Energy & Environmental Science



REVIEW

View Article Online
View Journal | View Issue



Cite this: Energy Environ. Sci., 2020, 13, 3950

Received 3rd July 2020, Accepted 28th September 2020

DOI: 10.1039/d0ee02111c

rsc.li/ees

Recent advances in developing organic electrode materials for multivalent rechargeable batteries

Kaiqiang Qin, Da Jinghao Huang, Kathryn Holguin and Chao Luo xab

Due to the low cost and abundance of multivalent metallic resources (Mg/Al/Zn/Ca), multivalent rechargeable batteries (MRBs) are promising alternatives to Li-ion and Pb-acid batteries for grid-scale stationary energy storage applications. However, the high performance of inorganic electrode materials in Li-ion batteries does not extend to MRBs, because the high charge density of multivalent cations dramatically reduces their diffusivity in the crystal lattice of inorganic materials. To achieve high-performance MRBs, organic electrode materials (OEMs) with abundant structural diversity and high structural tunability offer opportunities. This review presents an overview of the state-of-the-art OEMs in MRBs, including non-aqueous rechargeable Mg/Al/Zn and aqueous rechargeable Mg/Al/Zn/Ca batteries. The advantages, challenges, development, mechanism, structure, and performance of OEMs in MRBs are discussed in detail. To provide a comprehensive and thorough understanding of OEMs in MRBs, the correlation between molecular structure and electrochemical behavior is also summarized and discussed. This review offers insights for the rational structure design and performance optimization of advanced OEMs in MRBs.

Broader context

The rapid growth of consumer electronics, electric transportation, and grid-scale stationary energy storage has led to a demand for improved energy storage strategies. However, the state-of-the-art lithium ion batteries suffer from high cost, high toxicity, and scarcity of lithium and transition metal (cobalt) resources. To achieve safe, cost-effective and environmentally benign energy storage, it is essential to develop lithium-free and cobalt-free battery technology with affordable and sustainable resources. In this review, we present a comprehensive overview of recent advances in developing lightweight, abundant, inexpensive, sustainable, and recyclable transition metal-free organic electrode materials (OEMs) for multivalent rechargeable batteries (MRBs). We also focus on the advantages, challenges, mechanisms, structure, and performance of OEMs in MRBs. To gain fundamental insights and provide guidance for the rational structure design of advanced OEMs, this review not only discusses the development and applications of state-of-the-art OEMs in non-aqueous and aqueous MRBs, but also summarizes the correlation between structure and performance. Perspectives on future directions and outlooks for practical applications of organic MRBs, are proposed as well.

^b Quantum Science & Engineering Center, George Mason University, Fairfax, VA, 22030, USA



Kaiqiang Qin

Dr Kaiqiang Qin obtained his PhD from Tianjin University (China) in 2018. He joined the University of California, Los Angeles (UCLA, USA) as a postdoc from 2018 to 2020. He is currently a postdoc in Prof. Luo's lab at George Mason University (USA). His current research interests focus on organic electrode materials for next-generation energy storage.



Jinghao Huang

Jinghao Huang received his bachelor's degree in chemistry from University of California, Irvine (UCI). He is currently a student under supervision of Prof. Chao Luo in the Department of Chemistry and Biochemistry, George Mason University. His current research interests focus onorganic electrode materials for sodiumion batteries.

^a Department of Chemistry and Biochemistry, George Mason University, Fairfax, VA, 22030, USA. E-mail: cluo@gmu.edu

1. Introduction

With the advantages of lightweight, abundance, low cost, high sustainability and recyclability, organic electrode materials (OEMs) stand out as high-performance and universal electroactive materials for various rechargeable battery systems. The abundant structural diversity and tunability of OEMs, consisting of earth-abundant light elements such as C, H, O, N, and S, offer opportunities for developing advanced rechargeable batteries.¹⁻⁴ Unlike inorganic electrode materials, the electrochemical performance of OEMs depends on the active functional group rather than crystalline structure. The diverse molecular structures and universal electrochemical property of OEMs enable their promising electrochemical performance in lithium ion batteries (LIBs) and beyond. Up to date, OEMs have been applied in various types of energy storage devices, including non-aqueous alkali-ion batteries, multivalent batteries, dual-ion batteries, all-solid-state batteries, aqueous batteries, and redox flow batteries. Though the energy density of OEMs is still not comparable with their inorganic counterparts in LIBs, the low cost, abundance, and structural flexibility of OEMs render them ideal energy storage materials for cost-effective and sustainable energy storage devices.

After the debut in the market three decades ago, LIBs attracted considerable research interests from both academia and industry because of the high energy density and stable cycle life. To date, LIBs and lead acid batteries (LABs) dominate the market of energy storage devices for consumer electronics, automotive vehicles, uninterruptible power supply, telecommunications, and renewable energy.5-8 In 2018, the global LIB market was valued at \$36.2 billion, and the global LAB market was valued at \$39.7 billion. Although LABs ($\sim 40 \text{ W h kg}^{-1}$) provide much lower energy density than LIBs ($\sim 250 \text{ W h kg}^{-1}$), they have a larger market share because of their low cost, high safety, and high-power output. Cost and safety are critical for battery technology, especially when applied to large-scale

stationary electrical energy storage. However, the development of LIBs and LABs is impeded by the limited and unevenly distributed lithium resources and high toxicity of Pb/PbO2, respectively. 10-12 There is much anticipation for another leap of battery technology to achieve safe, cost-effective, and environmentally benign energy storage devices. Here, organic multivalent rechargeable batteries (MRBs) stand out as promising alternatives to LIBs and LABs due to the low cost and abundance of multivalent metals and OEMs.

In MRBs, the nontoxic multivalent metals such as Mg, Al, and Zn show high stability and capacity during battery charge/ discharge, rendering them ideal anodes for cost-effective and environmentally benign energy storage devices. 4 As shown in Table 1, the volumetric capacity of these multivalent metals is larger than Li. Additionally, Mg, Al, and Zn foils are stable when exposed to oxygen and moisture in the air, due to the formation of metal oxide passivation layers on the surface. Moreover, their autoignition temperatures are much higher than Li, demonstrating better safety for practical applications. As is well documented, lithium metal shows the highest specific capacity among all the anodes, but it cannot be used in commercial lithium batteries because of the safety concern for battery thermal runaway triggered by lithium dendrite growth. 15-17 Unlike in lithium metal batteries, the dendrite growth phenomenon is less favorable in non-aqueous Mg/Al metal batteries during the plating and stripping process, improving the safety of these batteries. 18-20 The inexpensive and abundant multivalent metals can be used as high capacity anodes in MRBs. The fundamental properties of various metal anodes in LIBs and MRBs such as cost, abundance, specific capacity, safety, standard potential, and volumetric capacity are compared in Fig. 1, demonstrating the advantages and challenges of MRBs and LIBs. 21-25 However, inorganic cathode materials such as transition metal oxides and transition metal phosphates do not extend their high performance in LIBs to MRBs when coupling



Kathryn Holguin

Kathryn Holguin received her BS in 2009 and MS in 2011 from George Mason University. She is currently a PhD candidate in the Department of Chemistry and Biochemistry, George Mason University. Her research interests focus on organic and polymer structure engineering for sodium ion and multivalent metal batteries.



Chao Luo

Prof. ChaoLuoreceived Bachelor's degree from Wuhan University in 2008. He joined Prof. Xuesong Wang's group and received Master's degree from Technical Institute of Chemistry and Physics, Chinese Academy of Sciences in 2011. Then, he joined Prof. Chunsheng Wang's group at University of Maryland, College Park, and obtained PhD degree in 2015. After that, he worked as a postdoc at University of Maryland, College Park from

2016 to 2019 and joined George Mason University as an Assistant Professor in 2019. His current research interests focus on developing new materials and new chemistries for highperformance and sustainable energy storage devices.

Table 1 A summary of fundamental chemical and physical properties of metal elements in various rechargeable battery systems¹³

	Atomic mass	Ionic radius (Å)	E^{0} (V) vs. SHE	Volumetric capacity (mA h mL^{-1})	Specific capacity (mA h g ⁻¹)	Air stability of metal foil	Autoignition temperature (°C)
Li	6.94	0.76	-3.04	2062	3861	Unstable	179
Mg	24.31	0.72	-2.37	3883	2205	Stable	473
Al	26.98	0.5335	-1.66	8046	2980	Stable	510
Ca	40.08	1.00	-2.87	2073	1337	Unstable	790
Zn	65.39	0.74	-0.76	5851	820	Stable	460

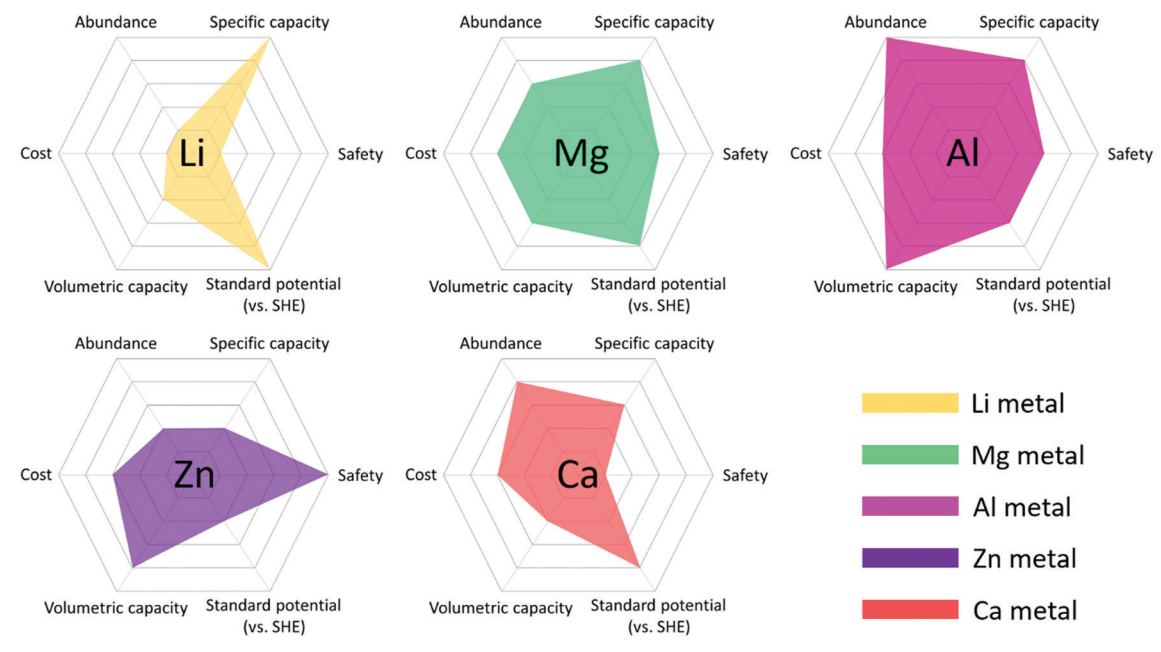


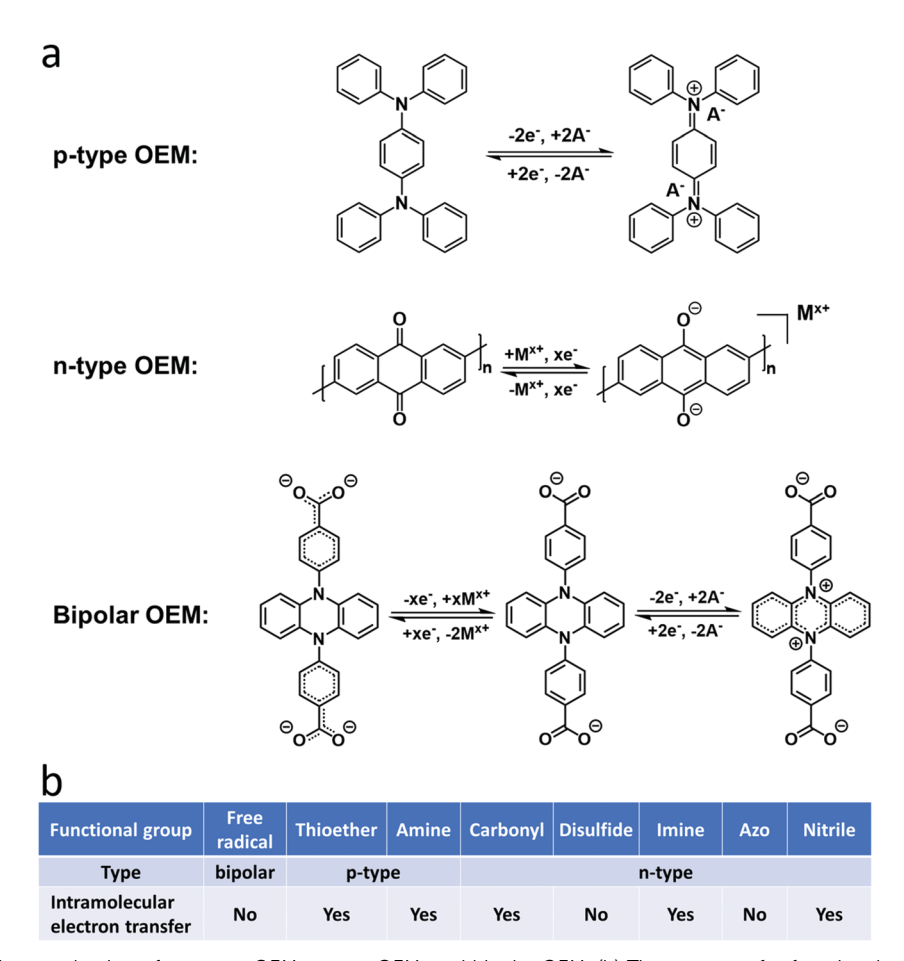
Fig. 1 Overview of fundamental properties of different types of metal anodes in rechargeable batteries.

with multivalent metal anodes. This is due to the high charge density of multivalent cations, which dramatically reduces their diffusivity in the crystal lattice of inorganic materials. The sluggish reaction kinetics of inorganic electrode materials impedes the development of MRBs. Though decreasing the particle size of inorganic materials to nanoscale circumvents this challenge, it sacrifices the cost and volumetric energy density of MRBs. To achieve cost-effective and high-performance MRBs, flexible and tunable OEMs provide new opportunities.

The first OEM, dichloroisocyanuric acid, was a carbonyl group-based organic compound introduced in lithium batteries in 1969, and the first attempt of OEMs in MRBs occurred in 1984 by using a conductive polymer, polypyrrole, in Al batteries (Fig. 2). 26,27 Since then, a number of functional groups have been introduced to the family of OEMs, including disulfide, free radical, imine, azo, nitrile, thioether, and primary/secondary/tertiary amines. 28–35 Different functional groups exhibit distinct reaction mechanisms and potentials. According to reaction mechanisms, OEMs can be divided into three categories: p-type OEMs, n-type OEMs, and bipolar OEMs. The reaction mechanisms of the representative OEMs for the three categories are summarized in Scheme 1a. The p-type OEMs containing thioether and amine, react with anions (ClO₄⁻, PF₆⁻, TFSI⁻) to carry positive charges during charge/discharge,

resulting in a high reaction potential, while n-type OEMs containing carbonyl, disulfide, imine, azo, and nitrile groups, react with metal cations to carry negative charges upon cycling, leading to a relatively low reaction potential.36-40 Bipolar OEMs contain free radicals or at least two types of other functional groups to react with both anions and cations, so they can serve as both cathodes and anodes to make an all-organic full cell. 41 The intramolecular electron transfer in the conjugated structure occurs in carbonyl, imine, nitrile, thioether, and amine-based OEMs, while there is no intramolecular electron transfer in disulfide, free radical, and azo group-based OEMs. A summary for functional groups, reaction types, and electron transfer mechanisms of OEMs is shown in Scheme 1b. Due to the superior structural tunability, the reaction potentials and specific capacity of OEMs can be altered in a wide range by tailoring the functional group and conjugated structure. The electron-withdrawing functional group could enhance the reaction potential, while the electron-donating functional group decreases the reaction potential. The reaction potentials of most OEMs are lower than the inorganic counterparts, resulting in a lower energy density in lithium batteries. However, the poor electrolyte stability in MRBs limits the selection of cathode materials.42,43 Most inorganic cathodes with reaction potentials above 3.5 V versus Li/Li⁺ cannot be used in non-aqueous MRBs, while the reaction potentials of OEMs are within the stability

Fig. 2 The development and timeline of organic electrode materials in various rechargeable batteries. The dates correspond to the first reported compound.



Scheme 1 (a) The reaction mechanisms for n-type OEM, p-type OEM, and bipolar OEM. (b) The summary for functional groups, reaction types, and electron transfer mechanisms of OEMs.

window of the electrolyte in MRBs. More importantly, the flexible and tunable structures facilitate the diffusivity of multivalent cations and related anions in OEMs. All these merits render OEMs promising electrode materials for MRBs.

This review focuses on the recent advances in developing OEMs for MRBs. As universal electrodes, OEMs are used in all types of MRBs with exceptional electrochemical performance, in terms of high capacity, high rate capability, and long cycle

life. To further stimulate the development of advanced OEMs and fulfill the aim of safe and cost-effective energy storage devices, it is pivotal to gain fundamental insights into the reaction mechanism and structure-performance correlation in MRBs. Therefore, this review not only provides an overview of the applications of OEMs in various MRBs but also exploits the relationship between chemical/physical structures and battery performances to offer insight for the rational structural

design of advanced OEMs for MRBs. The applications of OEMs in non-aqueous Mg/Al/Zn rechargeable batteries and aqueous Mg/Al/Ca/Zn rechargeable batteries are discussed in detail to explore the challenges and advantages in each energy storage system.

The discussion of the development of OEMs in MRBs is divided into two sections, non-aqueous organic MRBs and aqueous organic MRBs. We firstly present the OEMs in non-aqueous MRBs, including non-aqueous rechargeable Mg batteries (RMBs), rechargeable Al batteries (RABs), and rechargeable Zn batteries (RZBs), and then continue with a summary of OEMs in aqueous MRBs, including aqueous RMBs, RABs, rechargeable Ca batteries (RCBs), and RZBs. Systematic discussions about chemical structure, reaction mechanism, and electrochemical performance of OEMs in each type of non-aqueous and aqueous MRBs are provided to gain fundamental insights into the development and applications of OEMs in various MRBs. Eventually, the conclusion and outlook of advanced OEMs for low-cost, high-energy, safe, and stable MRBs are also discussed.

2. OEMs in non-aqueous MRBs

2.1. OEMs in non-aqueous RMBs

Non-aqueous RMBs are promising alternatives to LIBs and LABs for grid-scale stationary energy storage because of the low cost, abundance, and high volumetric/specific capacity of Mg metal anode. However, the sluggish reaction kinetics, low capacity, and fast capacity decay of inorganic cathode materials impede the development of RMBs. To obtain high-performance non-aqueous RMBs, the flexible and tunable OEMs stand out as promising cathodes. The reaction mechanisms and electrochemical behaviors of various types of OEMs in non-aqueous RMBs are summarized in Fig. 3, and Tables 2 and 3. This section further discusses the applications of state-of-the-art OEMs in detail.

2.1.1. Quinone monomers. Quinone monomers, which have been widely explored as cathode materials in LIBs, are

universal electrode materials in rechargeable battery systems, including alkali-ion batteries, MRBs, aqueous batteries, all-solidstate batteries, and redox flow batteries. As a typical quinone monomer, 2,5-dimethoxy-1,4-benzoquinone (DMBQ), has been used as a cathode material in LIBs. Moreover, the previous reports proved that DMBQ could also act as a cathode to reversibly accommodate Mg2+ ions in RMBs due to the interaction between two carbonyl groups in DMBQ and Mg²⁺ ion. Sano et al., 44 for the first time, tested DMBQ cathode in a Mg system with 0.5 M Mg(ClO₄)₂ in butyrolactone electrolyte. The DMBQ-based RMBs deliver a specific capacity of 260 mA h g⁻¹ at 20 mA g⁻¹ with an average discharge voltage of 0.9 V (Fig. 4a). The X-ray diffraction (XRD) and energy-dispersive X-ray spectroscopy (EDX) measurements verify that one DMBQ molecule can reversibly store/release one Mg ion, accompanied by a twoelectron redox reaction (Table 2). Although the voltage window is not satisfactory, this work reveals the promise of redox-active quinone derivatives as active materials in RMBs. Afterward, the same group utilized three different kinds of sulfones such as sulfolane (SL), ethyl-i-propyl sulfone (EiPS), and di-n-propyl sulfone (DnPS), as electrolyte solvents in RMBs. 45 Magnesium bis(trifluoromethanesulfonyl)imide (Mg(TFSI)2) was used as the salt to enlarge the stability window of the electrolyte. The Mg(TFSI)₂ salt shows a smaller effective solvated ionic radius and larger stability window in the SL-based electrolyte than EiPS and DnPS-based electrolytes owing to the higher stability of SL against oxidation. The as-fabricated Mg|Mg(TFSI)2/ SL|DMBQ cell provides a specific capacity of 100 mA h g⁻¹ and can be charged and discharged for more than 50 cycles over a wide voltage range of 0-4.0 V. Nonetheless, the cell suffers from large overpotential, low cycling stability, and a low discharge potential (0.9 V in 0.5 M Mg(ClO₄)₂ in γ -butyrolactone electrolyte, and 0.4 V in 0.5 M Mg(TFSI)2 in sulfone-based electrolytes). To circumvent these challenges, Pan et al.46 reported the development of DMBQ as a high voltage cathode (>2.0 V) for non-aqueous RMBs using non-nucleophilic Mg(TFSI)2 and MgCl2 in dimethoxyethane (DME) electrolyte. The non-nucleophilic electrolyte can avoid the nucleophilic attack of carbonyl moieties by the nucleophilic ions in the

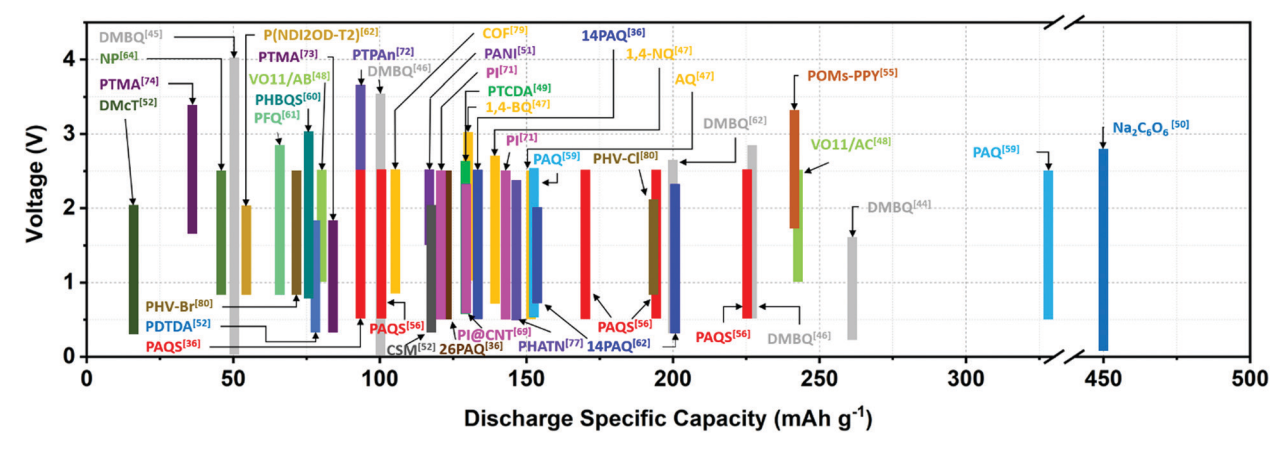


Fig. 3 Capacity versus voltage for the reported OEMs in non-aqueous RMBs

Reaction mechanisms and electrochemical behaviors of the OEMs in non-aqueous RMBs

Types		General redox mechanism	Classification	Average discharge voltage	Discharge capacity	Cycle life
Carbonyl monomer	Quinone monomer	R'' +Mg ²⁺ , 2e ⁻ R'' R''' -Mg ²⁺ , 2e ⁻ R''' -Mg ²⁺	n-Type	Medium	High	Low
	Anhydride	Ar Ar' -Mg ²⁺ , 2e -Mg ²⁺ , 2e -Mg ²⁺ , 2e				
	Quinone polymer	R" +Mg ²⁺ , 2e' R"				
Carbonyl polymer	Polyimide	R Mg ²⁺ Ar Ar' Ar Ar' Ar Ar' N O R N O O	n-Type	Medium	High	Medium
Disulfide polymer		$R-S-S-R' = \frac{+Mg^{2+}, 2e^{-}}{-Mg^{2+}, 2e^{-}} = R-S = \frac{-Mg^{2+}}{S-R'}$	n-Type	Low	Medium	Low
Imine polymer		R' A+, e R' R A+ -A+, e R'	n-Type	Medium	High	High
Amine polymer		R' +B', -e' R' B' R' B' R'' B': TFSI', 0.5 SO ₄ ² -, CIO ₄ -	p-Type	High	Medium	High
Nitroxide free radical	polymer	$ \begin{array}{c} & & & & & & & & & & & & & & & & & & &$	р-Туре	High	Low	Low

electrolyte and prevent the decomposition of DMBQ. Moreover, 0.5 M Mg(TFSI)₂-2MgCl₂ in DME electrolyte improves the magnesium plating/stripping efficiency (Coulombic efficiency, CE) to nearly 100%, and the Mg|Mg(TFSI)₂-MgCl₂/DME|DMBQ cell possesses an improved initial discharge capacity of 216 mA h g⁻¹. However, the capacity fading is still observed after 30 cycles due to the dissolution of DMBQ in the electrolyte, which is a major challenge for redox-active organic compounds in RMBs.

To circumvent the high solubility challenge and improve the cycle life of organic RMBs, another type of conjugated quinonebased OEMs, Anthraquinone (AQ) and its derivatives, are reported as promising cathode materials for RMBs due to the abundant structural tunability and high theoretical capacity. Bitenc et al. 47 investigated the performance of three quinonebased organic compounds (AQ, 1,4-naphthoquinone (1,4-NQ), and 1,4-benzoquinone (1,4-BQ)) using 0.6 M Mg(TFSI)₂-2MgCl₂ (MTC) in DME and 0.6 M MgCl2-AlCl3 (MAC) in DME as the electrolytes, respectively. In MTC electrolyte, AQ exhibits an initial capacity of 152 mA h g⁻¹ with a discharge potential of 1.55 V. The reaction potentials of the other two quinone-based organic compounds, 1,4-NQ and 1,4-BQ, are 0.2 V and 0.5 V higher than AQ, respectively. Furthermore, an additional potential upshift of 0.2 V was observed in the MAC electrolyte for all three compounds. However, their high solubility in the electrolyte results in fast capacity loss and short cycle life (40 cycles). Further improvement is required to enhance the performance of AQ derivatives. Another AQ derivate (Vat Orange 11) that contains three conjugated anthraquinone moieties, has been investigated as a promising cathode material for RMBs in PhMgCl-AlCl₃ (APC) electrolytes and non-nucleophilic ionic liquid-based electrolyte due to the highly reversible two-electron transfer process between carbonyl (-C=O) and magnesium enolate groups during charge and discharge cycles. 48 The dissolution of Vat Orange 11 in the APC electrolyte can be relatively suppressed by the addition of LiCl additive.

 Table 3
 Summary of OEMs as cathodes for non-aqueous RMBs

Compound	Structure	Electrolyte	Average discharge voltage	Initial reversible capacity at current density	Cycle life (n)	Rate capability
DMBQ ⁴⁴		0.5 M Mg(ClO ₄) ₂ /butyrolactone	0.9 V	260 mA h g^{-1} at	5	N/A
DMBQ ⁴⁵	Q.	0.5 M Mg(TFSA) ₂ /sulfone	0.4 V	20 mA g ⁻¹ 50 mA h g ⁻¹ at	50	N/A
DMBQ^{46}	OMe	0.5 M Mg(TFSI) ₂ -2MgCl ₂ in DME	2 V		30	N/A
DMBQ^{46}	MeO	0.5 M Mg(TFSI) ₂ in DEG/DME		U	30	N/A
DMBQ ⁶²	o	$0.25~M~Mg(TFSI)_2$ and $0.5~M~MgCl_2$ in DME	0.25 V 2 V	1C 200 mA h g ⁻¹ at 150 mA g ⁻¹	N/A	N/A
AQ^{47}		0.6 M Mg(TFSI) ₂ -2MgCl ₂ (MTC)	1.55 V	152 mA h g^{-1} at 100 mA g^{-1}	30	N/A
1,4-NQ ⁴⁷		0.6 M Mg(TFSI) ₂ –2MgCl ₂ (MTC)	1.75 V	138 mA h g^{-1} at 100 mA g^{-1}	40	N/A
1,4-BQ ⁴⁷		0.6 M Mg(TFSI) ₂ -2MgCl ₂ (MTC)	1.9 V	130 mA h $\rm g^{-1}$ at 100 mA $\rm g^{-1}$	40	N/A
Vat Orange 11/active carbon ⁴⁸		$0.4~\mathrm{M}~\mathrm{2PhMgCl\text{-}AlCl_3}~\mathrm{(APC)}$	~1.7 V	260 mA h g^{-1} at 100 mA g^{-1}	1000	26 mA h g^{-1} at 2000 mA g^{-1}
Vat Orange 11/active carbon ⁴⁸	NH NH	$0.4~\mathrm{M}~\mathrm{2PhMgCl-AlCl_3}~\mathrm{(APC)/1}~\mathrm{M}$ LiCl (LPC-LiCl)	~1.8 V	246 mA h g ⁻¹ at 100 mA g ⁻¹	1000	26 mA h g ⁻¹ at 2000 mA g ⁻¹
Vat Orange 11/acetylene black ⁴⁸		0.4 M 2PhMgCl-AlCl ₃ (APC)/ MMTP ₁₃ TFSI	~1.65 V	81 mA h g ⁻¹ at 100 mA g ⁻¹	500	15 mA h g ⁻¹ at 1000 mA g ⁻¹
PTCDA ⁴⁹	00	0.4 M APC electrolyte	1.7 V	130 mA h g^{-1} at	70	N/A
PTCDA ⁴⁹		0.4 M APC electrolyte + 1 M LiCl	1.7 V	100 mA g ⁻¹ 140 mA h g ⁻¹ at 100 mA g ⁻¹	150	40 mA h g^{-1} at 500 mA g^{-1}
$Na_{2}C_{6}O_{6}^{50}$	or which is a second of the se	0.25 M APC and 1 M LiCl/THF	1.8 V and	450 mA h g^{-1} at	50	100 mA h g ⁻¹ at
$Na_2C_6O_6/rGO^{50}$	O ONa O ONa	0.25 M APC and 1 M LiCl/THF	0.7 V 1.8 V and 0.7 V	50 mA g ⁻¹ 450 mA h g ⁻¹ at 50 mA g ⁻¹		5000 mA g ⁻¹ 175 mA h g ⁻¹ at 5000 mA g ⁻¹
$\mathrm{LiC_6O_6}^{50}$	O OLi O OLi	0.25 M APC and 1 M LiCl/THF	1.8 V and 0.7 V	400 mA h g^{-1} at 50 mA g^{-1}	50	25 mA h g^{-1} at 5000 mA g^{-1}
PANI ⁵¹		$0.025~\mathrm{M}~\mathrm{MgSO_4}$ in EMIES	2.1 V	116 mA h g ⁻¹ at 667 mA g ⁻¹	60	83 mA h g ⁻¹ at 6160 mA g ⁻¹
DMcT ⁵²	HS SH	0.25 M Mg(AlCl ₂ BuEt) ₂ /THF	1.4 V	16.8 mA h g^{-1} at 25 mA g^{-1}	26	N/A
PDTDA ⁵²	→ NH) _n s s S	$0.25~\mathrm{M}~\mathrm{MgAlCl_3Bu_2/THF}$	0.9 V	78 mA h g ⁻¹ 25 mA g ⁻¹	33	N/A
CSM ⁵²	S—S N N N n	0.25 M MgAlCl $_3\mathrm{Bu}_2/\mathrm{THF}$	1.35 V	117.3 mA h g ⁻¹ at 25 mA g ⁻¹	22	N/A
POMs-PPY ⁵⁵	$\left[\begin{array}{ccc} & & & & \\ $	0.1 M Mg(ClO ₄) ₂ /PC	2.4 V and 2.1 V	$242 \text{ mA h g}^{-1} \text{ at }$ 1C	50	N/A

Table 3 (continued)

Compound	Structure	Electrolyte	Average discharge voltage	Initial reversible capacity at current density	Cycle life (n)	Rate capability
PAQS ⁵⁶ PAQS ⁵⁶	+ °=	0.2 M MHCC 0.2 M MHCC	1.75 V 1.75 V	100 mA h g ⁻¹ 170 mA h g ⁻¹ at 50 mA g ⁻¹	80	N/A 75 mA h g ⁻¹ at 500 mA g ⁻¹
PAQS ⁵⁶		0.25 M MgCl ₂ and 0.075 M AlCl ₃ dissolved in THF (MACC)	1.5 V	191 mA h g ⁻¹		10 mA h g^{-1} at 500 mA g^{-1}
PAQS ⁵⁶	o s	0.37 M MgCl ₂ and 0.15 M Mg(TFSI) ₂ in THF/glyme = 3:2 (vol%) (MTCC)	1.5 V	225 mA h g ⁻¹ at 50 mA g ⁻¹	100	100 mA \hat{h} g^{-1} at 500 mA g^{-1}
PAQS ³⁶	0	0.3 M Mg(HMDS) ₂ -4MgCl ₂ /THF	1.5 V	90 mA h g ⁻¹ at 112 mA g ⁻¹	100	N/A
26PAQ ³⁶		0.3 M Mg(HMDS) ₂ -4MgCl ₂ /THF	1.71 V and 1.52 V	122 mA h g^{-1} at 130 mA g^{-1}	100	\sim 35 mA h g $^{-1}$ at 1300 mA g $^{-1}$
$14PAQ^{36}$	_	0.3 M Mg(HMDS) ₂ -4MgCl ₂ /THF	1.57 V and	132.7 mA h g^{-1} at 130 mA g^{-1}	1000	$\sim 45 \text{ mA h g}^{-1} \text{ at}$
PAQ ⁵⁹	° +	0.6 M Mg(TFSI) ₂ -2MgCl ₂ /DME	1.48 V 1.5 V	152 mA h g ⁻¹ at	500	1300 mA g ⁻¹ N/A
PAQ ⁵⁹		$0.6~\mathrm{M~MgCl_2-AlCl_3/DME}$	1.8 V	4	500	N/A
$14 \mathrm{PAQ}^{62}$, n	0.3 M Mg(HMDS) ₂ and 1.2 M MgCl ₂ in THF	1.5 V	155 mA h g ⁻¹ at 130 mA g ⁻¹	N/A	N/A
14PAQ ⁶²		0.2 M Mg(TFSI) ₂ in diglyme	1.5 V and 1.3 V	200 mA h g ⁻¹ at 16.2 mA g ⁻¹	100	125 mA h g ⁻¹ at 108 mA g ⁻¹
PHBQS ⁶⁰	ОН	0.48 M MgCl ₂ and 0.32 M Mg(TFSI) ₂ in tetraglyme and DOL	2 V	75 mA h g^{-1} at 50 mA g^{-1}	25	N/A
PHBQS ⁶⁰	+√>-s+ _n	0.48 M MgCl ₂ and 0.32 M Mg(TFSI) ₂ in tetraglyme	1.9 V	75 mA h g^{-1} at 50 mA g^{-1}	25	N/A
PFQ/rGO ⁶¹	+	0.6 M Mg(TFSI) ₂ -2MgCl ₂ in DME	1.8 V	65 mA h g^{-1} at 0.5C	400	$60 \text{ mA h g}^{-1} \text{ at}$ 5C
P(NDI2OD-T2) ⁶²	C ₁₀ H ₂₁ C ₈ H ₁₇	0.25 M Mg(TFSI) ₂ and 0.5 M MgCl ₂ in DME	1.5 V	54 mA h g ⁻¹ at 150 mA g ⁻¹	N/A	N/A
P(NDI2OD-T2) ⁶²	O N O S Y n	0.2 M Mg(TFSI) ₂ in diglyme	1.35 V	54.1 mA h g^{-1} at 11 mA g^{-1}	2500	38 mA h g ⁻¹ at 2700 mA g ⁻¹
64	O C ₁₀ H ₂₁	$0.4~M~Mg(TFSI)_2$ and $0.4~M~MgCl_2$		45 mA h σ^{-1} at		49 mA h o^{-1} at
NP ⁶⁴ NP ⁶⁴		in TEG/DME/DOL 0.4 M Mg(TFSI) ₂ and 0.4 M MgCl ₂	1.7 V	45 mA h g^{-1} at 50 mA g^{-1}	100 100	49 mA h g ⁻¹ at 500 mA g ⁻¹ N/A
W.	+N N+n	in TEG/DME	1.7 V	30 mA h g^{-1} at 50 mA g^{-1}	100	14/21
NDI-TFP polymer ⁶⁶	#+0}\$\{	DMSO, 0.1 M perchlorate supporting electrolyte	$-0.8~{ m V}~{ m vs.}$ Ag/AgClO $_4$	100 mA h g^{-1} at 70 uA	10	N/A
PI@CNT ⁶⁹	+N - N - O - O - O + n	PhMgCl/AlCl ₃ /THF	~1.7 V	130 mA h $\rm g^{-1}$ at 1C	200	71.5 mA h g^{-1} at 20C
PI1/CNTs ⁷¹	$+$ N \longrightarrow n	$Mg(HMDS)_2-4MgCl_2/2THF-PP_{14}TFSI$	1.45 V	\sim 120 mA h g ⁻¹ at 183 mA g ⁻¹	3000	59 mA h g ⁻¹ at 3660 mA g ⁻¹

Table 3 (continued)

Compound	Structure	Electrolyte	Average discharge voltage	Initial reversible capacity at current density	Cycle life (n)	Rate capability
PI2/CNTs ⁷¹	+N	Mg(HMDS) ₂ –4MgCl ₂ /2THF- PP ₁₄ TFSI	1.45 V	\sim 140 mA h g ⁻¹ at 158 mA g ⁻¹	8000	63 mA h g ⁻¹ at 20C, 3160 mA g ⁻¹
PTPAn ⁷²		Anhydrous Mg(ClO ₄) ₂ /acetonitrile	3.13 and 3.26 V	90 mA h g ⁻¹ at 50 mA g ⁻¹	2000	73 mA h g^{-1} at 1000 mA g^{-1}
PTMA ⁷³ PTMA ⁷⁴	/in	0.25 M Mg(AlCl ₂ BuEt) ₂ /THF 0.3 M Mg(TFSI) ₂ in glyme/diglyme	1 V ~2.6 and 1.8 V	81.2 mA h g^{-1} at 22.8 mA g^{-1} 37.6 mA h g^{-1} at 0.02C	21 4	N/A N/A
PHATN ⁷⁷	, , , , , , , , , , , , , , , , , , ,	1 M Mg(PF ₆) ₂ /DME	1.5 V	146 mA h g^{-1} at 20 mA g^{-1}	200	60 mA h g^{-1} at 200 mA g^{-1}
COF ⁷⁹		0.5 M Mg(TFSI)₂/DME	1.15 V	107 mA h g^{-1} at 22.8 mA g^{-1}	3000	$53 \text{ mA h g}^{-1} \text{ at}$ 1140 mA g^{-1}
PHV-Br ⁸⁰	 NNNN_Br	0.8 M PhMgCl + 0.4 M AlCl $_3$ in THF	1.7 and 1.2 V	68 mA h g ⁻¹ at 13 mA g ⁻¹	N/A	N/A
PHV-Cl ⁸⁰	$N = N \times $	0.8 M PhMgCl + 0.4 M AlCl ₃ in THF	1.69 and 1.33 V	192 mA h g ⁻¹ at 17 mA g ⁻¹	50	75 mA h g^{-1} at 850 mA g^{-1}

The resulting Vat Orange 11/active carbon-based cathode delivers a high initial capacity (246 mA h g⁻¹ at 100 mA g⁻¹), good cycling stability (~ 50 mA h g⁻¹ after 1000 cycles at 500 mA g⁻¹), and high rate capability (26 mA h g^{-1} at 2000 mA g^{-1}) (Fig. 4b). However, it still suffers from fast initial capacity decay from 246 mA h g^{-1} to below 100 mA h g^{-1} at 100 mA g^{-1} in 5 cycles. To further overcome the high solubility challenge, the Vat Orange 11/acetylene black cathode was tested in a non-nucleophilic electrolyte based on ionic liquid (Mg(HMDS)2-4MgCl2/2THF-PP₁₃TFSI, MMTP₁₃TFSI) in pure RMBs. The cathode provides a specific capacity of 120 mA h g⁻¹ at a current density of 100 mA g⁻¹ and retains a reversible capacity of 80 mA h g⁻¹ after 100 cycles, demonstrating the benefits of non-nucleophilic electrolyte to the electrochemical performance of Vat Orange 11 electrode. Therefore, this work demonstrates that extending the conjugated structure and using a non-nucleophilic electrolyte are effective approaches to enhance the performance of quinonebased OEMs in non-aqueous RMBs.

2.1.2. Anhydrides. 3,4,9,10-Perylenetetracarboxylic dianhydride (PTCDA) is another type of carbonyl group-based OEM for RMBs, which can transfer two electrons during the charge/discharge process (Table 2). As a small organic compound, it is challenging to avoid its dissolution in aprotic electrolyte solutions. Cui et al.49 provided an excellent Mg-storage performance using PTCDA as a cathode material through a saltdissolution inhibition approach. The use of the soluble salt additives (LiCl, KCl, or NaCl) in the aluminum chloride-THF complex/phenylmagnesium chloride (all phenyl complex, APC) electrolyte can effectively enhance the utilization of the active material and suppress the solubility of PTCDA, resulting in enhanced electrochemical performance. The PTCDA cathode shows a capacity of 130 mA h g⁻¹ at 100 mA g⁻¹ with a capacity retention of 67 mA h g^{-1} after 70 cycles in pure APC electrolyte. In comparison, the Mg|0.25 M APC-1 M LiCl|PTCDA cell delivers an initial discharge capacity of 140 mA h g⁻¹ at 100 mA g⁻¹ with a discharge plateau at 1.7 V and retains a

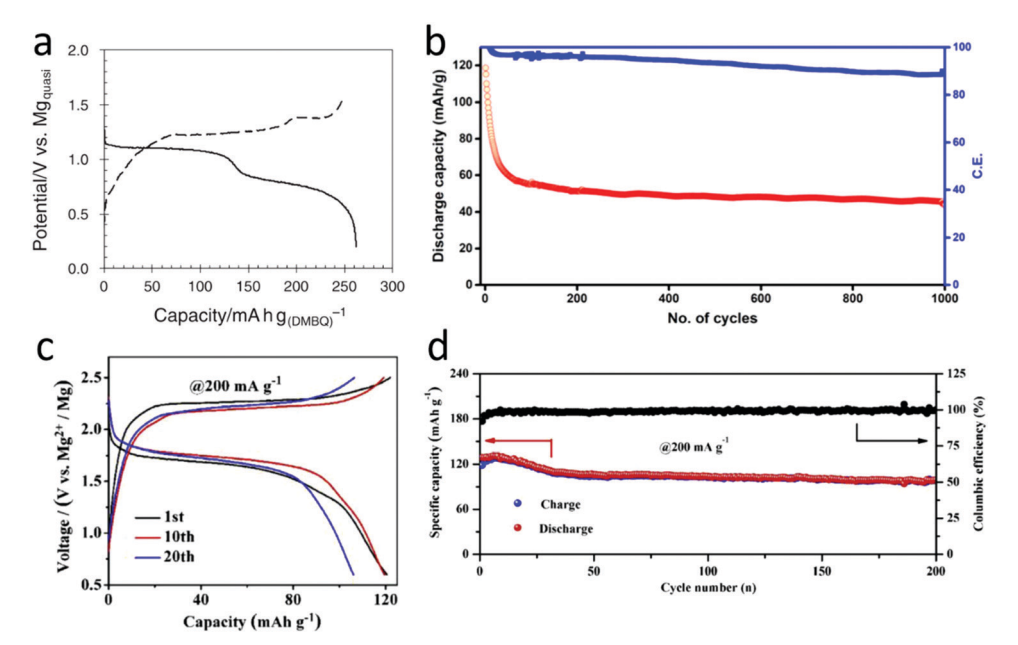


Fig. 4 (a) Typical charge–discharge curves of the DMBQ electrode (solid line: discharge; dashed line: charge). Reproduced with permission.⁴⁴ Copyright 2012 Chemical Society of Japan. (b) Long term cycling stability of the Vat Orange 11 electrode at 500 mA g^{-1} current density in APC-LiCl electrolyte. Reproduced with permission. 48 Copyright 2020 The Electrochemical Society. (c) Galvanostatic charge—discharge curves of PTCDA at a current density of 200 mA g^{-1} . (d) The long-term cycling stability of the PTCDA cathode at a current density of 200 mA g^{-1} . Reproduced with permission. ⁴⁹ Copyright 2019 Elsevier Ltd.

reversible capacity of 100 mA h g⁻¹ after 200 cycles with a CE of 98% (Fig. 4c and d). These excellent results are attributed to the synergistic effect of the capacitance-dominated reaction mechanism and the salt dissolution inhibition approach. This work opens up a door for developing high capacity, high potential, and stable organic cathodes in non-aqueous RMBs.

2.1.3. Conducting polymers and organosulfur polymers. Low-molecular-weight OEMs suffer from fast capacity loss in RMBs owing to their high solubility in the organic electrolyte. Polymerizing the redox-active compounds has been demonstrated as an effective approach to suppress the dissolution of organic electrodes. According to the charge storage mechanisms, these polymers are classified into six categories: conducting polymers, organosulfur polymers, quinone polymers, imine polymers, amine polymers, and nitroxide free radical polymers. The applications and electrochemical performances of these polymers are discussed in detail.

Among various types of conducting polymers, polyaniline (PANI) is a promising electrode material for RMBs due to environmental benignity, low cost, high conductivity, and good thermal stability. Ju et al.51 studied the performance of PANIbased cathode with MgSO₄-ionic liquid EMIES (1-ethyl-3methylimidazolium ethyl sulfate) electrolyte. The Mg metal anode displays high dissolution and deposition reversibility in this ionic liquid-based electrolyte. More importantly, the loose and porous structure of PANI is beneficial for the fast anion and electron transfer. As a result, the Mg|0.25 M MgSO₄/EMIES|PANI cell delivers a high average discharge potential of 2.1 V and an initial discharge capacity of 116 mA h g^{-1} at a high current density of 667 mA g^{-1} , as well as a high rate capability of 83 mA h g^{-1} at

 $6160~\mathrm{mA}~\mathrm{g}^{-1}$. Hence, PANI shows promising application prospects as the cathode for non-aqueous RMBs.

In addition to acting as an electroactive material, conducting polymers can also effectively enhance the electrochemical performance of other redox-active OEMs by increasing the conductivity of the organic electrode. For example, NuLi et al. 52 investigated three organosulfur cathode materials, 2,5-dimercapto-1,3,4-thiadiazole (DMcT), poly-2,2'-dithiodianiline (PDTDA), and conductive sulfur-containing material (CSM), for RMBs. Among them, DMcT undergoes a two-electron transfer process involved in the reversible cleavage and recombination of the disulfide bond. However, the DMcT-based RMBs must be operated at high temperatures (100–150 °C) due to the sluggish reaction kinetics of the disulfide group at ambient temperature. To improve the reaction kinetics, the conductive PANI is used to enhance the conductivity of the DMcT electrode.⁵³ After homogeneously mixing with PANI, the composite electrode of DMcT/PANI delivers a discharge capacity of 27.2 mA h g⁻¹ after 26 cycles at ambient temperature. As another organosulfur cathode material, PDTDA shows higher electrochemical activity and conductivity because of the existence of both S-S bond and aniline moiety. Hence, it was employed as a cathode for RMBs without the addition of PANI. As expected, the Mg|0.25 M MgAlCl₃Bu₂/THF|PDTDA cell shows an enhanced initial discharge capacity of 78 mA h g⁻¹ and slow capacity degradation over 30 cycles, due to the intramolecular electrocatalytic effect and conductive nature of the aniline moiety. After further investigation, the CSM with a stable and inactive backbone shows enhanced conductivity and redox reaction reversibility due to the extended π -conjugation structure and stable C-S-S-C bond. 54 However, the CSM cathode only delivers a

low capacity of 51.2 mA h g⁻¹ during the first discharge process due to the low reaction kinetics. After mixing with PANI, the composite electrode delivers a high initial capacity of 117.3 mA h g⁻¹, and retains 73 mA h g⁻¹ after 22 cycles. These results confirm the role of conductive PANI in improving the performance of OEMs in RMBs. Apart from increasing the electronic conductivity of OEMs, the conductive polymers also enhance the electron transfer of inorganic materials. Kenry et al. 55 synthesized a polyoxometalate-(poly)pyrrole (POMs-PPY) composite and used it as a cathode material for RMBs. The conductive polymer, PPY, not only enhances the electronic conductivity of the POMs-based electrode but also remarkably reduces the solubility of POMs active material in the electrolyte. Consequently, the POMs-PPY composite cathode delivers a high initial capacity of 242 mA h g⁻¹ and retains a reversible capacity of 145 mA h g⁻¹ after 50 cycles. Though the conductive polymers show high reaction potentials and fast reaction kinetics, the low specific capacity and short cycle life limit the further development and application. Therefore, more efforts are devoted to designing and synthesizing high capacity and stable polymeric materials for non-aqueous RMBs.

2.1.4. Quinone polymers. To achieve high capacity and stable OEMs, quinone polymers stand out as promising cathode materials for high energy density and high stability RMBs. Bitenc et al. 56 investigated poly(anthraquinoyl) sulfide (PAQS) as a cathode material for RMBs with three different nonnucleophilic electrolytes: (Mg2Cl3-6 THF) (HMDSAlCl3) in THF (MHCC), MgCl₂-AlCl₃ in THF (MACC), and MgCl₂-Mg(TFSI)₂ in a mixture of THF and glyme (MTCC). Additionally, modified Mg nanomaterials (200-500 nm) were used as the counter electrode to further improve the performance of the battery because of the higher electrochemical kinetics and a faster activation of Mg powder than Mg foil during the charge/discharge process.⁵⁷ Among the three electrolytes, the MTCC electrolyte displays the best performance. The Mg powder|MTCC|PAQS cell delivers a high initial capacity of 225 mA h g⁻¹ at a current density of 50 mA g⁻¹ and retains a reversible capacity of 100 mA h g⁻¹ at a current density of 500 mA g^{-1} (Fig. 5a). However, it still suffers from low cycling stability due to the dissolution of the anthraquinone polymer. To further improve the cycling stability, 2,6-polyanthraquinone (26PAQ), and 1,4-polyanthraquinone (14PAQ) were reported as promising cathode materials in RMBs.³⁶ Similarly, a non-nucleophilic 0.3 M Mg(HMDS)₂-4MgCl₂ (HMDS: hexamethyldisilazide) in THF solution was chosen as the electrolyte. Although PAQS, 26PAQ, and 14PAQ all show very limited solubility in THF, the magnesiated PAQS shows much higher solubility in THF than magnesiated 26PAQ and 14PAQ, resulting in the fast capacity decay of PAQS during long-term cycling. Also, the anthraquinonyl groups in 14PAQ show high rotation flexibility, because the redox-active quinonyl moieties lie on the branch of the polymer. The higher the rotation flexibility of the anthraquinonyl groups, the smaller the space hindrance and structural stress of the polymer. Therefore, 14PAQ shows the best structural stability among the three anthraquinone-based polymers.⁵⁸ The Mg-26PAQ battery shows an initial capacity of 122 mA h g⁻¹ at a current

density of 130 mA g⁻¹ and retains 100.2 mA h g⁻¹ after 100 cycles (Fig. 5b). Meanwhile, the Mg-14PAQ cathode delivers a high initial capacity of 132.7 mA h $\rm g^{-1}$ at a current density of 130 mA g^{-1} and retains 60 mA h g^{-1} after 1000 cycles at a current density of 260 mA g^{-1} (Fig. 5c). More importantly, the capacity and long-term cycling stability of PAQ-based cathodes are greatly impacted by the electrolyte. Bitenc et al. 59 explored and compared the electrochemical performance of PAO-based cathodes in two Mg electrolytes: 0.6 M Mg(TFSI)2-2MgCl2 and 0.6 M MgCl2-AlCl3 in DME. The PAQ-based cathode coupled with Mg(TFSI)2-2MgCl2 electrolyte shows higher capacity (165 mA h g⁻¹ at 1C) and cycling stability (120 mA h g⁻¹ after 500 cycles at 1C) than that with $MgCl_2$ -AlCl₃ (144 mA h g⁻¹ and 50 mA h g⁻¹ after 500 cycles at 1C), indicating the important role of electrolyte in RMBs (Fig. 5d). Inspired by the promising electrochemical performance of AQ-based polymers in RMBs, Bitenc et al. 60 synthesized a poly(hydrobenzoquinonyl-benzoquinonyl sulfide) polymer (PHBOS) to investigate the synergistic effect of benzoquinone and hydroquinone units. The Mg powder-PHBQS cell exhibits an average discharge voltage of 2 V and a high capacity of 140 mA h g⁻¹ after 25 cycles at a current density of 50 mA g^{-1} (Fig. 5e). Another high-performance cathode material for organic RMBs is an isomer of PAQ, poly-(9,10-phenanthrenequinone) (PFQ). PFQ shows high cycling stability due to the insolubility in the organic electrolyte. To enhance the utilization of PFQ, Vizintin et al. 61 developed a porous PFQ-based composite containing 21 wt% of reduced graphene oxide (rGO). The Mg|0.6 M Mg(TFSI)₂-2MgCl₂/ DME|PFQ/rGO cell delivers a specific capacity of 186 mA h g⁻¹ at 0.5C, and high capacity retention of 146 mA h g⁻¹ after 400 cycles, demonstrating a promising organic RMB.

Due to the superior electrochemical performance of polymeric materials in RMBs, considerable research efforts were devoted to exploiting the reaction mechanisms of organic RMBs. Dong et al. 62 proved that the MgCl+-storage chemistry is the mechanism for organic RMBs using carbonyl-based compounds as the cathodes and MgCl2-based electrolytes. The electrochemical storage of MgCl⁺ rather than Mg²⁺ leads to the low specific capacity of organic RMBs. To achieve the Mg²⁺-storage chemistry, the chloride-free electrolyte is the key. 63 When coupling with a chloride-free electrolyte (0.2 M Mg(TFSI)₂ in diglyme), the 14PAQ-based RMBs deliver a much higher initial capacity of 200 mA h g⁻¹ at a current density of 16.2 mA g⁻¹. The excellent electrochemical performance can be maintained even under lean electrolyte condition (Fig. 5f). This work sheds light on the development of organic RMBs for practical applications. Therefore, exploiting chloride-free electrolytes and polymeric cathode materials is critical for the further development and applications of organic RMBs.

2.1.5. Polyimides (PIs). PIs, which are synthesized by polycondensation between aromatic dianhydride and diamine, are widely used as cathode materials in LIBs. The superior electrochemical performance of PIs in LIBs is extended to RMBs that the PI-based cathodes exhibit fast reaction kinetics and good cycling stability in RMBs. Bančič *et al.*⁶⁴ investigated the electrochemical behavior of naphthalene-hydrazine diimide

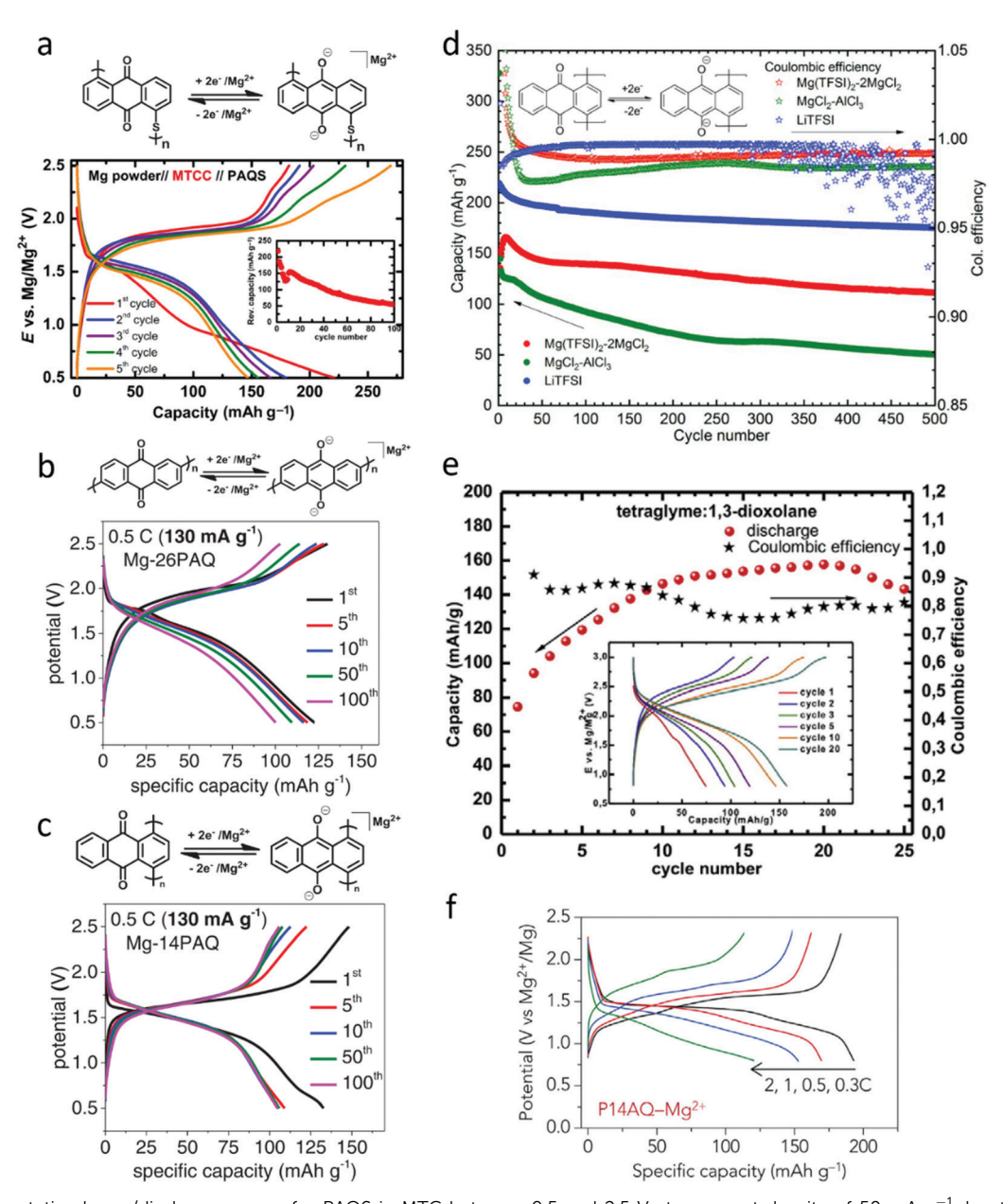


Fig. 5 (a) Galvanostatic charge/discharge curves for PAQS in MTC between 0.5 and 2.5 V at a current density of 50 mA g⁻¹. Insets show capacity retention in the first 100 cycles. Reproduced with permission. 56 Copyright 2015 Wiley-VCH Verlag GmbH & Co. KGaA (b) Galvanostatic charge/discharge curves for Mg-26PAQ. (c) Galvanostatic charge/discharge curves for Mg-14PAQ. Reproduced with permission. 36 Copyright 2016 Wiley-VCH Verlage GmbH & Co. KGaA. (d) Discharge capacity (left y-axis) and Coulombic efficiency (right y-axis) of long-term cycling of PAQ cathode at 1C from 0.5 to 2.5 V in Mg(TFSI)₂-2MgCl₂ (red) and MgCl₂-AlCl₃ (green). Reproduced with permission. So Copyright 2019 Elsevier B.V. (e) Discharge capacity and Coulombic efficiency in Mg system at 50 mA q^{-1} in tetraglyme/dioxolane electrolyte. Inset: Selected galvanostatic cycles. Reproduced with permission.⁶⁰ Copyright 2016 Elsevier B.V. (f) Voltage profiles of P14AQ at different current densities. Electrolyte: 0.2 M Mq(TFSI)₂ in diglyme. Reproduced with permission.⁶² Copyright 2018 Elsevier Inc.

polymer (NP) as a cathode in RMBs. It was proven that only two of the four carbonyl groups in the repeating unit of NP are electrochemically active. 65 As a result, a capacity corresponding to 42% of theoretical capacity of NP is achieved in two different electrolytes (0.4 M Mg(TFSI)₂ and 0.4 M MgCl₂ in TEGDME/DOL = 1:1 (v/v%) and in TEGDME alone) (Fig. 6a). In addition to NP, porous polymer networks (PPNs) are also attractive electrode materials for RMBs, because they offer a large surface area and

open structures that enable pseudocapacitive energy storage. DeBlase et al.66 investigated a 2D PPN-functionalized thin film electrode, naphthalenediimide diamine and triformylphloroglucinol polycondensation (NDI-TFP) polymer. The polymer possesses distinct and counter cation-dependent electrochemical behavior, which is quite different from monomer NDI.⁶⁷ The reduction potentials of polymer films were shifted to more positive values due to the strong interaction between NDI

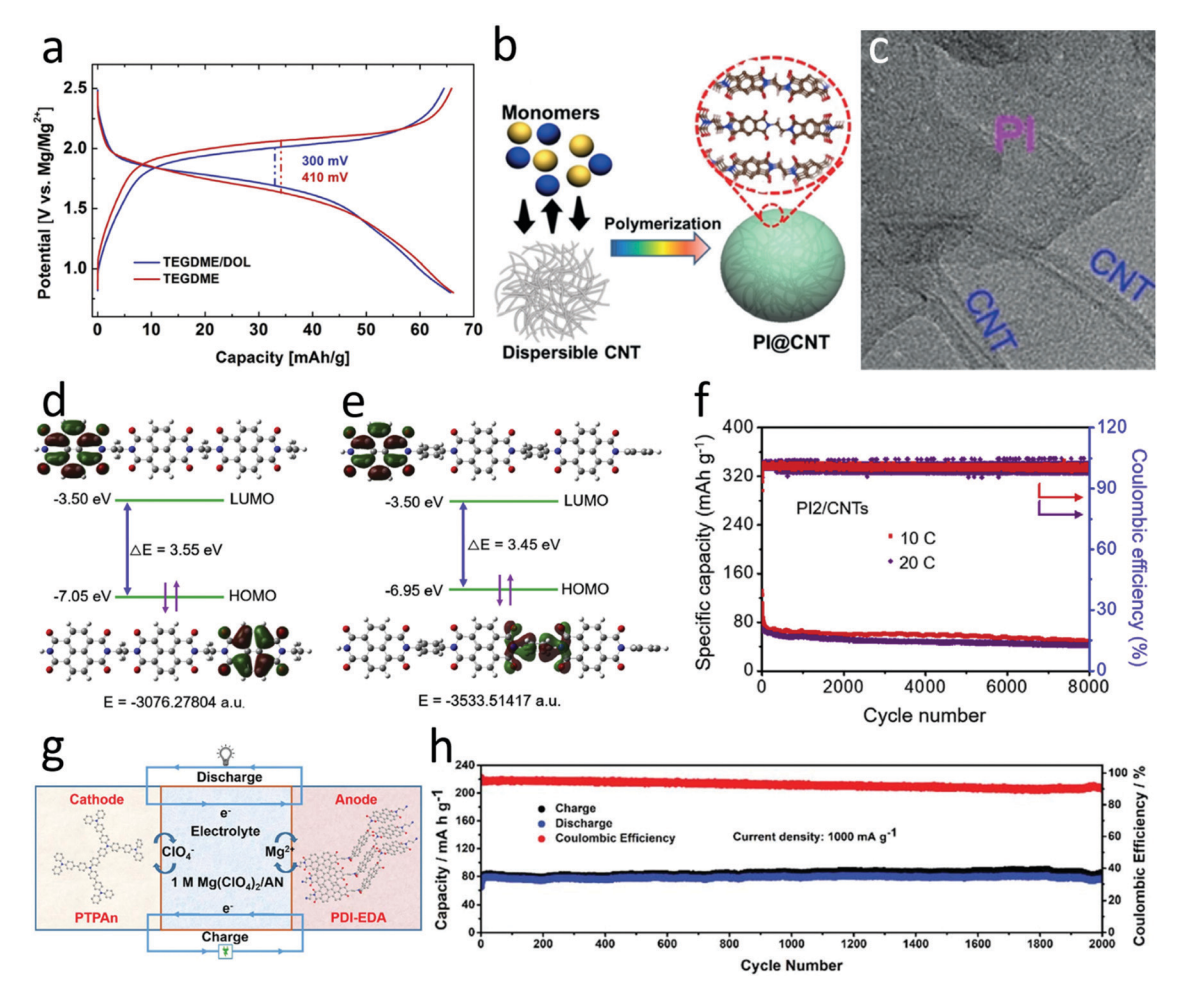


Fig. 6 (a) Comparison of voltage hysteresis of NP in both TEGDME/DOL and TEGDME electrolytes in the 10th cycle. Reproduced with permission.⁶⁴ Copyright 2018 Elsevier B.V. (b) Illustration of PI@CNT synthesis. (c) HRTEM image of the PI@CNT composite. Reproduced with permission.⁶⁹ Copyright 2018 Wiley-VCH Verlag GmbH & Co. KGaA. DFT calculated HOMO and LUMO energy levels of (d) PI1 and (e) PI2 with the polymerization degree n=3, respectively. (f) Long-term cycling tests of PI2/CNTs cathodes at 10C and 20C, respectively. Reproduced with permission. 71 Copyright 2019 Elsevier B.V. (g) The schematic illustration of the, which consists of PDI-EDA anode $|Mg(CIO_4)_2|$ AN electrolyte PTPAn cathode. (h) The cycling performances of the MIOB at a current density of 1000 mA q⁻¹. Reproduced with permission.⁷² Copyright 2018 The Royal Society of Chemistry.

dianions and small cations, such as Li⁺, K⁺ and Mg²⁺. The NDI-TFP polymer-based RMBs delivers a capacity of 100 mA h g⁻¹ at a current of 70 µA and negligible capacity decay was observed after 10 cycles.

Although great progress has been achieved for organic RMBs, they still suffer from low round-trip efficiency and low power density compared with LIBs due to the low intrinsic ion diffusion rate of multivalent ions and large potential hysteresis during charge and discharge.⁶⁸ To circumvent these challenges, Fan et al. 69 prepared a polyimides@carbon nanotubes (PI@CNTs) cathode for RMBs with extremely high cycling stability and rate capability (Fig. 6b). The dispersible CNTs contact with each other to form a 3D electron conductive matrix, and the in situ formed PI is filled into the spaces between CNTs, ensuring an excellent electronic conductivity and ultra-short ion transport pathway (Fig. 6c).⁷⁰ Consequently, the Mg|PhMgCl/AlCl₃/THF|PI@CNTs cell delivers a high reversible capacity of 130 mA h g⁻¹ at 1C $(1C = 150 \text{ mA g}^{-1})$ and excellent rate capability of 55% capacity retention when increasing the current density from 0.5C to 20C.

The exceptional electrochemical performance is mainly attributed to the surface reaction-dominated pseudocapacitance behavior and viable ion-coordination charge storage mechanism. More interestingly, the PI@CNTs composite can even deliver a reversible capacity of 65 mA h g^{-1} at -40 °C, confirming the fast reaction kinetics. Additionally, the π -conjugated molecular units in PIs provide abundant redox-active sites for Mg2+ storage, making PIs ideal cathode materials for RMBs with high output voltage and high specific capacity. Wang et al.71 synthesized two different kinds of aromatic dianhydride-derived PIs, naphthalene-1,4,5,8tetracarboxylic acid dianhydride-ethylene diamine copolymer (PI1) and naphthalene-1,4,5,8-tetracarboxylic acid dianhydride-pphenylenediamine copolymer (PI2), and blended them with CNTs for RMB cathodes. The smaller highest occupied molecular orbital-lowest unoccupied molecular orbital (HOMO-LUMO) gap of PI2 (3.45 eV) than PI1 (3.55 eV) indicates the better electronic conductivity of PI2. The high conductivity is beneficial for Mg-ion storage and the electrochemical performance of PI2. Consequently, the relatively narrow HOMO-LUMO energy gap,

compact π - π stacking structure, and the 3D-crosslinked CNTs networks dramatically enhance the Mg²⁺ storage performance of PI2 (Fig. 6d and e). The PI2/CNTs cathodes exhibit ultralong cycle life of 8000 cycles in non-nucleophilic Mg(HMDS)₂-4MgCl₂/ 2THFPP₁₄TFSI electrolyte due to the capacitive-controlled reaction mechanism (Fig. 6f).

In addition to the organic cathodes, there are several kinds of OEMs can be used as the anode materials for RMBs. Lu et al. 72 used perylene diimide-ethylene diamine (PDI-EDA) as an anode for RMBs. After coupling with a p-type conductive polymer, polytriphenylamine (PTPAn), as the cathode and anhydrous acetonitrile solution of magnesium perchlorate (Mg(ClO₄)₂/AN) as the electrolyte, an all-organic dual-ion battery was demonstrated, in which Mg²⁺ and ClO₄⁻ are reversibly inserted into and extracted from the anode and cathode, respectively (Fig. 6g). This dual-ion battery delivers a high capacity of 90 mA h g⁻¹ at a current density of 50 mA g⁻¹ and retains 88% of its initial capacity at 1000 mA g⁻¹ for 2000 cycles (Fig. 6h). The design of the all-organic dual-ion battery opens up a door for the development of low cost and high stability lithium-free and transition metal-free energy storage devices.

2.1.6. Nitroxide free-radical polymers. Nitroxide freeradical polymers represent a kind of aliphatic or nonconjugated polymers with free radicals as the redox-active centers in RMBs. As shown in Table 2, the nitroxide free radicals undergo an anion-insertion reaction mechanism with high reaction potentials. Chen et al. 73 reported a composite of poly(2,2,6,6tetramethyl-piperidinyl-1-oxy-4-yl methacrylate) (PTMA) nanoparticles and graphene as a cathode material for RMBs. The Mg|0.25 M Mg(AlCl₂EtBu)₂/THF|PTMA/graphene cell delivers an initial discharge capacity of 81.2 mA h g⁻¹ at a current density of 22.8 mA g⁻¹. However, the PTMA-based cathode suffers from rapid capacity decline, large polarization and low voltage window of 0.3-1.8 V due to the high solubility of PTMA in the electrolyte and poor stability of the electrolyte at high reaction potentials. To overcome these challenges, Ha et al.74 proposed a new class of electrolyte containing 0.3 M Mg(TFSI)₂ in glyme/diglyme (Fig. 7a), which shows excellent anodic stability exceeding 4.0 V with Al current collector (Fig. 7b). The PTMA-based RMBs using this novel electrolyte show two discharge plateaus at 2.6 V and 1.8 V (Fig. 7c). However, obvious capacity fading is still observed in the second cycles due to the high solubility of PTMA in the electrolyte. More work is required to reduce the solubility of the nitroxide free radical polymer and enhance the cyclic stability upon long-term cycling. A possibility is to chemically attach the polymer to insoluble substrates such as carbon nanotubes and porous carbon, which not only stabilize the polymer but also increase the conductivity of the organic electrode.⁷⁵

2.1.7. Imine polymers. Though great advances have been achieved, organic RMBs are still not comparable with the commercial LIBs, in terms of energy density and cycle life. It is critical to exploit new materials, new structures, and new chemistries for high-performance RMBs.⁷⁶ To date, porous polymers and covalent organic frameworks (COFs) are widely used in the fields of gas adsorption/storage, separation, catalysis, environmental remediation, energy, optoelectronics, and health. With rational structure design, these emerging polymers can also be applied in RMBs. Mao et al. 77 polymerized hexaazatrinaphthalene (HATN) to generate poly-hexaazatrinaphthalene (PHATN) and studied its electrochemical performance as a cathode in rechargeable Na, Mg, and Al batteries. PHATN particles possess an amorphous structure and abundant C=N bonds. Benefitting from the stable and reversible multi-electron-deficient pyrazine sites in redox-active centers, Mg-PHATN battery renders a high initial capacity of 146 mA h g^{-1} , high cycling stability of 200 cycles, and fast reaction kinetics up to 1C (Fig. 7d-f). This work paves the way for the applications of pyrazine-based polymer cathodes in non-aqueous MRBs.

COFs as another type of porous polymer materials can also be used as promising cathodes in RMBs due to their insolubility in organic electrolyte, highly ordered porous structure, and large surface area, which enhance Mg-ion diffusion and accommodate the volume change during the electrochemical process.⁷⁸ Sun et al.⁷⁹ synthesized a triazine-based porous COF material from rational polymerization of 1,4-dicyanobenzene. The resulting COF material exhibits a porous structure with an average pore size of 1.35 nm, which provides a large surface area and more active sites to enhance the Mg²⁺ diffusion and facilitate the reaction kinetics (Fig. 7g). Consequently, this COFbased RMB delivers a high reversible capacity (107 mA h g⁻¹ at 22.8 mA g⁻¹), excellent cycling stability (30 mA h g⁻¹ after 3000 cycles at 570 mA g⁻¹), and high rate capability (53 mA h g^{-1} at 1140 mA g^{-1}) in a chloride-free ether-based electrolyte (0.5 M Mg(TFSI)₂/DME) (Fig. 7h and i). The exceptional electrochemical performance is mainly attributed to the pseudocapacitive behavior. Moreover, as the redox-active sites in the porous COF material, the triazine rings enable each repeating unit to reversibly react with nine Mg ions during the charge/discharge process, providing a high theoretical capacity (561.4 mA h g^{-1}) in RMBs (Fig. 7j). However, the reversible capacity of the COF is much lower than its theoretical capacity. There is a great potential to further improve the performance of COF-based OEMs. Therefore, more efforts are demanded to design and synthesize high porosity and large surface area COFs with multiple electroactive functional groups (C=O, C=N, N≡N, C≡N, and free radicals) for high-performance RMBs.

2.2. OEMs in non-aqueous RABs

Aluminum, one of the most abundant metallic elements in the earth's crust, possesses a high gravimetric capacity of 2980 mA h g^{-1} , a high volumetric capacity of 8046 mA h mL⁻¹, a low reaction potential of -1.66 V versus standard hydrogen electrode (SHE), and high safety in the air. Hence, Al metal is a promising anode for the next generation high-safety and lowcost rechargeable batteries. 81–83 However, the poor electrochemical performance of inorganic electrode materials hampers the development of non-aqueous RABs. As universal electrode materials, the low cost and abundant OEMs offer opportunities. 84 In this section, the reaction mechanisms and electrochemical behaviors of various types of OEMs in

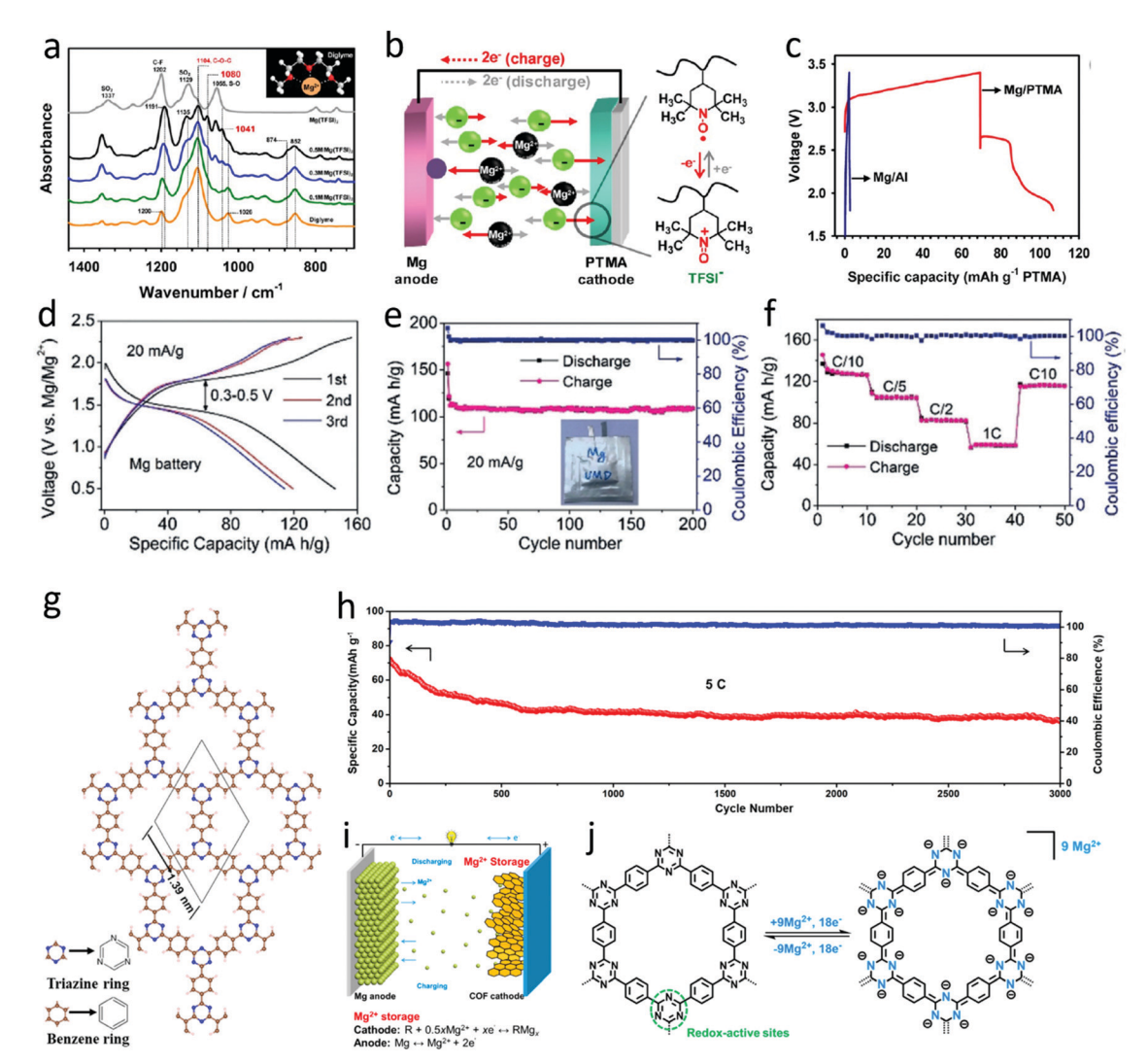


Fig. 7 (a) FT-IR spectra of diglyme solvent, 0.1, 0.3, and 0.5 M Mg(TFSI)₂ dissolved in diglyme, and Mg(TFSI)₂ salt. The inset shows a schematic drawing of the ion-dipole interaction between Mg²⁺ ions and diglyme solvent. (b) Schematic of electrochemical oxidation and reduction of the PTMA cathode in an Mg/PTMA cell. (c) First charge (Mg plating on a Mg anode) and discharge (Mg stripping from a Mg anode) curves of Mg/PTMA and Mg/aluminum cells. Reproduced with permission.⁷⁴ Copyright 2014 American Chemical Society. (d) The discharge-charge curves of PHATN cathode for the first three cycles in RMB at 20 mA g^{-1} . (e) Cycling performance and CE of the first 200 cycles at 20 mA g^{-1} in RMBs. (f) Rate capabilities of PHATN in RMBs at various current rates from C/10 to 1C. Reproduced with permission.⁷⁷ Copyright 2019 Wiley-VCH Verlag GmbH & Co. KGaA. (g) Schematic illustration of the COF. (h) Long-term cycling performance of the COF at 5C. (i) Schematic illustrations of the reaction mechanism and equations of COF cathodes in chloride-free electrolytes. (i) Chemical structure and possible electrochemical redox mechanism of the COF. Reproduced with permission.⁷⁹ Copyright 2020 American Chemical Society

non-aqueous RABs are summarized in Fig. 8, and Tables 4 and 5. We also discuss the development and application of state-ofthe-art OEMs in non-aqueous RABs in detail.

2.2.1. Conducting polymers. Conducting polymers are promising cathode materials for RABs due to their high stability and highly reversible redox properties in chloroaluminate ionic liquid electrolyte. In 1984, Osteryoung et al.27 prepared PPY films using an oxidative electrochemical polymerization approach in the 1:1 mol ratio of AlCl₃: N-1-butylpyridinium chloride (BuPyCl) molten salt, which is a pure BuPyAlCl₄ ionic liquid at temperatures above 27 °C. A Lewis basic environment can be generated after adding the extra BuPyCl to the 1:1 molten salt. The electrochemical performance of the prepared

PPY was tested in 0.8:1 mol ratio of AlCl₃: BuPyCl basic melt at 40 °C with a three-electrode system using Al wire as the reference electrode and Pt foil as the working electrode. This work demonstrates the feasibility of organic materials in electrodes for RABs in a liquid electrolyte at ambient temperature (Fig. 9a). In the ensuing year, the same group demonstrated the electrochemical activity of PPY in AlCl₃ and 1-ethyl-3methylimidazolium chloride (AlCl₃:EMIC) molten salts, which exhibits higher conductivity and can be used at lower temperatures than the AlCl₃:BuPyCl melt.⁸⁵ Furthermore, the porous PPY shows better electrochemical performance and a much faster redox reaction rate in this electrolyte than that in acetonitrile (CH₃CN), indicating that the AlCl₃:EMIC melt is

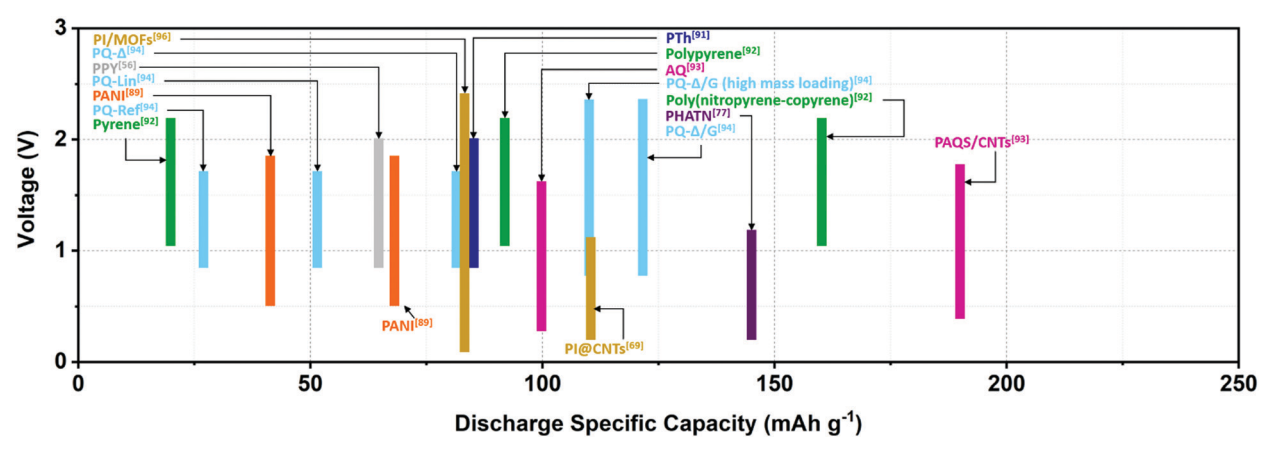


Fig. 8 Capacity versus voltage for the reported OEMs for non-aqueous RABs.

Table 4 Reaction mechanisms and electrochemical behaviors of the OEMs in non-aqueous RABs

Types		General redox mechanism	Classification	Average discharge voltage	Discharge capacity	Cycle life
Carbonyl monomer	Quinone monomer	R' +A ²⁺ , 2e R' R'' A ²⁺ : AlCl ₂ + R'' A ²⁺ , 2e R'' A ²⁺ : AlCl ₂ + R'' A ⁴ , e R'' A ⁴ : AlCl ₂ + R'' R''	n-Type	Medium	Low	High
Carbonyl	Quinone polymer	R" +A ²⁺ , 2e R"	_		1	
polymer	Polyimide	R O N O Ar Ar -2A ⁺ , 2e ⁻ O A ⁺ : AlCl ₂ ⁺ O A	n-Type	Medium	High	Medium
Imine polym	er	R' -A', e - R' -A', e - R'	n-Type	Low	High	Low
Amine polym	er	R' +B', +e' R' B' R'' B': AICI4'	p-Type	Medium	Low	Low
Pyrene polym	ner	+B', -e' -B', +e' B': AlCl ₄ '	р-Туре	High	High	Medium

suitable as an electrolyte for conducting polymer-based RABs. Afterward, they successively prepared a variety of conducting polymers, such as polythiophene (PTh), polybithiophene (PBTh), PANI, and poly (p-phenylene) (PPP) films^{86–88} by anodic

oxidation approach in AlCl₃:EMIC melt, and demonstrated their electrochemical properties in the same solution. The results indicate that the polymers are conductive in their oxidation state and become nonconductive after reduction.

 Table 5
 Summary of OEMs as cathodes for non-aqueous RABs

Compound	Structure	Electrolyte	Average discharge voltage	Initial reversible capacity at current density	Cycle life (n)	Rate capability
1		AlCl ₃ : EMIC	~1 V	42 mA h g ⁻¹ at 0.4 mA cm ⁻²	N/A	N/A
PANI ⁸⁹	- ((2:1 molar ratio) AlCl ₃ :BPC (2:1 molar ratio)	~1 V ~1 V	0.4 mA cm^{-2} $68 \text{ mA h g}^{-1} \text{ at}$ 0.4 mA cm^{-2}	N/A	N/A
PPP ⁹⁰	$+$ $\longrightarrow_{\mathbf{n}}$	AlCl ₃ : BPC (2:1 molar ratio)	0.8 V	\sim 53 mA h g ⁻¹ at 1 mA cm ⁻²	N/A	N/A
PPY ⁹¹	√N H N N N N N N N N N N N N N N N N N N	AlCl $_3$: EMIC (1.5:1 molar ratio)	1.2 V	65 mA h g^{-1} at 20 mA g^{-1}	100	N/A
PTh ⁹¹	(s)n	AlCl $_3$: EMIC (1.5:1 molar ratio)	1.4 V	85 mA h g^{-1} at 16 mA g^{-1}	100	N/A
Pyrene ⁹²		AlCl ₃ : EMIC (1.3:1 molar ratio)	1.7 V	$20 \text{ mA h g}^{-1} \text{ at}$ 200 mA g^{-1}	300	N/A
Polypyrene ⁹²	in the second se	AlCl ₃ : EMIC (1.3:1 molar ratio)	1.7 V	92 mA h g^{-1} at 200 mA g^{-1}	300	N/A
Poly(nitropyrene- copyrene) ⁹²	NO ₂	AlCl ₃ : EMIC (1.3:1 molar ratio)	1.7 V	160 mA h g^{-1} at 200 mA g^{-1}	1000	48 mA h g ⁻¹ at 2000 mA g ⁻¹
AQ^{93}		AlCl ₃ : EMIC (1.5:1 molar ratio)	1.1 V	100 mA h g $^{-1}$ at 0.2C	50	N/A
BQ^{93}	MeO O OMe	AlCl ₃ : EMIC (1.5:1 molar ratio)	1.5 V	210 mA h g $^{-1}$ at 0.15C	3	N/A
PAQS/CNTs ⁹³		AlCl ₃ : EMIC (1.5:1 molar ratio)	1.1 V	190 mA h $\rm g^{-1}$ at 0.5C	500	$>$ 120 mA h g $^{-1}$ at 10C
PQ-Ref ⁹⁴		AlCl ₃ : EMIC (1.3:1 molar ratio)	1.3 V	\sim 27 mA h g ⁻¹ at 200 mA g ⁻¹	200	N/A
PQ-Lin ⁹⁴		AlCl ₃ : EMIC (1.3:1 molar ratio)	1.3 V	\sim 51 mA h g ⁻¹ at 200 mA g ⁻¹	200	N/A
PQ-Δ ⁹⁴ PQ-Δ/graphite ⁹⁴		AlCl ₃ : EMIC (1.3:1 molar ratio) AlCl ₃ : EMIC (1.3:1 molar ratio)	1.4 V 1.4 V and 1.8 V	81.5 mA h g^{-1} at 200 mA g^{-1} 121.3 mA h g^{-1} at 200 mA g^{-1}	5000 500	70 mA h g ⁻¹ at 10 000 mA g ⁻¹ 98.2 mA h g ⁻¹ at 1000 mA g ⁻¹
PI@CNT ⁶⁹	+N-\\N-\\\-\-\\\	AlCl $_3$: EMIC (1.5:1 molar ratio)	~0.65 V	110 mA h g ⁻¹ at 1C	100	\sim 55 mA h g ⁻¹ at 10C
PI/MOFs ⁹⁶		AlCl ₃ : EMIC (1.3:1 molar ratio)	~1 V	83 mA h g^{-1} at 1000 mA g^{-1}	1800	40 mA h g^{-1} at 10 A g^{-1}
PHATN ⁷⁷		AlCl ₃ -[BMIm]Cl ionic liquid electrolyte	0.7 V	145 mA h g^{-1} at 50 mA g^{-1}	100	N/A

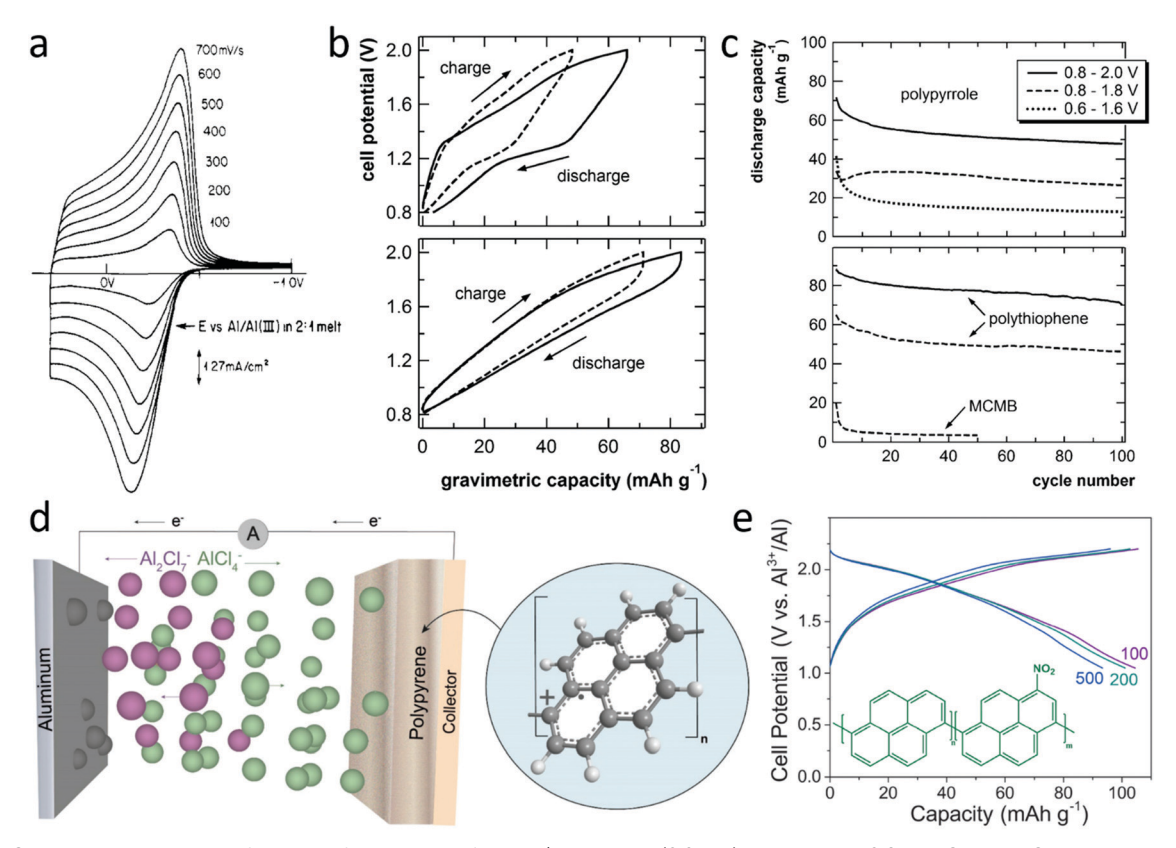


Fig. 9 (a) Cyclic voltammetry as a function of scan speed for a Pt/polypyrrole (0.2 μm) electrode in 0.8:1 AlCl₃: BuPyCl melt. Reproduced with permission.²⁷ Copyright 1984 American Chemical Society. (b) Charge and discharge profiles of PPy (top) and PTh (bottom). The 5th (solid line) and 100th (dashed line) cycles are presented. (c) Cycling performance of PPy (top) and PTh (bottom). Reproduced with permission.91 Copyright 2014, American Chemical Society. (d) Schematic of the working principle of a rechargeable aluminum battery during charge with a polypyrene cathode and chloroaluminate ionic liquid. (e) Charge-discharge voltage curves of poly(nitropyrene-co-pyrene) based Al ion battery for the 100th, 200th, and 500th cycles. Reproduced with permission.⁹² Copyright 2018, Wiley-VCH Verlag GmbH & Co. KGaA.

The high conductivity and low melting point of AlCl₃:EMIC melt make it a promising electrolyte for non-aqueous RABs. Subsequently, Koura et al. 89 also investigated the electrochemical performance of PANI as a cathode material in RABs with AlCl₃: EMIC electrolyte. The PANI-based RAB delivers a discharge capacity of 42 A h kg⁻¹ with a CE of 90%. To further improve the electrochemical performance, an Al₂Cl₇⁻ doped PANI was prepared and tested in AlCl₃-1-butylpyridiniumchloride (BPC) electrolyte, exhibiting an excellent discharge capacity of 68 A h kg⁻¹ and an excellent CE of 99%. In addition to the PANI-based cathode, the AlCl₃-BPC electrolyte also improves the electrochemical performance of PPP-based RABs.90

Although previous demonstrations indicated that the conducting polymers can be used as cathodes in non-aqueous RABs, the fundamental reaction mechanism and quantitative performance in a two-electrode battery system are still poorly understood. Hence, Hudak et al. 91 synthesized anionic (AlCl₄and Al₂Cl₇⁻) doped PPY and PTh using an electrochemical polymerization process in chloroaluminate ionic liquid (CIL) AlCl₃:EMIC solution and tested them as cathodes in RABs. The PPY-based Al cell shows a specific capacity of ~ 65 mA h g⁻¹ at 20 mA g⁻¹ in the cutoff window of 0.8-2.0 V, and capacity retention of \sim 48 mA h g⁻¹ after 100 cycles. However, the broad

potential range of the PPY-based Al cell, especially at lower voltages, is less useful for practical application. In contrast, PTh-based RABs deliver a much higher capacity of ~ 85 mA h g⁻¹ at 16 mA g⁻¹ in the cutoff window of 0.8-2.0 V and higher capacity retention of \sim 70 mA h g⁻¹ after 100 cycles (Fig. 9b and c). Though using the same cutoff window, the redox potential of PTh was about 1 V higher than PPY, demonstrating a much higher energy density of PTh than PPY. To further improve the electrochemical performance, optimization of the CIL electrolyte to enhance the ionic conductivity and enlarge the stability window offers opportunities.

To date, AlCl₃:EMIC is still considered to be the best electrolyte for conducting polymer-based RABs. Walter et al. 92 investigated the amorphous polypyrene and poly(nitropyreneco-pyrene) as cathodes for RABs in AlCl₃:EMIC ionic liquid electrolyte using tungsten as the current collector (Fig. 9d). In comparison to pyrene, the amorphous polypyrene not only shows suppressed solubility in the chloroaluminate ionic liquid but also shows higher electronic conductivity due to the extended π -conjugation system. Furthermore, the amorphous and flexible nature of polypyrene chains is favorable for the diffusion of AlCl₄ ions. Consequently, polypyrene-based RABs deliver an initial capacity of \sim 92 mA h g⁻¹ at a high current density of 200 mA g⁻¹ with an average discharge voltage of 1.7 V. The

excellent performance is retained for 300 cycles at 70 mA h g⁻¹, which is much better than that of pyrene (initial capacity of \sim 20 mA h g⁻¹ at a high current density of 200 mA g⁻¹, and then remains stable for 300 cycles at 10 mA h g⁻¹). To further improve the electrochemical performance of polypyrene, an amorphous copolymer of 1-nitropyrene and pyrene (poly(nitropyrene-copyrene)) was synthesized. Compared with homopolymer, poly-(nitropyrene-co-pyrene) shows better dispersibility in N-methyl-2-pyrrolidone (NMP) to enable better contact with the conductive carbon additive when preparing the organic electrodes. Moreover, the unique structure of the copolymer can effectively enhance the utilization of active materials. As a result, poly(nitropyrene-copyrene)-based RABs deliver an excellent cycling performance with a reversible capacity of 100 mA h g⁻¹ for 1000 cycles at a current density of 200 mA g⁻¹, an average discharge voltage of 1.7 V, and a high rate capability of 48 mA h g^{-1} after 500 cycles at 2000 mA g^{-1} (Fig. 9e). The superb battery performance of this copolymer stimulates the development of low-cost and high-flexibility polycyclic aromatic polymer-based RABs.

2.2.2. Quinone monomers and polymers. Although conducting polymers represent huge potentials as cathode materials

for RABs and show enhanced electrochemical performance in AlCl₃:EMIC ionic liquid electrolyte, the battery energy density is still limited by the quantity of AlCl₃-based electrolyte, as it relies on AlCl₄ anion intercalation. Hence, it is vital to search for highenergy-density cathode materials for non-aqueous RABs. Among the cathode materials, quinone-based OEMs are promising for the high-performance RABs due to the highly reversible reaction between carbonyl groups and AlCl₂⁺ species during the discharge/ charge process (Fig. 10a). Bitenc et al. 93 investigated AQ as a cathode for RABs in AlCl₃: EMIC (1.5:1 molar ratio) electrolyte. The AQ-based RABs provide a specific capacity of 183 mA h g^{-1} at 0.2C with a discharge voltage of 1.1 V (Fig. 10b). To suppress the dissolution of AO into the electrolyte and improve the capacity retention, PAQS/CNTs composite was prepared by an in situ polymerization approach. As expected, the cell with PAQS/CNTs composite exhibits a high initial capacity (190 mA h g⁻¹ at 0.5C with a discharge voltage of 1.0 V), excellent cycling stability (114 mA h g^{-1} after 500 cycles) (Fig. 10c). In addition to AQ and PAQS, a phenanthrenequinone (PQ)-based cathode material was also introduced as a cathode for RABs, which has better cycle life and a 0.2 V higher redox potential than AQ. As redox-active OEMs,

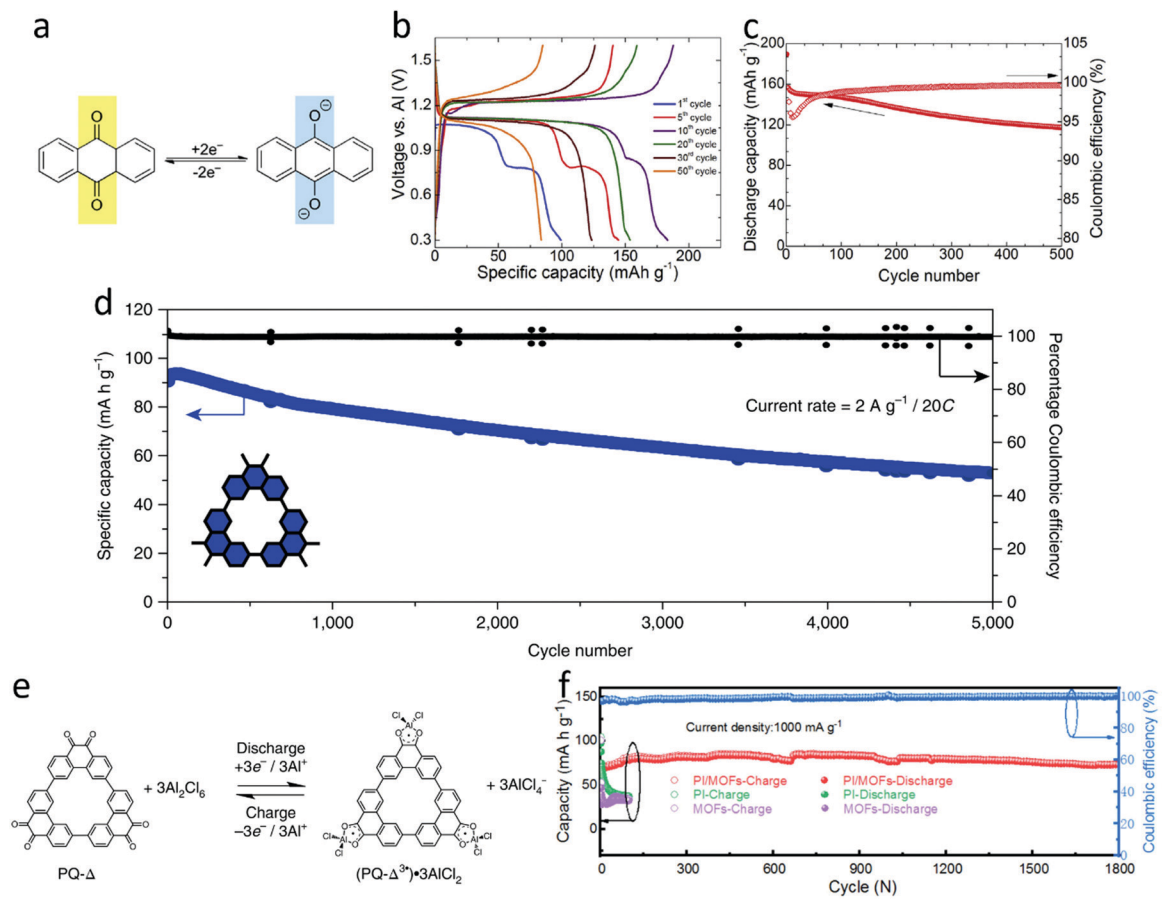


Fig. 10 (a) The electrochemical mechanism of AQ. (b) Galvanostatic charge/discharge curves of an Al-AQ battery cell cycled at C/5 rate from 0.3 to 1.6 V. (c) Discharge capacity and Coulombic efficiency of PAQS/MWCNT cell at 0.5C and 0.4–1.8 V. Reproduced with permission.⁹³ Copyright 2019 Elsevier B.V. (d) Extended cycling test of PQ- Δ at a current rate of 2 A g⁻¹ (20C). (e) Structure and redox mechanism of PQ- Δ upon discharge and charge. The Coulombic efficiency is defined on the right-hand axis.⁹⁴ Copyright 2018, Springer Nature. (f) Cycling stability of pure PI, pure MOFs, and PI/MOFs hybrid. Reproduced with permission. 96 Copyright 2020 Published by Elsevier B.V.

PQ-based monomers and polymers are promising cathode materials for RABs because of their reversible redox nature and high structural tunability. Kim et al.94 demonstrated an amorphous redox-active triangular PQ-based macrocycles (PQ-Δ) for RABs with AlCl₃: EMIC (1.3:1 molar ratio) ionic liquid electrolyte. The organic RABs preserve a reversible capacity of 53 mA h g^{-1} at a high current density of 2 A g⁻¹ (20C) after 5000 cycles, representing the best cycle life in organic RABs (Fig. 10d). The exceptional cycling stability is ascribed to the flexibility of the triangularly shaped molecule and its π - π stacked superstructure, allowing for the accommodation of AlCl₂⁺ ion (Fig. 10e). To further improve the capacity and conductivity of the organic RABs, a graphite-flake-blended PO triangle hybrid (PO-Δ-HY) electrode was prepared by sonicating an equal molar weight of PO- Δ and graphite flakes in NMP. The cell-based on PO- Δ -HY delivers an enhanced initial capacity (121.3 mA h g⁻¹ at 200 mA g^{-1}), high cycling stability (114 mA h g^{-1} after 500 cycles) and rate capability (98.2 mA h g⁻¹ at 1000 mA g⁻¹). More importantly, even at a high areal loading of 9 mg cm⁻², the PQ-Δ-HY electrode can still achieve a high capacity (110 mA h g⁻¹ at 100 mA g⁻¹), high cyclability (108 mA h g⁻¹ after 100 cycles) and excellent rate capability (51 mA h g⁻¹ at 1000 mA g⁻¹) due to the efficient electron transport contributed by the high conductivity of graphite and π - π interactions between PQ- Δ and graphite. This work sheds lights on the development of redox-active organic molecules with well-defined geometries for RABs. 95

2.2.3. PIs and imine polymers. Due to the universal nature of OEMs in metal-ion batteries, PIs and imine-based polymers, which were applied as cathode materials in non-aqueous RMBs, are also promising cathode materials in non-aqueous RABs. The surface reaction-dominated pseudocapacitance behavior and viable ion-coordination charge storage mechanisms enable the fast reaction kinetics of PIs. Similar to that in RMBs, CNTs are also used to enhance the electronic conductivity of the PI-based cathode in RABs. The Al|AlCl₃:EMIC|PI@CNTs cell delivers a high reversible capacity (110 mA h g^{-1} at 1C (1C = 150 mA g^{-1})), excellent cycling stability (100 mA h g⁻¹ after 100 cycles), and high rate capability (55% of capacity retention at 20C compared to that

at 0.5C). 69 The excellent performance of PI@CNTs attracts more research interests in developing PI-based cathodes for RABs. Recently, Zhou et al.96 developed a PI/metal-organic frameworks (MOFs) hybrid material as a cathode for non-aqueous RABs by a one-pot solvothermal method. The -C=O groups in PI possess high reactivity with AlCl₂⁺ ions (Table 4), and the MOFs effectively prevent the aggregation of PI and provide a favorable ion transport pathway due to the ordered porous structure. The resulting PI/MOFs cathode delivers a capacity of 83 mA h g⁻¹ at 1000 mA g⁻¹, as well as superior cycling stability of 1800 cycles (Fig. 10f). In addition to PIs, the imine polymers based on the π -conjugated aromatic structure and abundant redox-active C=N groups also exhibited excellent performance in non-aqueous RABs. Mao et al. 77 reported PHATN, which is active in RMBs, also possesses reversible AlCl₂⁺ insertion/de-insertion capability in RABs. The PHATN/Al pouch cell shows an initial discharge capacity of 145 mA h g⁻¹ with a plateau at 0.7 V and a capacity of 92 mA h g^{-1} after 100 cycles, demonstrating that the pyrazine sites are the universal redox-active centers for non-aqueous MRBs. The success of OEMs in non-aqueous RABs offers opportunities for the development of affordable and sustainable energy storage devices.

2.3. OEMs in non-aqueous RZBs

Similar to RMBs and RABs, the low cost and high volumetric capacity of Zn resources attract research interests toward RZBs. However, due to the high reaction potential of Zn/Zn^{2+} (-0.76 V) versus SHE, the potential of non-aqueous RZBs is low, compared to non-aqueous rechargeable Li/Mg/Al batteries.⁹⁷ There are only a few reports about the applications of OEMs in non-aqueous RZBs because of the low energy density. The electrochemical behaviors of various types of OEMs in non-aqueous RZBs are summarized in Table 6. Herein, we provide a brief discussion in this section.

2.3.1. Conducting polymer. As universal cathode materials, conducting polymers are also applied in non-aqueous RZBs. Guerfi et al.98 investigated a PANI/CNTs cathode for RZBs in the organic electrolyte (0.3 M Zn(TFSI)₂/PC). The PANI-based cathode delivers a high capacity of 148 mA h g⁻¹ at 1C together with excellent cycling stability of 85% capacity retention after

Table 6 Summary of OEMs as cathodes for non-agueous RZBs

Compound	Structure	Electrolyte	Average discharge voltage	Initial reversible capacity at current density	Cycle life (n)	Rate capability
PANI ⁹⁸		0.3 M Zn(TFSI) ₂ /PC	~0.9 V	148 mA h g ⁻¹ at 0.5C	2000	70 mA h g ⁻¹ at 12C
PEDOT ⁹⁹	s s n	[C ₂ mim][dca] + 3 wt% H ₂ O+10 mol% Zn(dca) ₂	1.2 V	42 mA h g^{-1} at 0.17 A g^{-1}	100	$\sim 25 \text{ mA h g}^{-1}$ at 8 A g ⁻¹
PQ-Δ ¹⁰⁰		0.5 M Zn(CF ₃ SO ₃) ₂ /DMF	0.66 V	145 mA h g^{-1} at 50 mA g^{-1}	20 000	60 mA h g^{-1} at 50 A g^{-1}

2000 cycles at 1C. However, the battery still suffers from a severe self-discharge of 48% due to the dissolution of the Zn anode. To suppress the dissolution and achieve efficient deposition of the Zn anode in an organic electrolyte, Simons $et\ al.^{99}$ invented a novel imidazolium-based ionic liquid electrolyte (1-ethyl-3-methylimidazolium dicyanamide [C₂mim][dca] + 3 wt% H₂O +

self-discharge of 48% due to the dissolution of the Zn anode. To suppress the dissolution and achieve efficient deposition of the Zn anode in an organic electrolyte, Simons et al. 99 invented a novel imidazolium-based ionic liquid electrolyte (1-ethyl-3methylimidazolium dicyanamide [C₂mim][dca] + 3 wt% H₂O + 10 mol% Zn(dca)2), in which Zn shows high cyclability, smooth morphology and insolubility. They also synthesized ploy(3,4ethylenedioxythiophene)/poly(diallyl dimethyl ammonium) (PEDOT/ PDDA) as cathode materials in RZBs with this electrolyte. However, the PEDOT/PDDA-based RZBs show a low capacity of 9 mA h g⁻¹ at 25 mA g⁻¹ due to its poor adhesion and poor conductive property. After blending with carbon black, the composite cathode displays a higher capacity of 42 mA h g⁻¹ at 170 mA g⁻¹ and maintains a capacity of 36 mA h g⁻¹ after 100 cycles due to the increased conductivity. Hence, it is necessary to optimize the morphology and conductivity of PEDOT-based materials to further enhance the electrochemical performance of organic non-aqueous RZBs.

2.3.2. Quinone monomers. In addition to the conducting polymer, quinone monomers are also applicable in non-aqueous RZBs. PQ- Δ , which has been reported as a high-performance cathode material for non-aqueous RABs, also shows high potential as the cathode material for non-aqueous RZBs. ¹⁰⁰ Moreover, a new ZnTFMS/DMF electrolyte with high Zn plating/ stripping efficiency was employed in the organic RZBs. The abundant C=O groups endow the PQ- Δ |ZnTFMS/DMF|Zn battery a high discharge capacity of 145 mA h g⁻¹ at 50 mA g⁻¹, together with an ultra-long cycle life of 20 000 cycles and negligible capacity fading. More importantly, this full cell can be operated in a wide temperature range from -70 to 150 °C due to the low freezing point, high boiling point, and superior stability of the ZnTFMS/DMF electrolyte. This work opens up a door for the development of ultralow-temperature and ultrahigh-temperature batteries for

3. OEMs in aqueous MRBs

Aqueous batteries are promising for developing affordable, sustainable and environmentally benign energy storage devices because of low cost, nonflammability, and high safety of the aqueous electrolyte. However, the electrochemical stability window of the aqueous electrolyte is narrow due to the electrochemical water splitting at high and low potentials. Numerous high-capacity electrode materials such as lithium metal, silicon, magnesium metal, aluminum metal, carbon, and high-potential transition metal oxides cannot be used in aqueous batteries. Herefore, extensive work has been done to search for high-performance electrode materials for aqueous batteries.

3.1. OEMs in aqueous RMBs

Aqueous RMBs represent a promising type of energy storage devices because of the low cost, abundance, high sustainability, and environmental benignity of magnesium resources, as well as the aqueous electrolyte. Additionally, the aqueous electrolyte in RMBs can effectively avoid the drawbacks shown in a non-aqueous electrolyte such as limited power density and sluggish Mg-ion diffusivity.¹¹¹ In this section, we discuss the recent advances of OEMs in aqueous RMBs. The electrochemical behaviors of various types of OEMs in aqueous RMBs are summarized in Table 7.

Table 7 Summary of OEMs for aqueous RMBs

Compound	Structure	Electrolyte	Average discharge voltage	Initial reversible capacity at current density	Cycle life (n)	Rate capability
PTCDA ³⁰		Saturated Mg(NO ₃) ₂	−0.2 V vs. Ag/AgCl	125 mA h $\rm g^{-1}$ at 137 mA $\rm g^{-1}$	N/A	N/A
Eumelanin ¹⁰⁸	O N R= H or COOH	0.5 M Mg(NO ₃) ₂	−0.4 V vs. SCE	$61.6\pm0.3~\text{mA}~\text{h}~\text{g}^{-1}$ at 100 mA g^{-1}	500	40 mA h g ⁻¹ at 1000 mA g ⁻¹
PPTO ¹¹⁰	H N N N N N N N N N N N N N N N N N N N	4.5 M Mg(NO ₃) ₂	0.2 V νs. SHE	144 mA h $\rm g^{-1}$ at 280 mA $\rm g^{-1}$	1000	120 mA h $\rm g^{-1}$ at 560 mA $\rm g^{-1}$
PNTCDA ¹¹¹	+N	1 M MgSO ₄	−0.5 V vs. Ag/AgCl	140 mA h g ⁻¹ at 1000 mA g ⁻¹	2000	N/A
PPMDA@MCNTs ¹¹³	$+$ N \longrightarrow n	4 M Mg(TFSI) ₂	2.0 V vs. Mg/Mg ²⁺	110 mA h $\rm g^{-1}$ at 100 mA $\rm g^{-1}$	500	N/A

3.1.1. Anhydrides. Unlike most inorganic electrode materials, OEMs are universal electroactive materials for metal-ion batteries. A couple of OEMs used in LIBs are also applied as electrode materials in aqueous RMBs. For instance, Rodríguez-Perez et al.³⁰ studied a carbonyl group-based crystalline organic solid, PTCDA, as an anode material in aqueous RMBs (Fig. 11a). The PTCDAbased anode provides an initial capacity of 125 mA h g⁻¹ at a low current density of 20 mA g⁻¹ and retains a reversible capacity of 75 mA g⁻¹ when the current density increases to 500 mA g⁻¹, demonstrating robust reaction kinetics (Fig. 11b). This work proves that the crystalline organic solids are promising electrodes for the reversible storage of Mg²⁺ ion in aqueous batteries.

3.1.2. Carbonyl polymers. In addition to the carbonyl group-based small organic compounds, the carbonyl-based polymers are also applicable in aqueous RMBs. The metal cation-catechol complexes play crucial roles in many biochemical behaviors, such as transduction of biological energies, Fe(III) uptake in microbial siderophores. 105,106 Catechols have tight, but reversible and complicated coordination with many metal cations such as Li⁺, Mg²⁺, and Al³⁺. 107 It has been discovered that catechols exhibit excellent electrochemical performances in

monovalent and multivalent batteries. Kim et al. 108 employed a redox-active catechol-quinone system (Eumelanin) in the cathode for aqueous RMBs. The quinone becomes a catechol after discharge, which has a much stronger affinity for Mg²⁺ (0.95 eV) than the original o-quinone. 109 Therefore, Mg2+ can coordinate with catechol to form the complex. It is extracted when the catechol was oxidized back to o-quinone (Fig. 11c). This mechanism was proved by Fourier-transform infrared (FT-IR) and Raman spectroscopy. The eumelanin cathode delivers a capacity of 61.6 mA h g^{-1} at 0.1 A g⁻¹ along with negligible capacity decay after 500 cycles in aqueous RMBs (Fig. 11d). Although eumelanin exhibits excellent cycle life, more work needs to be done to further improve its reversible capacity by improving the conductivity and optimizing the chemical structure.

Apart from eumelanin, several other polymers have also been synthesized and proved to be reliable electrode materials for aqueous RMBs (Fig. 11e). Liang et al. 110 studied a quinonebased monomer, pyrene-4,5,9,10-tetraone (PTO), as an anode material in aqueous batteries. However, it is soluble in a neutral electrolyte, and thus suffers from fast capacity decay. To overcome this challenge, they polymerized PTO to form insoluble

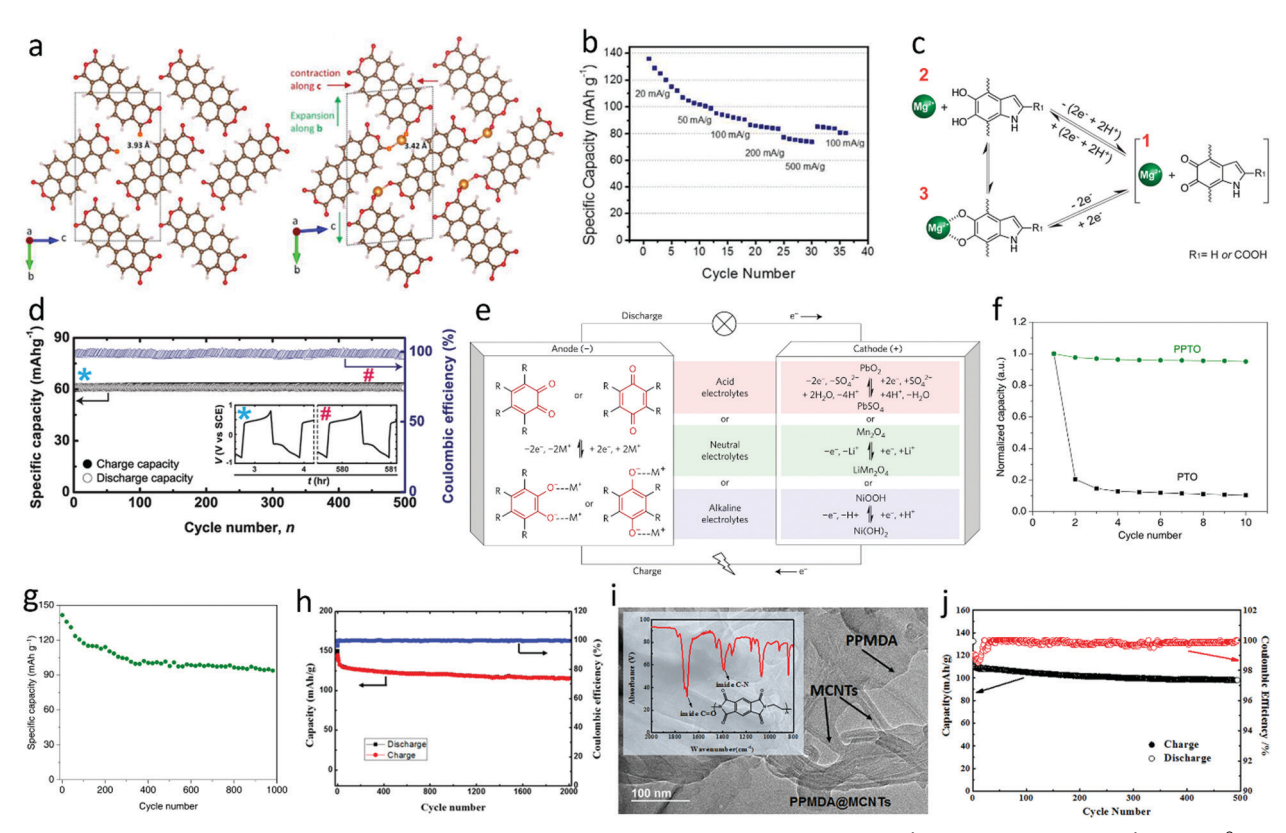


Fig. 11 (a) Calculated distances between two oxygen atoms from two different PTCDA molecules (3.93 Å (pristine, left) and 3.42 Å (with Mq²⁺ inserted, right)). (b) Rate capability measurements at 20, 50, 100, 200, 500, and 200 mA g⁻¹. Reproduced with permission. ³⁰ Copyright 2017 American Chemical Society. (c) The redox reaction of the eumelanin-catechol system and the formation of the Mg-catechol complex. (d) Reversible charge-discharge cycles (500 cycles) of eumelanin cathode. Insets represent the curves from the initial (*) and final (#) charge-discharge cycles. Reproduced with permission.¹⁰⁸ Copyright 2014 Wiley-VCH Verlag GmbH & Co. KGaA. (e) Schematics of aqueous rechargeable batteries based on quinone anodes at different pH values (with corresponding redox chemistries). (f) Cycling performance of PPTO and PTO in a neutral electrolyte. (g) Cycling performance of PPTO at C/2. Reproduced with permission. 110 Copyright 2017 Macmillan Publishers Limited. (h) Cycling stability test for PNTCDA electrodes. Reproduced with permission.¹¹¹ Copyright 2017 American Chemical Society. (i) TEM for PPMDA@MCNTs composite (inset: FTIR spectrum). (j) Cycling stability and Coulombic efficiency of PPMDA@MCNTs at 1C. Reproduced with permission. 113 Copyright 2017 American Chemical Society.

PPTO. The resultant PPTO exhibits much better cyclic stability (Fig. 11f). When working in 4.5 M Mg(NO₃)₂ electrolyte, PPTO delivers a specific capacity of 144 mA h g⁻¹ and exhibits a high cycling stability for 1000 cycles in a voltage range of -0.4 to 0.5 V vs. Ag/AgCl (Fig. 11g). Besides quinone-based polymers, Chen et al. 111 designed an aqueous RMB, consisting of 1,4,5,8naphthalenetetracarboxylic dianhydride (NTCDA)-derived polyimide (PNTCDA)112 as an anode material. The computational studies of the monomer (NTCDA) and Mg²⁺ disclosed the redox reaction mechanism of PNTCDA in aqueous RMBs, which is similar to that in non-aqueous RMBs. The carbonyl groups in PNTCDA act as active centers to reversibly react with Mg²⁺. In 1 M MgSO₄ aqueous electrolyte, the polyimide exhibits a specific capacity of 140 mA h g⁻¹ in the voltage window of 0 to -0.8 V vs. Ag/AgCl at a current density of 1 A g⁻¹ and retains 90% of its initial capacity after 2000 cycles (Fig. 11h). In addition to PNTCDA, Wang et al. 113 reported another polyimide named poly-pyromellitic dianhydride (PPMDA) as an anode material for aqueous RMBs. To improve the electronic conductivity, 5% multiwall carbon nanotubes (MCNTs) were added into the in situ polymerization process of PPMDA to generate the PPMDA@MCNTs composite (Fig. 11i). Attenuated total reflectance Fourier-transform infrared spectroscopy (ATR-FTIR) measurements were carried out to verify that MCNTs were uniformly distributed in the composites to form a highly conductive 3D network. The resulting composite provides a specific capacity of 110 mA h g⁻¹ at a current density of 0.1 A g⁻¹ in the 4 M Mg(TFSI)₂ aqueous electrolyte, and excellent cycling stability

of 500 cycles with 87% capacity retention (Fig. 11j). The exceptional electrochemical performance of PNTCDA and PPMDA demonstrates that carbonyl-based polymers are promising anode materials in aqueous RMBs. Since the plating/stripping potential of Mg metal is below the stability window of aqueous electrolytes, more research efforts are demanded to develop high-performance polymer anodes for aqueous RMBs.

3.2. OEMs in aqueous RABs

Aqueous RABs is another alternative to LIBs due to the low cost, abundance, and environmental benignity of aluminum resources and aqueous electrolyte. To date, the major research direction of OEMs in aqueous RABs focuses on the anode, because the high-capacity Al metal anode is not compatible with the aqueous electrolyte. 114 It is critical to find high-performance anodes for aqueous RABs. The electrochemical behaviors of various types of OEMs in aqueous RABs are summarized in Table 8. Herein, we provide a brief discussion in this section.

Analogous to aqueous RMBs, the development of high-performance anode materials based on redox-active polymers (RAPs) is the major research direction in aqueous RABs. Compared with the inorganic counterparts, RAPs have large cavities and soft structures, which enable the Al³⁺ intercalation/de-intercalation process and accommodate the large volume change. Patil *et al.*¹⁰⁷ designed a series of catechol-based RAPs as anode materials for RABs. They focus on the P(DA₇₀-stat-SSA₃₀) copolymer contains both dopamine acrylamide (DA) and 4-styrenesulfonic acid (SSA) units, which improve the specific

Table 8 Summary of OEMs for aqueous RABs and RCBs

Compound	Structure	Electrolyte	Average discharge voltage	Initial reversible capacity at current density	Cycle life (n)	Rate capability
P(DA ₇₀ -stat-SSA ₃₀) ¹⁰⁷	stat 30 70 NH O=S=O OH OH	1.0 M $AlCl_3$	−0.4 V vs. Ag/AgCl	142 mA h g^{-1} at 182 mA g^{-1}	10 000	47 mA h g^{-1} at 21 840 mA g^{-1}
PPTCDI ¹¹⁵	-N	0.5 M AlCl ₃	−0.4 V vs. SCE	185 mA h g ⁻¹ at 100 mA g ⁻¹	1000	95 mA h g ⁻¹ at 1000 mA g ⁻¹
PTCDA ³⁰		Saturated Ca(NO ₃) ₂	0.7 V	87 mA h g ⁻¹ at 137 mA g ⁻¹	N/A	N/A
PANI/CC ¹¹⁸	$+$ $\left\langle -\right\rangle_{n}$	2.5 M Ca(NO ₃) ₂	−0.1 V vs. Ag/AgCl	123 mA h g^{-1} at 150 mA g^{-1}	200	101 mA h g^{-1} at 500 mA g^{-1}
PNDIE ¹¹⁹	+N N N N	2.5 M Ca(NO ₃) ₂	−0.6 V vs. Ag/AgCl	148 mA h g ⁻¹ at 183 mA g ⁻¹	1000	115 mA h g ⁻¹ at 3660 mA g ⁻¹
SBA-15/PPTCDI ¹²⁰	+N	1.0 M Ca(NO ₃) ₂	−0.5 V vs. SCE	199 mA h g ⁻¹ at 100 mA g ⁻¹	1500	46 mA h g ⁻¹ at 1000 mA g ⁻¹

capacity and rate capability. The resultant copolymer electrode shows a specific capacity of 142 mA h g^{-1} at 1C (1C = 182 mA h g^{-1}), and a 78% capacity retention after 10 000 cycles at a high current rate of 30C in the 1 M Al(NO₃)₃ aqueous electrolyte. The excellent electrochemical performance renders it a promising anode material for aqueous RABs. Poly(3,4,9,10-perylentetracarboxylic diimide) (PPTCDI) is another promising anode material for aqueous RABs. To optimize the performance of the polymer anode, Cang et al. 115 synthesized PPTCDI at various temperatures: 120 °C, 160 °C, and 180 °C. Then, the galvanostatic charge-discharge method was carried out to evaluate their electrochemical performance. The result indicates that PPTCDI-160 °C shows the best performance with a specific capacity of 185 mA h g⁻¹ at a current density of 100 mA g⁻¹ and retains nearly 99% of its initial capacity after 1000 cycles. Moreover, the PPTCDI-160 °C electrode delivers an excellent rate capability that a capacity of 95 mA h g⁻¹ can be retained at 1000 mA g⁻¹. The superior electrochemical performance of RAP anodes attracts more research interests from energy storage for the development of aqueous RABs.

Despite several outstanding RAPs that have been studied as anode materials for aqueous RABs, there is still a high demand for further improvement in this field. To fulfill this goal, three strategies are feasible. Firstly, there are a myriad of highperformance polymers in LIBs that are also capable anodes in aqueous RABs. More efforts are required to evaluate their performance in aqueous RABs. Secondly, the conductivity of RAPs can be further improved to achieve better reaction kinetics and electrochemical performance. For instance, designing and synthesizing composites with highly conductive materials such as carbon nanotubes (CNTs) and graphene, and extending the π -conjugated aromatic structure in RAPs are two effective methods to enhance the material conductivity. Thirdly, the specific capacity of RAPs needs to be improved. Reducing the molecular weight and increasing the electroactive centers in the repeating units of polymers will enhance the theoretical specific capacity of RAPs. These aspects can be used as references for future research directions of RAP anode materials in aqueous RABs. 116

3.3. OEMs in aqueous RCBs

Among the MRBs, aqueous RCBs are also attractive alternatives to LIBs because of the low cost and abundance of Ca resources. Moreover, the redox potential of Ca metal (-2.87 V vs. SHE) is close to that of Li metal (-3.04 V vs. SHE), and it also has a high theoretical volumetric capacity of 2073 mA h cm⁻³. 117,118 However, the development of RCBs is still in its infancy because of the low stripping/plating efficiency of Ca metal in the electrolyte. There are only a few reports about the nonaqueous RCBs, but none of them is related to OEMs. The application of OEMs in RCBs mainly focuses on the aqueous electrolyte. Therefore, we summarized the electrochemical behaviors of various types of OEMs in aqueous RCBs in Table 8. In this section, the development and application of OEMs in aqueous RCBs are discussed in detail.

As reported by Rodríguez-Pérez et al. the crystalline organic solid, PTCDA, was a universal electrode material in metal-ion

batteries. 30 It delivers an initial specific capacity of 87 mA h g⁻¹ in aqueous RCBs but suffers from fast capacity fading from the second to 10th cycle due to the high solubility and poor structural stability of PTCDA in the aqueous electrolyte (Fig. 12a). To improve the electrochemical performance, developing stable, insoluble and highly conductive OEMs is the key. Therefore, similar to aqueous RMBs and RABs, the major OEMs in aqueous RCBs are conducting and carbonyl-based polymers, which are stable and insoluble in aqueous electrolytes. Adil et al. 118 employed the conducting polymer, PANI, as an anode material in aqueous RCBs. They prepared a PANI-coated carbon cloth (PANI/CC) composite to further increase the conductivity of the organic anode. In a voltage window of -0.5 to 0.4 V vs. Ag/AgCl reference electrode, the PANI/CC composite delivers a specific capacity of 123 mA h g⁻¹ at a current density of 150 mA g⁻¹ in the 2.5 M Ca(NO₃)₂ aqueous electrolyte, and retains 84% of its initial capacity after 200 cycles (Fig. 12b). Due to the superior electrochemical performance, the PANI/CC anode is coupled with a potassium copper hexacyanoferrate cathode to make a full Ca-ion cell, which also exhibits excellent electrochemical behaviors. In addition to conducting polymer, carbonyl-based polymers are also used in aqueous RCBs. Gheytani et al. 119 developed a polyimide anode, poly [N,N'-(ethane-1,2-diyl)-1,4,5,8-naphthalenetetracarboxiimide] (PNDIE), for aqueous RCBs (Fig. 12c). In the potential range of -0.9 to 0 V vs. Ag/AgCl reference electrode, the polyimide provides a specific capacity of 148 mA h g^{-1} at a current density of 183 mA g^{-1} (1C) in 2.5 M Ca(NO₃)₂ aqueous electrolyte. It also displays good cyclic stability that it retains 80% of its initial capacity and high CE of >99% at a current rate of 5C (925 mA g⁻¹) after 4000 cycles (Fig. 12d). Recently, Cang et al. 120 synthesized mesoporous silica SBA-15/ PPTCDI composite as an organic anode for aqueous RCBs. The composite delivers an initial discharge capacity of 199 mA h g⁻¹ at a current density of 100 mA g⁻¹ and retains a reversible capacity of 196.5 mA h g⁻¹ after 100 cycles. Even at a high current rate of 1000 mA g⁻¹, the composite still shows a negligible capacity loss for 1500 cycles, demonstrating outstanding cycle life and robust reaction kinetics (Fig. 12e). The superior electrochemical performance of these electroactive polymers confirms that developing stable, insoluble and highly conductive polymer anodes is a promising research direction for aqueous RCBs.

The lack of high-capacity anode stimulates the rapid development of high-performance OEMs in aqueous RMBs, RABs, and RCBs. However, the capacity of state-of-the-art polymer anodes is still much lower than that of the commercial LIB anode, graphite (372 mA h g⁻¹), resulting in a low energy density of aqueous batteries. Additionally, the improvement of cycle life, CE and power density of the polymer anodes is also required for the applications of aqueous batteries in grid-scale stationary energy storage. As we mentioned previously, there are a couple of approaches to enhance the performance of polymer electrodes by tailoring the chemical/physical structures and attaching to conductive and insoluble carbon matrix. To fulfill the aim of affordable, sustainable, and environmentally benign energy storage devices, more research efforts are demanded to design

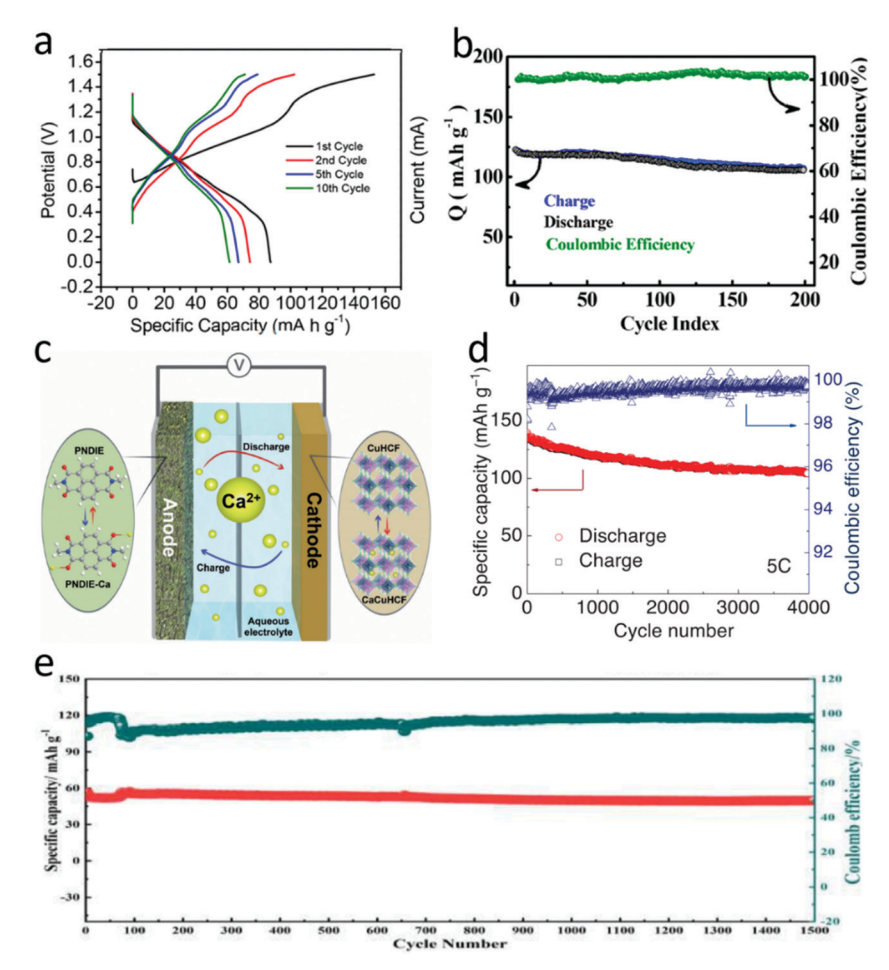


Fig. 12 (a) Galvanostatic charge-discharge potential profiles of 1st, 2nd, 5th, and 10th cycles of PTCDA in saturated Ca(NO₃)₂ electrolyte. Reproduced with permission. 30 Copyright 2017 American Chemical Society. (b) Long-term cycling performance of PANI/CC anode at the current rate of 0.15 A g $^{-1}$. Reproduced with permission. 118 Copyright 2020 American Chemical Society. (c) Schematic illustration of the polyimide—CaxCuHCF aqueous rechargeable Ca-ion battery. (d) Capacity stability and Coulombic efficiency of PNDIE at 5C current rate (925 mA g⁻¹). Reproduced with permission. 119 Copyright 2017 Wiley-VCH Verlag GmbH & Co. KGaA. (e) The cycle performance of SBA-15@PPTCDI at 100 mA g^{-1} . Reproduced with permission: ¹²⁰ Copyright 2020 Wiley-VCH Verlag GmbH & Co. KGaA.

and synthesize high-capacity, fast-charge and stable polymers for aqueous RMBs, RABs, and RCBs.

3.4. OEMs in aqueous RZBs

Unlike the other metals (Li, Mg, Al, and Ca), Zn metal is stable in the aqueous electrolyte during the charge and discharge of aqueous RZBs due to the high reaction potential of Zn/Zn²⁺ versus SHE. Hence, Zn metal is used as a low-cost and highcapacity anode in aqueous RZBs, which is a major advantage of this battery system. 121-123 The reaction mechanisms and electrochemical behaviors of various types of OEMs in aqueous RZBs are summarized in Fig. 13 and Tables 9 and 10. This section further discusses the development and applications of state-of-the-art OEMs in detail.

3.4.1. Conducting polymers. Conducting polymers show higher conductivity than small organic compounds due to their extended π -conjugated structures. Among them, PANI is the first organic material used in RZBs with an aqueous electrolyte containing ZnCl₂ and NH₄Cl.^{47,124,125} However, the electrochemical activity of PANI is limited by the pH value of the electrolyte, because the deprotonation of PANI at pH > 1 leads to low electrochemical activity, while the acidic electrolyte (pH < 1) is corrosive to Zn anode. To circumvent this challenge, the copolymerization of aniline with a monomer that is electrochemically active at a wide pH range offers opportunities to enhance the electrochemical activity of PANI. Rahmanifar et al. 126 synthesized a copolymer, consisting of aniline and m-aminobenzoic acid (MABA). The copolymer exhibits electrochemical activity over a wide pH range due to the presence of carboxylate anions. The copolymer was investigated as a cathode in RZBs with 1.0 M $ZnCl_2 + 0.5$ M NH_4Cl aqueous electrolyte (pH = 5). It delivers a capacity of 146.4 A h kg⁻¹ at 1 mA cm⁻² in the cutoff window of 0.8-1.6 V, together with a 62.5% capacity retention after 200 cycles (Fig. 14a). Also, another copolymer, poly(aniline-co-m-aminophenol), possesses good electrochemical properties at pH < 10.6 and high electronic conductivity, owing to the reversible redox behaviors of hydroxyl groups in the copolymer chain (Fig. 14b). 127 The poly(aniline-co-m-aminophenol)-based aqueous RZBs provides a high capacity of 137.5 A h kg⁻¹ at 0.5 mA cm⁻² and 88.6% capacity retention after 120 cycles at

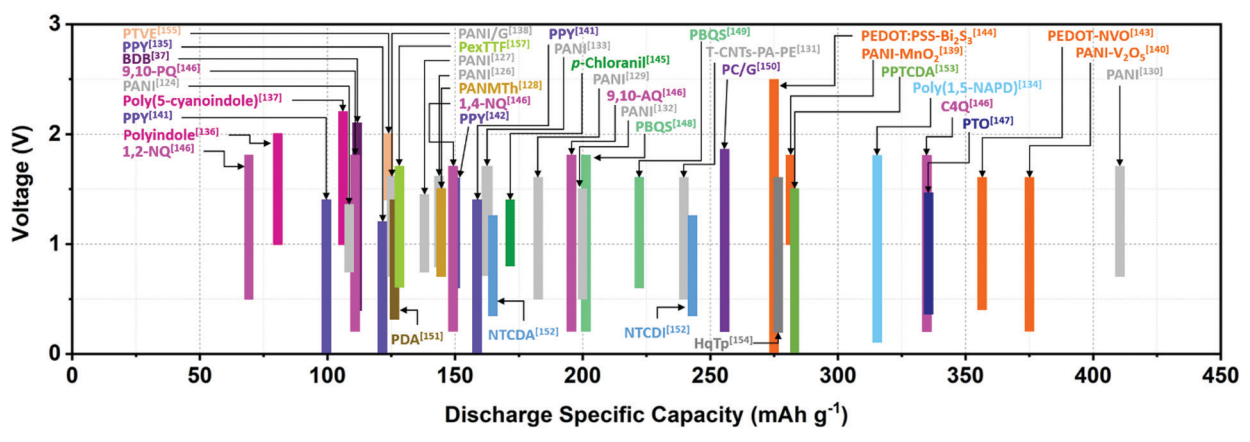


Fig. 13 Capacity versus voltage for the reported OEMs for non-aqueous rechargeable Al batteries.

Table 9 Reaction mechanisms and electrochemical behaviors of the OEMs in aqueous RZBs

Types		General redox mechanism	Classification	Average discharge voltage	Discharge capacity	Cycle life
Carbonyl onomer	Quinone monomer	R'' +Zn ²⁺ , 2e' R''' R''' R''' +Zn ²⁺ , 2e' R''' R''' +Zn ²⁺ , 2e' R''' R''' R''' R''' R''' R''' R''' R'''	n-Type	Low	High	Low
	Anhydride	O O O O O O O O O O O O O O O O O O O				
	Quinone polymer	$\begin{array}{c} \begin{array}{c} & & & \\ & & \\ & & \\ & & \end{array}$				
Carbonyl polymer	Catechol polymer	$\begin{array}{c ccccccccccccccccccccccccccccccccccc$	n-Type	Medium	High	High
	Polyimide	Ar Ar' -Zn ²⁺ , 2e Ar Ar' -Zn ²⁺ , 2e N N N N N N N N N N N N N				
Amine polymer		R' +B', -e' R' B'. R' -B', +e' R R' R'' B': CI', CF ₃ SO ₃ ',TFSI', 0.5 SO ₄ ² -	р-Туре	High	Medium	Medium
Nitroxide free ra	ndical polymer	+B', -e' -B', +e' -B', +e' (R'\), R'),	р-Туре	High	Low	Medium

Another example of using a copolymer to improve the

2.5 mA cm⁻² in 2.0 M ZnCl₂ + 3.0 M NH₄Cl aqueous electrolyte. performance of PANI is incorporating redox-active Nmethylthionine unit into the PANI chain via electrochemical

 Table 10
 Summary of OEMs as cathodes for aqueous RZBs

			Average	Initial reversible	Cycle	
Compound	Structure	Electrolyte	discharge voltage	capacity at current density	Cycle life (n)	Rate capability
PANI ¹²⁴		1.0 M ZnSO ₄	~1.1 V	108 mA h g ⁻¹ at 30 μA cm ⁻²	2000	N/A
PANI ¹²⁶		$1.0~\mathrm{M~ZnCl_2} + 0.5~\mathrm{M~NH_4Cl}$	~1 V	146.4 mA h g ⁻¹ at 1 mA cm ⁻²	200	N/A
PANI ¹³⁰		$2~M~ZnCl_2 + 3~M~NH_4Cl$	1.2 V	$412.7 \text{ mA h g}^{-1}$	1500	218 mA h g^{-1} at
t-CNTs-PA-PE ¹³¹		2 M ZnSO ₄	1.1 V	at 0.5 A g ⁻¹ 238 mA h g ⁻¹ at	1500	16 A g ⁻¹ 145 mA h g ⁻¹ at
PANI ¹³²		1 M Zn(CF ₃ SO ₃) ₂	1.1 V	0.2 A g^{-1} $200 \text{ mA h g}^{-1} \text{ at}$	3000	10 A g ⁻¹ 95 mA h g ⁻¹ at
PANI ¹³³	, <u> </u>	1 M ZnCl ₂	~1.1 V	50 mA g ⁻¹ 162 mA h g ⁻¹ at	100	5 A g ⁻¹ 30 mA h g ⁻¹ at
PANI/graphite ¹³⁸		2 M Zn(ClO ₄) ₂ + 1 M	1.2 V	1C 125.43 mA h g ⁻¹	100	234C N/A
$\mathrm{PANI\text{-}MnO_2}^{139}$		$NH_4ClO_4 + Triton-X100$ 2 M $ZnSO_4 + 0.1$ M $MnSO_4$	1.3 V	at 50 mA g ⁻¹ 280 mA h g ⁻¹ at	200	110 mA h g ⁻¹ at
$PANI-V_2O_5^{143}$		3 M Zn(CF ₃ SO ₃) ₂	0.9 and 0.5 V	0.2 A g ⁻¹ 375.2 mA h g ⁻¹ at 1 A g ⁻¹	2000	3 A g ⁻¹ 197.1 mA h g ⁻¹ at 20 A g ⁻¹
Poly(aniline-co-m-aminophenol) ¹²⁷	HO —NH—NH) _n	$2.0~\mathrm{M~ZnCl_2} + 3.0~\mathrm{M~NH_4Cl}$	1.05 V	137.5 mA h g ⁻¹ at 0.5 mA cm ⁻²	120	N/A
PANMTh ¹²⁸	NHCH ₃ *	$2.0~\mathrm{M~ZnCl_2} + 3.0~\mathrm{M~NH_4Cl}$	1.1 V	146.3 mA h g ⁻¹ at 1 mA cm ⁻²	150	110.5 mA h g ⁻¹ at 5 mA cm ⁻²
PANI-S ¹²⁹	(N-NH-NH-NH-NH-NH-NH-NH-NH-NH-NH-NH-NH-NH	1.0 M ZnSO ₄	1.1 V	184 mA h g ⁻¹ at 0.2 A g ⁻¹	2000	130 mA h g^{-1} at 10 A g^{-1}
BDB ³⁷		19 M Li-N(SO ₃ CF ₃) ₂ + 1 M Zn(CF ₃ SO ₃) ₂	1.27 and 0.89 V	112 mA h g^{-1} at 3C	1000	$>$ 80 mA h g $^{-1}$ at 6C
Poly(1,5-NAPD) ¹³⁴	HN—H ₂ N—H ₂ N—HN—	2 M ZnSO ₄	0.8 V	315 mA h g^{-1} at 0.19 A g^{-1}	10 000	145 mA h g^{-1} at 14.8 A g^{-1}
PPY ¹³⁵	2	PVA-KCl-Zn(CH ₃ COO) ₂ gel	0.5 V	123 mA h g^{-1} at 1.9 A g^{-1}	200	N/A
PPY ¹⁴¹	<i>"</i> —» Н	electrolyte 2 M Zn(CH ₃ COO) ₂	~0.7 V	$100 \text{ mA h g}^{-1} \text{ at}$	50	N/A
PPY ¹⁴¹	HN N N N N N N N N N N N N N N N N N N	2 M Zn(CH ₃ COO) ₂ in choline acetate + 70%	~0.7 V	0.5 A g ⁻¹ 160 mA h g ⁻¹ at 0.5 A g ⁻¹	50	N/A
PPY^{142}	,	water 2 M ZnCl ₂ + 3 M NH ₄ Cl	~1.1 V	151 mA h g^{-1} at 0.5 A g^{-1}	1000	87.6 mA h g ⁻¹ at 16 A g ⁻¹
Polyindole ¹³⁶	NH n	1 M ZnCl ₂	~1.5 V	80 mA h g^{-1} at 200 A m^{-2}	200	60 mA h $\rm g^{-1}$ at 1000 A $\rm m^{-2}$
Poly(5-cyanoindole) ¹³⁷	N≡C N n	1 M ZnCl ₂	~1.7 V	$107~\mathrm{mA}~\mathrm{h~g}^{-1}$ at $0.2\mathrm{C}$	800	$61 \text{ mA h g}^{-1} \text{ at}$ 10C
PEDOT-NVO ¹⁴⁰	s s n	3 M Zn(CF ₃ SO ₃) ₂	1 V	356.8 mA h g^{-1} at 0.05 A g^{-1}	5000	163.6 mA h g ⁻¹ at 10 A g ⁻¹

Table 10 (continued)

Review

Compound	Structure	Electrolyte	Average discharge voltage	Initial reversible capacity at current density	Cycle life (n)	Rate capability
PEDOT:PSS/Bi $_2$ S $_3^{144}$	+ n SO ₃ - SO ₃ H	1 M Zn(TFSI) ₂ + 21 M LiTFSI	1.3 V	275 mA h g ⁻¹ at 0.3 A g ⁻¹	5300	105 mA h g ⁻¹ at 6 A g ⁻¹
<i>p</i> -Chloranil ¹⁴⁵	CICI	1 M Zn(CF ₃ SO ₃) ₂	1.1 V	$170~\mathrm{mA~h~g^{-1}}$ at $0.2\mathrm{C}$	200	118 mA h g^{-1} at 1C
1,2-NQ ¹⁴⁶		3 M Zn(CF ₃ SO ₃) ₂	~1 V	68 mA h g ⁻¹ at 20 mA g ⁻¹	5	N/A
1,4-NQ ¹⁴⁶		3 M Zn(CF ₃ SO ₃) ₂	0.8 V	149 mA h g^{-1} at 20 mA g^{-1}	5	N/A
9,10-AQ ¹⁴⁶		3 M Zn(CF ₃ SO ₃) ₂	0.9 and 0.55 V	194 mA h g^{-1} at 20 mA g^{-1}	40	N/A
9,10-PQ ¹⁴⁶		3 M Zn(CF ₃ SO ₃) ₂	0.5 V	111 mA h g^{-1} at 20 mA g^{-1}	5	N/A
$C4Q^{146}$		3 M Zn(CF ₃ SO ₃) ₂	1 V	335 mA h g^{-1} at 20 mA g^{-1}	1000	172 mA h $\rm g^{-1}$ at 1000 mA $\rm g^{-1}$
PTO ¹⁴⁷		2 M ZnSO ₄	1 and 0.6 V	336 mA h g^{-1} at 40 mA g^{-1}	1000	113 mA h g^{-1} at 20 000 mA g^{-1}
PBQS ¹⁴⁸ PBQS ¹⁴⁹	o o s	3 M Zn(CF ₃ SO ₃) ₂ 3 M Zn(OTf) ₂	0.9 V ~1 V	203 mA h g^{-1} at 0.1C 220 mA h g^{-1} at 400 mA h g^{-1}	50 1000	126 mA h $\rm g^{-1}$ at 5C N/A
PC/G ¹⁵⁰	HO OH	3 M ZnSO ₄	~1 V	255 mA h g^{-1} at 0.1C	3000	171 mA h $\rm g^{-1}$ at 10C
PDA ¹⁵¹	NH HO OH	3.3 M ZnSO ₄	0.8 V	126.2 mA h g ⁻¹ at 0.02 A g ⁻¹	500	43.2 mA h g ⁻¹ at 5 A g ⁻¹
NTCDA ¹⁵²		2 M ZnSO ₄	0.6 and 0.4 V	\sim 165 mA h g ⁻¹ at 0.1 A g ⁻¹	30	$<\!20$ mA h $\rm g^{-1}$ at 2 A $\rm g^{-1}$

Table 10 (continued)

Compound	Structure	Electrolyte	Average discharge voltage	Initial reversible capacity at current density	Cycle life (n)	Rate capability
NTCDI ¹⁵²	NH NH	2 M ZnSO ₄	0.5 V	240 mA h g ⁻¹ at 0.1 A g ⁻¹	2000	140 mA h g ⁻¹ at 2 A g ⁻¹
PPTCDA/GA ¹⁵³	+N-C ₂ H ₄ -N-C ₂ H ₄	2 M ZnSO ₄	0.6 and 0.3 V	281 mA h g^{-1} at 0.1 A g^{-1}	300	102 mA h g ⁻¹ at 1 A g ⁻¹
HqTp ¹⁵⁴	HO HN OH HO HH OH HO HO	3 M ZnSO ₄	1 V	276 mA h g ⁻¹ at 0.125 A g ⁻¹	1000	85 mA h g^{-1} at 3.75 A g^{-1}
PTVE ¹⁵⁵	n O O	$0.1~\mathrm{M}~\mathrm{ZnCl_2-NH_4Cl}$	1.75 V	124 mA h $\rm g^{-1}$ at 60C	500	N/A
PTAm ¹⁵⁶	HN O	$0.1~\mathrm{M}~\mathrm{ZnCl_2-NH_4Cl}$	1.2 V	114 mA h g^{-1}	1000	N/A
PexITF ¹⁵⁷	S S S	1 M Zn(BF ₄) ₂	1.1 V	128 mA h g^{-1} at 20C	10 000	110 mA h g^{-1} at 120C
P(DA ₇₀ -stat-SSA ₃₀) ¹⁰⁷	O NH OH OH	1 M ZnSO ₄	0.2 V vs Ag/AgCl	$132 \text{ mA h g}^{-1} \text{ at } 1\text{C}$	50 000	67 mA h g^{-1} at 120C

copolymerization. The resulting copolymer cathode, poly(aniline-co-N-methylthionine) (PANMTh), exhibits dramatically enhanced electrochemical performance in aqueous RZBs at a pH of 10.¹²⁸ It delivers a high capacity of 146.3 A h kg⁻¹ at 1 mA cm⁻² together with excellent cycling stability of 99.4% capacity retention after 150 cycles at 2 mA cm⁻². The superior electrochemical performance in the alkaline electrolyte is attributed to the redox-active phenothiazine ring of *N*-methylthionine in the copolymer chain (Fig. 14c). These results confirm that copolymerization of aniline with other redox-active monomers is an effective approach to obtain conducting polymers with a high electrochemical performance for aqueous RZBs.

In addition to incorporating other redox-active monomers, altering the chemical environment is another effective strategy

for improving the physicochemical properties and functionality of PANI. Shi $et~al.^{129}$ synthesized a sulfo-self-doped PANI (PANI-S) cathode for RZBs by a facile electrochemical copolymerization approach, in which the $-\mathrm{SO_3}^-$ was used as an internal proton reservoir to retain a high local H⁺ concentration and facilitate the redox process in zinc sulfate electrolyte (Fig. 14d). The PANI-S based cathode provides a high capacity (184 mA h g⁻¹ at 0.2 A g⁻¹ with a voltage range of 0.5–1.6 V), excellent rate capability (130 mA h g⁻¹ at 10 A g⁻¹), and long lifetime (110 mA h g⁻¹ after 2000 cycles at 10 A g⁻¹) in 1.0 M ZnSO₄ aqueous electrolyte (Fig. 14e). This work resolves the electrochemical activity mismatch of PANI cathode and Zn anode in the aqueous electrolyte by using the pH adjustable ability of self-dopants.

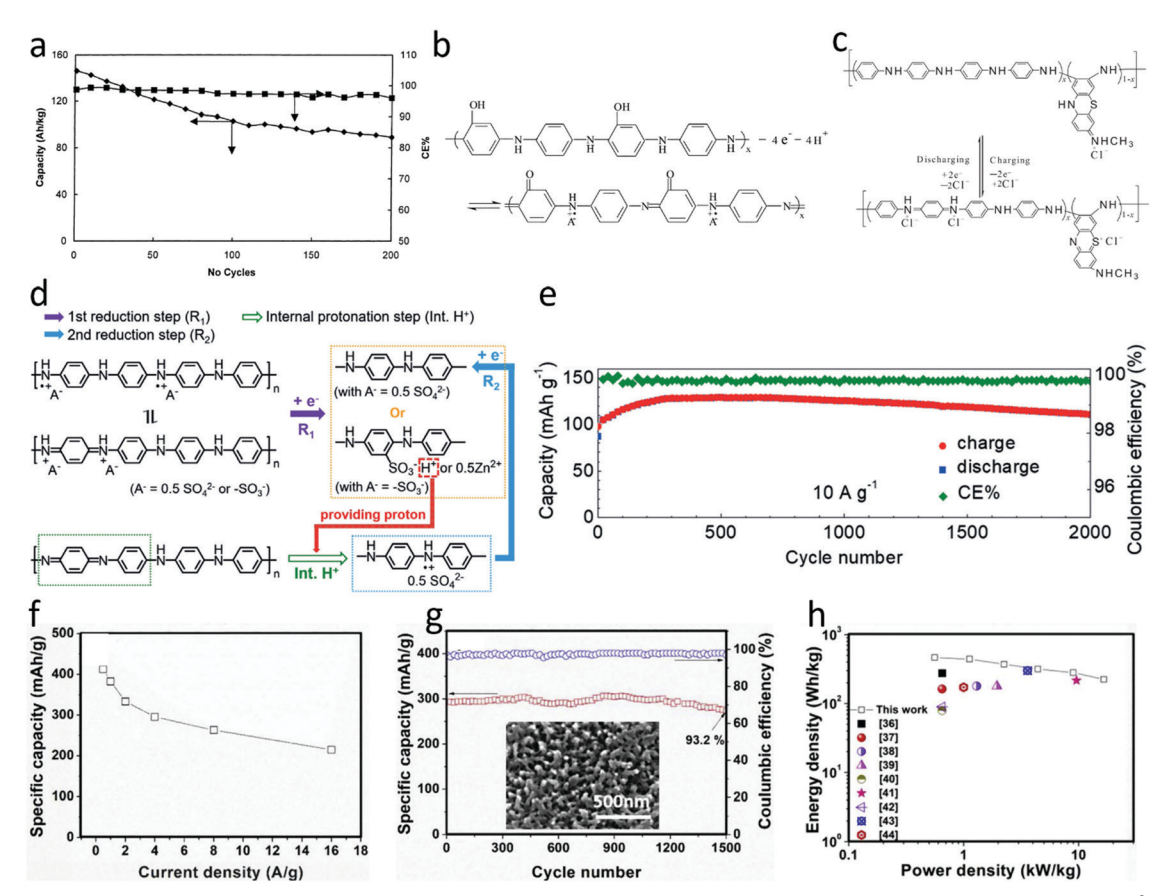


Fig. 14 (a) Discharge capacity and Coulombic efficiency vs. cycle number for SDPA-Zn cell at a constant current density of 1 mA cm⁻². Reproduced with permission.¹²⁶ Copyright 2002 Elsevier Science B.V. (b) The structure and the electrode reaction of poly(aniline-com-aminophenol). Reproduced with permission. ¹²⁷ Copyright 2006 Elsevier Science B.V. (c) Schematic representation of the charging-discharging processes of the cathode for Zn copolymer rechargeable battery. Reproduced with permission. 128 Copyright 2015 Elsevier Ltd. (d) Proposed reduction processes after conditioning cycles (only PANI fragments of the polymer chain are drawn for the components on the right side of the scheme for simplicity). (e) Capacity and Coulombic efficiency evolution during long-term cycling at the current density of 10 A g⁻¹. Reproduced with permission: ¹²⁹ Copyright 2018 Wiley-VCH Verlag GmbH & Co. KGaA. (f) Specific capacity versus current density of PANI cathode. (g) Cyclic stability at 4 A g⁻¹ (the inset SEM image after 1500 cycles). (h) Ragone plot of energy density versus power density of PANI-based device. Reproduced with permission. 130 Copyright 2019 Elsevier Ltd.

Apart from tailoring the chemical structure, the morphology of PANI also shows a great influence on its electrochemical performance in aqueous RZBs. Li et al. 130 synthesized an ultrahigh-energy cathode, consisting of PANI nanopillars grown on the surface of cracked carbon fiber. The PANI nanopillars facilitate the redox reaction kinetics due to short ion diffusion pathways across the solid/liquid interfaces. The PANI nanopillarbased cathode delivers an ultrahigh specific capacity of 412.7 mA h g⁻¹ at 0.5 A g⁻¹ and superior cyclic stability with 93.2% capacity retention over 1500 cycles at 4 A g⁻¹ (Fig. 14f and g). Moreover, the resulting Zn/PANI full cell presents a high energy density of 464.1 W h kg⁻¹ at a power density of 0.56 kW kg⁻¹ (close to that of LIBs with organic electrolytes) and a high power density of 16.6 kW kg⁻¹ at an energy density of 223.5 W h kg⁻¹ (comparable to that of supercapacitors with aqueous electrolytes) (Fig. 14h). The high power and energy densities of this aqueous RZB render it a promising candidate for fast-charge batteries in consumer electronics and electric transportations.

The high performance of PANI-based OEMs attracts considerable research interests to exploit new battery configurations

for PANI-based aqueous RZBs. Due to the rapid growth of smart technology and wireless electronic devices, the requirements for thin and flexible batteries that can be designed and fabricated in customized size and shape stimulate the development of battery technology. Liu et al. 131 reported a PANI-based cathode for aqueous RZBs by constructing a π -electron conjugated system between PANI and poly(3,4-ethylenedioxythiophene) polystyrene sulfonate (PEDOT:PSS) on CNTs substrate (named as CNTs-PANI-PEDOT:PSS (t-CNTs-PA-PE)). The -SO₃-H⁺ groups in PSS, as an internal proton reservoir, provide enough H⁺ for PANI's protonation to promote its electrochemical activity and reversibility. Meanwhile, the strong π - π conjugation interaction between PANI and PEDOT:PSS leads to enhanced electronic conductivity (Fig. 15a). The t-CNTs-PA-PE based cathode achieves a high capacity of 238 mA h g^{-1} at 0.2 A g^{-1} , together with excellent cycling stability (113 mA h g^{-1} after 1500 cycles at 10 A g^{-1}) and high rate capability (145 mA h g^{-1} at 10 A g^{-1}) (Fig. 15b). Moreover, the freestanding t-CNTs-PA-PE enables a highperformance flexible RZB, expanding the applications of PANIbased cathode for flexible energy storage devices. In addition,

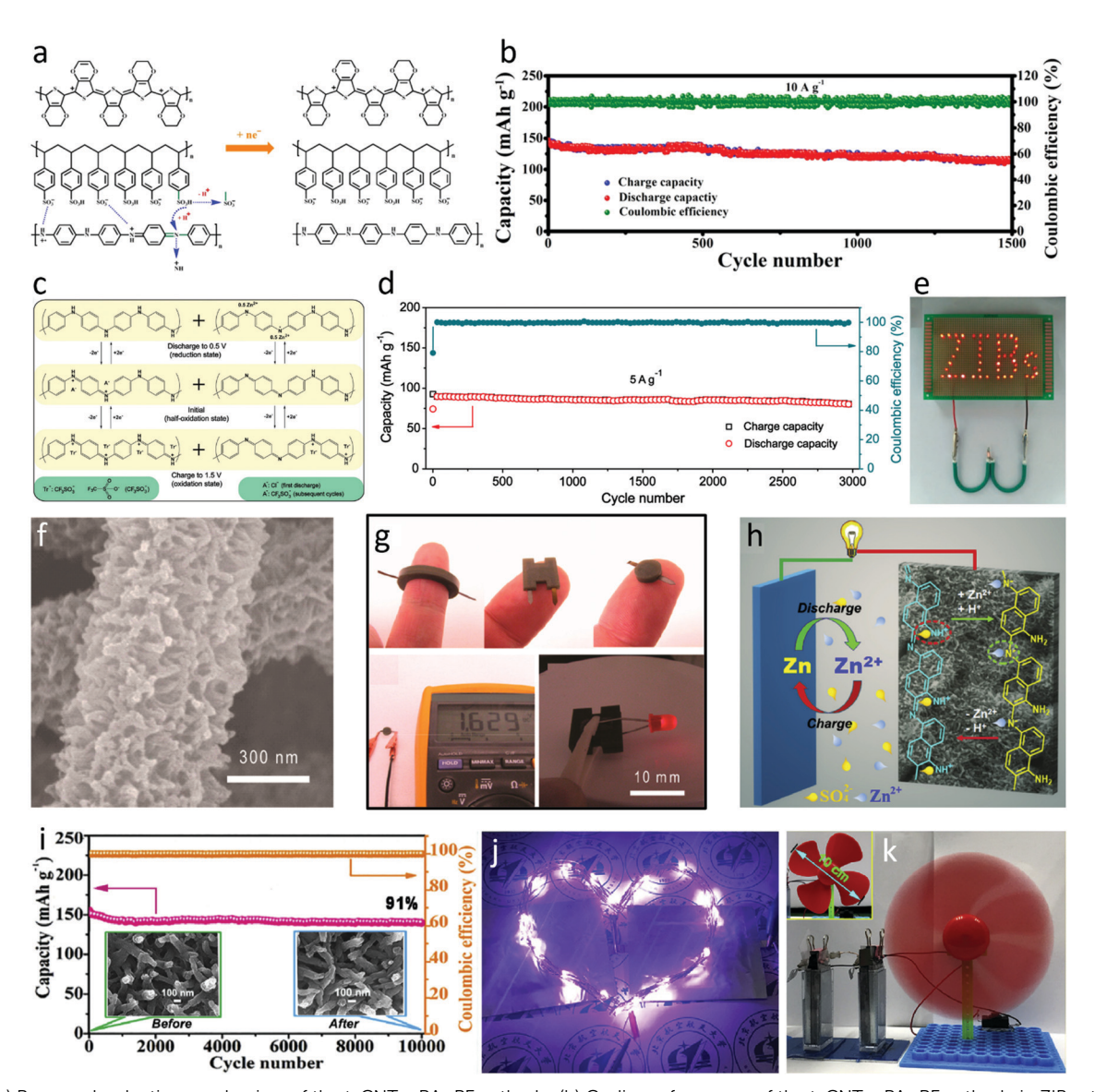


Fig. 15 (a) Proposed reduction mechanism of the t-CNTs-PA-PE cathode. (b) Cyclic performance of the t-CNTs-PA-PE cathode in ZIBs at 10 A g^{-1} . Reproduced with permission. ¹³¹ Copyright 2019 American Chemical Society. (c) The proposed redox mechanism of PANI/CFs. (d) Cycling performance of PANI/CFs at 5 A g^{-1} . (e) An LED array powered by two soft-packaged quasi-solid-state batteries in series and two cable-type quasi-solid-state batteries in series, respectively. Reproduced with permission. ¹³² Copyright 2018 Wiley-VCH Verlag GmbH & Co. KGaA. (f) High-magnification SEM images of the CF mat after PANI coating. (g) Optical images of assembled Zn-PANI batteries in ring-, H-, and cylindrical shapes. Reproduced with permission. ¹³³ Copyright 2018 American Chemical Society. (h) Illustration for the charge storage mechanism of poly(1,5-NAPD). (i) Cycling stability of a typical button-type cell tested at 10 A g^{-1} over 10 000 cycles. The insets depict the poly(1,5-NAPD) nanorods before and after the long-term cycling test. (j) Violet LEDs and (k) electric fan powered up by cells. Reproduced with permission. ¹³⁴ Copyright 2020 Elsevier B.V.

Wan *et al.*¹³² developed an aqueous Zn/PANI battery using PANI/carbon felts (PANI/CFs) as a cathode in 1 M Zn(CF₃SO₃)₂ electrolyte. The Zn(CF₃SO₃)₂ electrolyte passivated the Zn anode to improve the Zn plating/stripping efficiency. Moreover, the bulky $CF_3SO_3^-$ stabilizes the oxidized PANI by decreasing the number of H_2O molecules nearby the oxidized PANI and forming hydrogen bonds with oxidized PANI (Fig. 15c). The resulting aqueous Zn/PANI battery delivers a capacity of 200 mA h g⁻¹ at 0.05 A g⁻¹ with an average discharge voltage of 1.1 V and retains a capacity of 95 mA h g⁻¹ at a high current density of 5 A g⁻¹ with a capacity retention of 92% after 3000 cycles (Fig. 15d). Furthermore, the high conductivity and flexibility

of PANI-coated carbon fiber (PANI/CF) cathodes endow the aqueous Zn/PANI battery with the ability to serve as flexible energy storage devices (Fig. 15e). To further explore the potential of PANI-based cathode for flexible batteries, Kim $et\ al.^{133}$ demonstrated an integrated design and manufacturing method for aqueous RZBs composed of PANI/CF cathodes, laser micromachined Zn anodes, and porous separators (Fig. 15f). The batteries were housed within three-dimensional printed geometries, including rectangular, cylindrical, H- and ring-shapes (Fig. 15g). A small (\sim 8 mm) RZB pack delivers a high capacity of 162 mA h g $^{-1}$ at 1C together with an excellent rate capability of 30 mA h g $^{-1}$ at 234C. This work opens up a door for the

application of polymer-based aqueous RZBs in customized wearable devices. The exceptional electrochemical performance and flexibility of PANI-based cathodes demonstrate that conducting polymers are promising cathode materials for aqueous RZBs.

Due to the success of PANI-based cathodes, other conducting polymers are also being explored for aqueous RZBs. For example, an amino-containing polymer electrode based on poly(1,5-naphthalenediamine) (poly(1,5-NAPD)) was prepared by electrodepositing the polymer onto nanoporous activated carbon (AC) granules. 134 Interestingly, both Zn2+ and H+ can be reversibly inserted into/extracted from poly(1,5-NAPD) during repeated charge/discharge process. Additionally, the helix-structured molecular chains of poly(1,5-NAPD) provide unhindered pathways along the chains for the back-and-forth diffusion of ions upon cycling, resulting in superb cycling stability of RZBs (Fig. 15h). As a result, the poly(1,5-NAPD)-based Zn battery delivers a high capacity of 315 mA h g⁻¹ at 0.19 A g⁻¹, superior rate capability of 145 mA h g⁻¹ at 14.8 A g⁻¹ and excellent cycling stability of 91% capacity retention after 10 000 cycles at 10 A g^{-1} (Fig. 15i). The excellent electrochemical performances are retained even at a high areal mass loading of 20 mg cm⁻², demonstrating great potential for practical application. Moreover, the poly(1,5-NAPD)/ AC composite can also be used as a cathode for flexible quasisolid-state RZBs, providing another candidate for flexible energy storage (Fig. 15j and 15k). In addition to poly(1,5-NAPD), PPY can also be used as a cathode for electrochromic and flexible RZBs. Wang et al. 135 coupled flexible and electrochromic nanostructured PPY cathode with nano-spherical Zn anode and a polyvinyl alcohol (PVA)-KCl-Zn(CH3COO)2 gel electrolyte to form a solid-state rechargeable Zn//PPY battery, which delivers a high capacity (123 mA h g⁻¹ at 1.9 A g⁻¹ within a voltage ranges from 0-1.2 V), fast charge/discharge, high flexibility, and 38% capacity retention after 200 cycles at a high current density of 4.4 A g⁻¹. More importantly, when the flexible Zn battery is under short circuit conditions (i.e., the voltage is 0 V), the color of the battery turns yellow immediately, enabling the safety diagnosis of this Zn//PPY battery to avoid battery short circuit. Polyindole is another type of conducting polymer, exhibiting a higher redox potential, slower degradation rate, and higher electrical conductivity in comparison to PANI and PPY in aqueous RZBs. During the charge/discharge process, the chloride anion is reversibly inserted into/extracted from polyindole to react with the nitrogen in the secondary amine. Cai et al. 136 made a polyindole-based Zn battery, which achieves a discharge capacity of 60-80 A h kg⁻¹ at a current density of 200-1000 A m⁻². Furthermore, the same group utilized an electrospinning technique for the fabrication of poly(5-cyanoindole) fibers as a cathode in aqueous RZBs. It delivers a higher capacity (107 A h kg⁻¹ at 0.2C), better cycling stability (75% capacity retention after 800 cycles at 0.2C), and rate capability (61 A h kg⁻¹ at 10C) than polyindole.137 The exceptional performance of conducting polymers in aqueous RZBs demonstrates that the p-type OEMs based on anion insertion mechanism are promising for developing affordable, sustainable, and environmentally benign energy storage devices.

Conducting polymers can also be used as additives to improve the electrochemical performance of redox-active inorganic cathode materials for aqueous RZBs. Manganese dioxide (MnO₂) and vanadium oxide are the most common inorganic cathode materials for aqueous RZBs due to their high theoretical capacity, low cost, and low toxicity. However, the MnO₂ cathode suffers from substantial phase change during cycling, leading to poor cyclic stability. Intercalating a guest polymer into the layered MnO₂ has proven to be a promising approach to strengthen the extended layered structure. Huang et al. 139 inserted PANI into MnO2 nanolayers to form a mesoporous structure through an interface reaction, which avoids phase transformation and achieves a stable cyclic performance in aqueous RZBs (Fig. 16a). The as-prepared PANI-intercalated MnO2 nanolayers exhibit a high capacity of 280 mA h g^{-1} at 0.2 A g^{-1} together with a high rate capability (110 mA h g^{-1} at 3 A g^{-1}) and 90% capacity retention after 200 cycles (Fig. 16b). In contrast to MnO2, the performance of vanadium oxide cathode strongly relies on the interlayer spacing distance. The large molecular weight and volume of Zn2+ will lead to an unstable structure change of vanadium oxide upon repeated Zn²⁺ insertion and extraction. The organic/inorganic hybrid materials with extended interlayer spacing and reinforced layered structures facilitate the Zn²⁺ storage and improve the cycle life. Bin et al. 140 designed an organic-inorganic intercalated layered composite based on 3,4-ethylenedioxythiophene (PEDOT) and ammonium vanadate oxide (NVO) (Fig. 16c). The interplanar spacing of the crystal lattice for NVO is effectively enlarged (10.8 Å) by the intercalation of PEDOT, leading to improved mobility of Zn²⁺ in the crystal lattice. As a result, the PEDOT-NVO cathode presents a high capacity (356.8 mA h g⁻¹ at 0.05 A g⁻¹), superior cycling stability (capacity retention of 94.1% after 5000 cycles at 10 A $\rm g^{-1}$), and excellent rate capability (163.6 mA h $\rm g^{-1}$ at 10 A $\rm g^{-1}$) (Fig. 16d). In addition to the PEDOT-NVO cathode, Liu et al. 143 synthesized a PANIintercalated V2O5 (PVO) with an enlarged interlayer distance of 13.9 Å to further facilitate the insertion/extraction kinetics of Zn²⁺ (Fig. 16e). The resultant PVO-base RZBs deliver a high capacity of 375.2 mA h g⁻¹ at 0.05 A g⁻¹ and a high rate capability of 197.1 mA h g⁻¹ at 20 A g⁻¹ (Fig. 16f), together with excellent cycling stability of 95.3% capacity retention after 1000 cycles at 10 A g⁻¹ (Fig. 16g). The exceptional electrochemical performance of organic/inorganic hybrid materials demonstrates a promising research direction of using conducting polymers to enhance the performance of inorganic aqueous RZBs.

3.4.2. Carbonyl monomer and polymer. Quinone monomers and polymers as universal OEMs for various MRBs are also widely used in aqueous RZBs. Kundu et al. 145 reported a quinone monomer, tetrachloro-1,4-benzoquinone (p-chloranil), as a cathode for aqueous RZBs. The DFT calculations indicate that the molecular columns in p-chloranil undergo a twisted rotation to accommodate Zn²⁺. Due to this phase transformation, taking place at the boundary of the solid and liquid phase, unrestricted growth of the charged/discharged phases occurs, compromising the electrochemical behavior of p-chloranil (Fig. 17a). To prevent the unrestricted phase change, p-chloranil

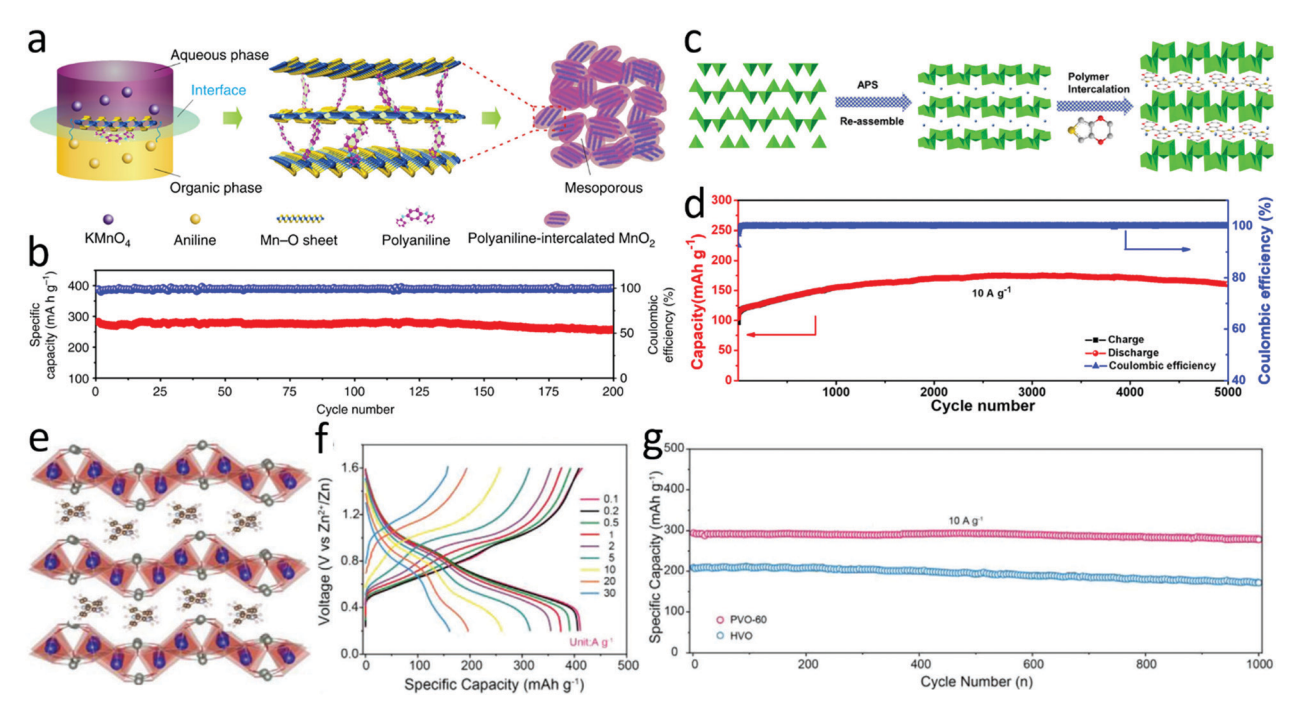


Fig. 16 (a) Schematic illustration of the expanded intercalated structure of polyaniline (PANI)-intercalated MnO₂ nanolayers. (b) Cycling performance in terms of specific capacity (red) and the corresponding Coulombic efficiency (blue) at a current density of 200 mA g⁻¹. Reproduced with permission. ¹³⁹ Copyright 2018 Springer Nature. (c) Schematic illustration of the preparation process of PEDOT-intercalation NVO-layered material. (d) Long-term cycling performance of the Zn/PEDOT-NVO battery at 10 A g^{-1} . Reproduced with permission. ¹⁴⁰ Copyright 2020 Elsevier Inc. (e) Schematic illustration of PANI intercalated V₂O₅. (f) Charge-discharge curves of PVO-60 at the indicated current densities. (g) Cycling performance of PVO-60 and HVO at 10 A g⁻¹. Reproduced with permission. A g⁻¹. Reproduced with permission. A g⁻¹. Reproduced with permission.

was confined inside nanochannels of mesoporous carbon (CMK-3), which restricts the growth of discharge/charge phases, and thus significantly enhances the electrochemical reversibility and cyclability. The resultant p-chloranil/CMK-3 cathode shows a high capacity of 170 mA h g^{-1} at 0.2C (1C = 217 mA g^{-1}) and retains a reversible capacity of 90 mA h g⁻¹ after 100 cycles (Fig. 17b). This work not only provides fundamental insights for the phase structure evolution but also offers guidance for the rational structure design of advanced OEMs. In addition to p-chloranil, other quinone monomers were also reported as promising cathodes for aqueous RZBs. Zhao et al. 146 reported a series of quinones with carbonyl groups at para-positions (1,4-naphthoguinone (1,4-NQ), 9,10-anthraguinone (9,10-AQ), and calix[4]quinone (C4Q)) and ortho-positions (1,2-naphthoquinone (1,2-NQ) and 9,10- phenanthrenequinone (9,10-PQ)) as cathodes for aqueous RZBs (Fig. 17c). The results indicate that the quinones with carbonyl groups at para-positions deliver higher capacity and lower charge/discharge gap than those with carbonyl groups at ortho-position. Among the monomers, C4Q, with a bowl-like structure, shows small steric hindrance. Moreover, the carbonyl groups at para-positions in C4Q are more favorable for Zn²⁺ ion uptake due to the lower electrostatic potential (ESP) than the ortho-position carbonyl groups (Fig. 17d). Consequently, the C4Q cathode displays a low potential hysteresis of 70 mV and a high capacity of 335 mA h $\rm g^{-1}$ at 20 mA $\rm g^{-1}$, corresponding to the uptake of three Zn²⁺ ions and utilization of six carbonyl groups. More importantly, the C4Q-based RZBs with the Nafion membrane delivers high cycling stability (a capacity retention

of 87% after 1000 cycles at 500 mA g⁻¹) and decent rate capability (172 mA h g^{-1} at 1000 mA g^{-1}) owing to the ion-selective Nafion membrane, which blocks the diffusion of $C4Q^{2x-}$ anions from the cathode to the anode. However, the Nafion separator is unfeasible for flexible devices. To overcome this challenge, it is of great importance to use insoluble OEMs in aqueous RZBs such as quinone polymers. Hence, Guo et al.147 proposed a pyrene-4,5,9,10-tetraone (PTO)-based RZB using conventional porous glass fiber membrane as the separator (Fig. 17e). The PTObased RZBs deliver a remarkably high capacity (336 mA h g⁻¹ at 0.04 A g⁻¹), excellent cycling stability (a capacity retention of 70% after 1000 cycles at 3 A g⁻¹), and a high rate capability (113 mA h g^{-1} at 20 A g^{-1}) (Fig. 17f). For practical application, a flexible belt-shape PTO//Zn battery was fabricated and provided a high capacity of 337 mA h $\rm g^{-1}$ at 0.04 A $\rm g^{-1}$ and an excellent rate capability of 122 mA h g^{-1} at a high current density of 10 A g^{-1} . Therefore, the polymerization of small carbonyl compounds is an effective approach to reduce the solubility of carbonyl monomers and enhance their electrochemical performance. Another example 148 for carbonyl polymers is the poly(benzoquinonyl sulfide) (PBQS), which was employed as a cathode in RZBs with 3 M Zn(CF₃SO₃)₂ aqueous electrolyte. As we discussed before, the bulky CF₃SO₃ anions can decrease the number of water molecules surrounding the Zn2+ cations and reduce the solvation effect, facilitating Zn2+ charge transfer. Owing to the fast reaction kinetics of the benzoquinone units and the high ionic conductivity of the aqueous electrolyte, the resultant PBQS cathode exhibits a high specific capacity of 203 mA h g⁻¹ at 0.1C

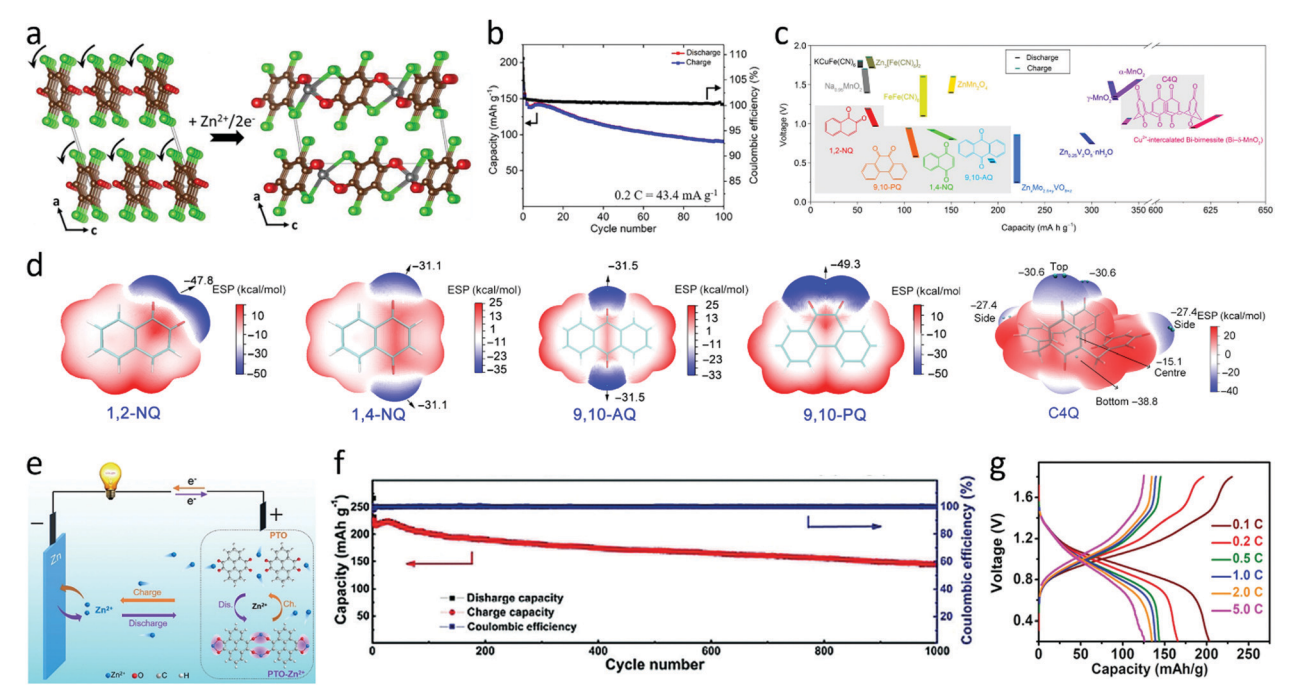


Fig. 17 (a) Structural models of p-chloranil and Zn-p-chloranil ($Zn \cdot C_6Cl_4O_2$) as obtained from DFT structural optimization. The curved arrows in (a) show the direction of the rotation of the p-chloranil molecular columns upon Zn^{2+} insertion. Color code: C (brown), Cl (green), O (red), and Zn (gray). (b) Galvanostatic cyclability and corresponding Coulombic efficiency of the p-chloranil infused CMK-3 electrode at 0.2C (1C: 217 mA g⁻¹). Reproduced with permission. 145 Copyright 2018 American Chemical Society. (c) Discharge/charge voltages and capacities of selected quinone compounds (1,2-NQ, 1,4-NQ, 9,10-PQ, 9,10-AQ, and C4Q) in agueous ZBs. (d) The ESP- mapped molecular van der Waals surface of 1,2-NQ, 1,4-NQ, 9,10-AQ, 9,10-PQ, and C4Q. Surface local minima of ESP are represented as blue spheres, and the corresponding ESP values are marked out by numbers. Reproduced with permission. 146 Copyright 2018 American Association for the Advancement of Science. (e) Illustration of the reversible reaction mechanism of the aqueous PTO//Zn battery. (f) Cycle stability at a current density of 3 A g^{-1} . Reproduced with permission. ¹⁴⁷ Copyright 2018 Wiley-VCH Verlag GmbH & Co. KGaA. (g) Typical discharge/charge curves of aqueous Zn-PBQS batteries. Reproduced with permission. 148 Copyright 2018 the Partner Organizations.

 $(1C = 200 \text{ mA g}^{-1})$ with an average discharge voltage of 0.95 V, good capacity retention of 86% after 50 cycles at 0.2C, and a high rate capability of 126 mA h g^{-1} at 5C (Fig. 17g). Apart from PBQS, polydopamine (PDA) with low water solubility, low cytotoxicity, and high bio-adhesion nature was also used as a cathode in aqueous RZBs. Yue et al. 151 developed a flexible free-standing PDA/CNTs film by spontaneous polymerizing PDA on CNTs, followed by a vacuum-filtering processes. The resultant PDA/ CNTs cathode delivers a specific capacity of 126.2 mA h g⁻¹ at 0.02 A g⁻¹ and retains a reversible capacity of 80 mA h g⁻¹ after 500 cycles. The exceptional electrochemical performance renders quinone polymers promising cathode materials for highperformance, low-cost, sustainable and flexible aqueous RZBs.

In addition to quinones, other types of carbonyl monomers and polymers can also be used for aqueous RZBs. As typical conjugated carbonyl monomers, NTCDA and 1,4,5,8-naphthalene diimide (NTCDI) were employed as cathodes for aqueous RZBs. However, the large size of oxygen in the anhydride group of NTCDA and the existence of insertion/extraction of hydronium hinder the reversible reaction between Zn2+ and C=O bonds, leading to poor electrochemical performance. Replacing oxygen in the anhydride group with nitrogen to generate NTCDI facilitates the Zn2+ ion diffusion and reaction kinetics because the NTCDI molecules with smaller crystal size can effectively increase the contact possibility for Zn²⁺ and C=O bonds (Fig. 18a). 152 As a result, the NTCDI-based cathode delivers a high capacity of 240 mA h g⁻¹ at 0.1 A g⁻¹, with 73.7% capacity retention after 2000 cycles and superior rate capability of 140 mA h g^{-1} at 2 A g^{-1} (Fig. 18b and 18c). The excellent electrochemical performance of NTCDI confirms that chemical structure optimization is an effective way to enhance the performance of OEMs. Besides that, polymerizing the small organic compounds to make insoluble polymer is another way to improve the electrochemical performance of OEMs. A dianhydride-based polymer, poly 3,4,9,10-perylentetracarboxylic dianhydride (PPTCDA), shows high promise as a cathode for aqueous RZBs but suffers from low electronic conductivity. To improve the conductivity of the PPTCDA cathode, Cang et al. 153 used a one-step synthesis method to prepare a binder-free and conductive additive-free PPTCDA/ graphene aerogel (GA) (PPTCDA/GA) cathode for RZBs with 2 M ZnSO₄ aqueous electrolyte. The PPTCDA/GA cathode delivers a high capacity of 281 mA h g⁻¹ at 0.1 A g⁻¹ together with an excellent capacity retention of 99% after 300 cycles and a superior rate capability of 102 mA h g^{-1} at 1 A g^{-1} . The ex situ FT-IR and X-ray photoelectron spectroscopy (XPS) results indicate that the zinc ion intercalation in PPTCDA converted the carbonyl groups (C=O) into enolate groups. Also, the intercalation/de-intercalation process of Zn ion in PPTCDA/ GA cathode does not compromise the structure of GA. The excellent structure integrity contributes to the high cycling

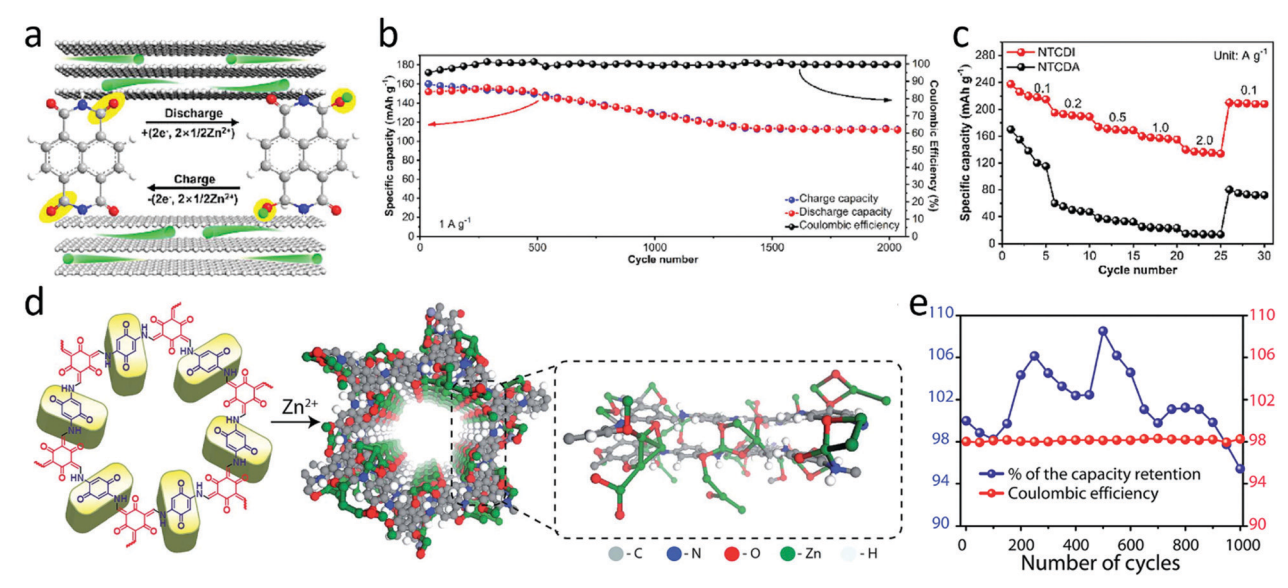


Fig. 18 (a) Electrochemical redox mechanism of NTCDI for ZIBs. (b) Cycling performance of NTCDI at 1 A g^{-1} . (c) Comparison of rate performance of NTCDI and NTCDA. Reproduced with permission. 152 Copyright 2019 Wiley-VCH Verlag GmbH & Co. KGaA. (d) The electrochemical oxidation of hydroquinone to guinone in HgTp. (e) Long-life cyclic stability and CE plot of Zn/HgTP cell at 3.75 A g⁻¹. Reproduced with permission. ¹⁵⁴ Copyright 2019 The Royal Society of Chemistry.

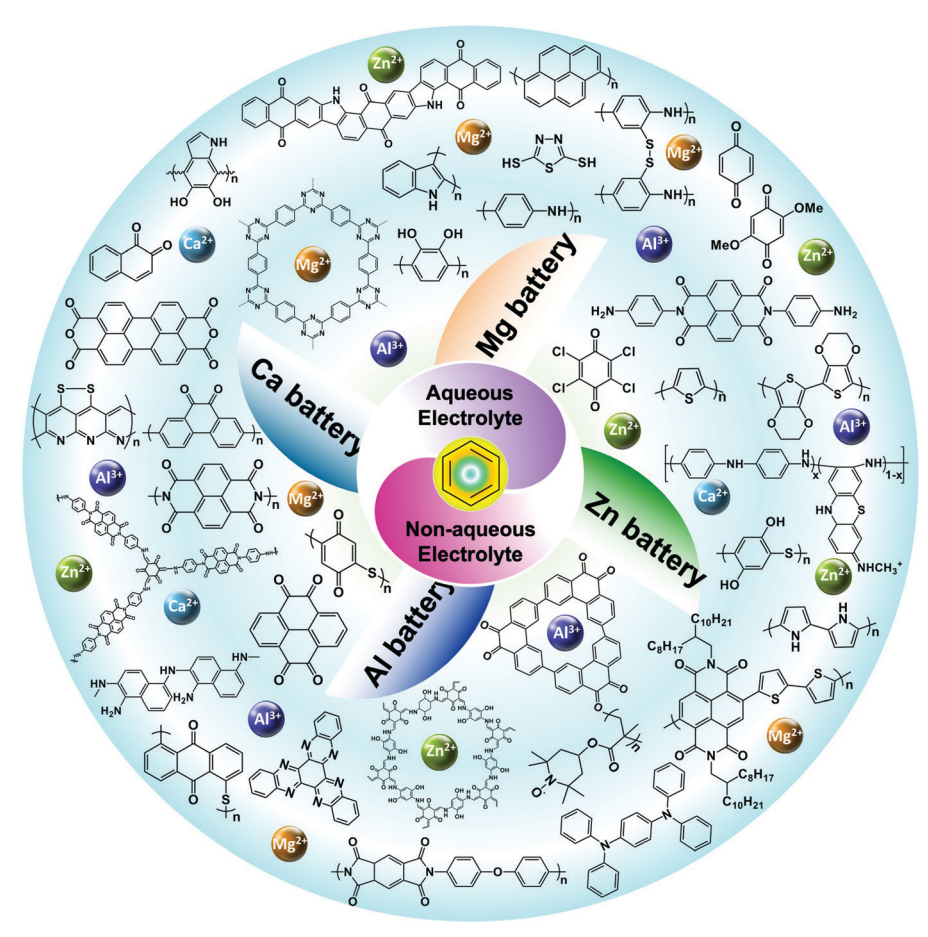
stability of PPTCDA/GA cathode. To further improve the electrochemical performance in aqueous RZBs, the large surface area and porous COFs offer opportunities. However, there are only a few reports about the electrochemical storage of Zn²⁺ ion in COFs. Khayum et al., 154 for the first time, utilized hydroquinone linked β-ketoenamine COF (HqTp) as a cathode material in aqueous RZBs. The electron-rich backbone in HqTp facilitates the efficient interaction between the COF and Zn²⁺ ions (Fig. 18d). Due to the strong interaction between O/N in COF and Zn²⁺ ions, as well as the well-defined nanopores and structural organization, the HqTp cathode exhibits an excellent capacity of 276 mA h g⁻¹ at 125 mA g⁻¹ and superior cycling stability of 95% capacity retention after 1000 cycles at 3.75 A g⁻¹ (Fig. 18e). The superior electrochemical performance of carbonyl monomers and polymers further confirms that OEMs are promising for developing high-performance, affordable, sustainable and environmentally benign aqueous RZBs. More research efforts are demanded to exploit porous polymers, COFs, and metal organic frameworks to further enhance the performance of aqueous RZBs.

3.4.3. Other redox-active polymers. Another type of promising polymers for aqueous RZBs is the nitroxide radical polymer, which is a category of p-type OEMs with high reaction potentials. For example, polyacrylamide, a well-known hydrophilic soft material in the biological, medical, and agricultural fields, can also be used in aqueous RZBs due to the rapid, reversible, and stoichiometrical redox property of 2,2,6,6-tetramethylpiperidin-1-oxyl-4-yl (TEMPO) groups. Koshika et al. 155 investigated a hydrophilic radical polymer, poly(2,2,6,6-tetramethylpiperidinyloxy-4-yl vinyl ether) (PTVE), as a cathode in RZBs with 0.1 M ZnCl₂-NH₄Cl aqueous electrolyte. The PTVE-based cathode exhibits a discharge capacity of 131 mA h g-1 and 65% capacity retention after 500 cycles. To further improve the hydrophilic property of the polymer in aqueous electrolyte, the same research group 156

designed and synthesized a water-swellable polyacrylamidebased radical polymer, poly(2,2,6,6-tetramethylpiperidinyloy-4yl acrylamide) (PTAm). The PTAm-based aqueous RZBs displays an output voltage of 1.2 V, an excellent cycle life of 2000 cycles, and a fast charge capability up to 60C. In addition to the nitroxide radical polymers, there is also another category of p-type polymers such as thioether-based polymers. Häupler et al. 157 reported a novel poly(acetylene)-based polymer, poly(9,10-di(1,3dithiol-2-ylidene)-9,10-dihydroanthracene) (PexTTF), as a cathode material in aqueous RZBs. It delivers a high capacity of 128 mA h g⁻¹ at 20C with an average discharge voltage of 1.1 V, and excellent cycling stability of 1000 cycles at 120C and 10000 cycles at 10C, as well as superior rate capability up to 120C. The exceptional performance of these p-type polymers in aqueous RZBs sheds lights on the development of affordable, sustainable and environmentally benign energy storage devices. More efforts are demanded to enhance the specific capacity of p-type polymers by reducing the molar mass of the repeating units and incorporating more redox-active centers in the polymers.

4. Summary and outlook

OEMs are universal electrode materials for affordable, sustainable, and environmentally benign MRBs, including nonaqueous Mg/Al/Zn rechargeable batteries and aqueous Mg/Al/ Zn/Ca rechargeable batteries (Fig. 19). In the carbonyl-based OEMs (n-type OEMs), a pair of carbonyl groups (-C=O) connected by a conjugated structure undergoes a two-electron reduction process to yield a dianion with intramolecular electron transfer, when interacting with cations (Mg²⁺, AlCl²⁺, AlCl₂+, Ca²⁺ or Zn²⁺). Likewise, imine groups (-C=N-) in



The schematic illustration for the application of OEMs in non-aqueous and aqueous rechargeable Mg/Al/Zn/Ca batteries.

imine-based OEMs (n-type OEMs) can reversibly gain and lose electrons during the discharge/charge process due to the reversible reaction between N in the imine group and multivalent cations. Different from carbonyl and imine compounds, disulfide-based OEMs (n-type OEMs) do not show intramolecular electron transfer when interacting with cations. Instead, disulfide-based OEMs undergo reversible cleavage and regeneration of disulfide bonds during the interaction with cations, corresponding to electrochemical reduction and oxidization between disulfide and thiolate. In p-type OEMs, such as amine-based OEMs, an amine group loses one electron to generate a N cation during the charging process. Meanwhile, the anion, TFSI or Cl, can simultaneously associate with the cation to balance the charge. During the discharge process, the cation gains one electron, followed by the disassociation with the anion. The low electronic conductivity and high solubility of OEMs in an organic electrolyte are two major challenges for organic MRBs. Polymerizing the redox-active compounds to achieve long-term π -conjugated structure has been demonstrated as an effective method to enhance the intrinsic electronic conductivity and suppress the dissolution of the OEMs in the electrolyte. Another approach to circumvent these challenges is to attach the OEMs to insoluble inorganic substrates such as carbons and SiO₂ nanoparticles, which stabilize the OEMs at the price of decreasing the overall capacity of the

electrodes. After considerable contributions from scientists in the last decade, a large number of OEMs were employed as electrodes in MRBs with long cycle life and high-power density. Though remarkable progress has been made for organic MRBs, the electrochemical performance of MRBs is still not comparable to commercial LIBs because of the low reaction potential and low capacity of OEMs. More efforts are necessitated to probe new materials and chemistries for organic MRBs. Future research should focus on the design and synthesis of high reaction potential and high capacity OEMs to achieve low-cost, high-energy, safe, and stable MRBs.

To shed light on the development of advanced OEMs in MRBs, it is pivotal to understand the correlation between molecular structure and electrochemical performance. As we discussed in this review, a large variety of OEMs are used in non-aqueous RMBs, RABs, and aqueous RZBs, thus we used the OEMs in these three types of MRBs as representatives to gain fundamental insights into the relationship between structure and performance. In Fig. 20, we correlate the electrochemical behaviors of the OEMs such as the average discharge voltage, discharge capacity, and cycle life to the molecular structure and chemical composition. The key goal is to provide guidance for the rational structure design and performance optimization in organic MRBs. In OEMs for non-aqueous RMBs, there are six types of functional groups, including carbonyl, imine,

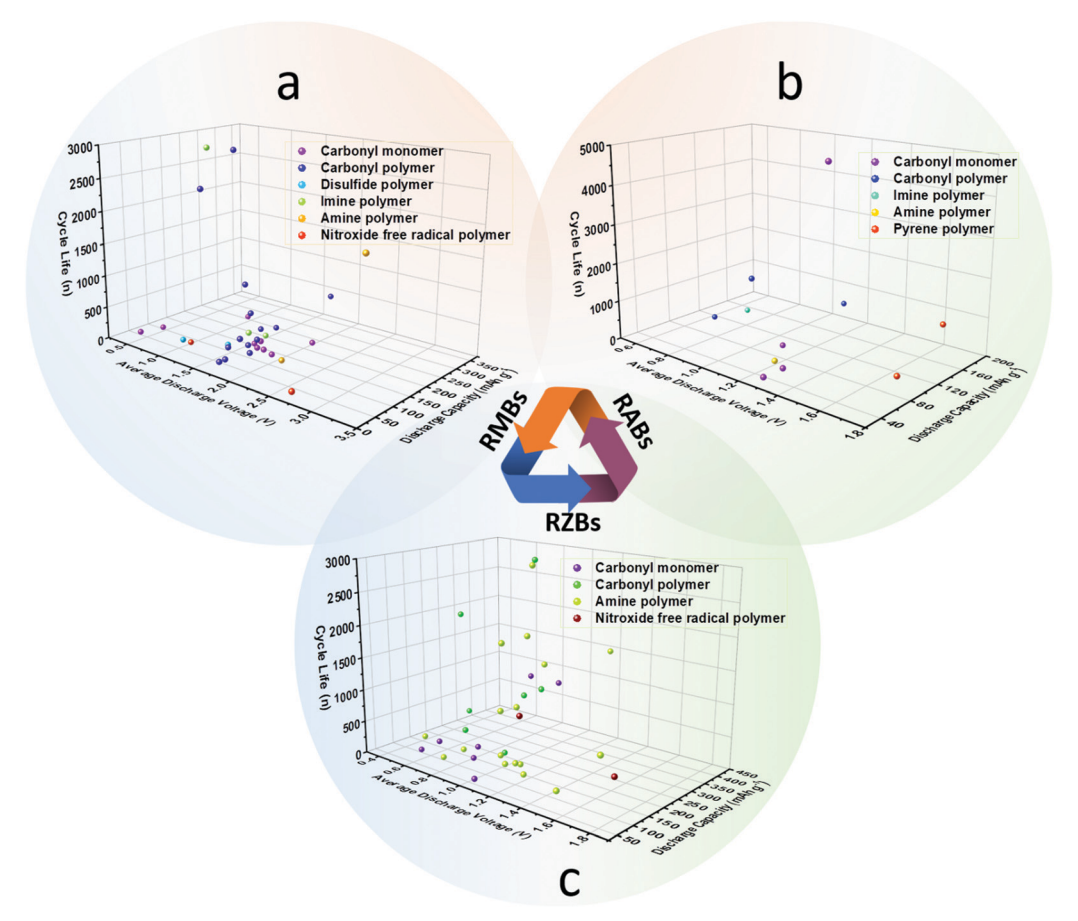


Fig. 20 The summary of discharge capacity, average discharge voltage, and cycle life of OEMs in (a) non-aqueous RMBs, (b) non-aqueous RABs, and (c) aqueous RZBs

disulfide, organosulfur, nitroxide free radical, and secondary/ tertiary amine groups. As shown in Fig. 20a, carbonyl-based monomers and polymers represent the majority of OEMs in non-aqueous RMBs. Most carbonyl group-based small molecules suffer from poor cycle life due to the high solubility in the electrolyte, but increasing the molecular weight to form highmolecular-weight organic compounds or polymers could enhance the cycle life to over 1000 cycles, demonstrating that polymeric materials are promising cathodes for non-aqueous RMBs. The tertiary amine-based polymers and imine-based polymers also exhibit stable cycle life of thousands of cycles. Analogous to non-aqueous RMBs, the high-molecular-weight and polymeric OEMs also show superior cyclic stability in nonaqueous RABs (Fig. 20b), confirming that increasing the molecular weight of OEMs is an effective method to fulfill stable organic MRBs. To further improve the electrochemical performance, the porous COFs and MOFs offer new opportunities. The porous structure and large surface area of these polymeric materials increase the electroactive sites and shorten the multivalent cation diffusion pathways, facilitating the reaction kinetics of the batteries. Nevertheless, the reaction potentials of most n-type OEMs containing carbonyl, imine, and disulfide groups are lower than 2.0 V versus Mg/Mg²⁺ and 1.5 V versus Al/Al³⁺. To obtain high potential cathodes, the p-type OEMs

containing nitroxide free radical, amine groups, and pyrene are promising candidates because the anion insertion mechanism provides high reaction potentials in non-aqueous RMBs and RABs (Fig. 20a and b). Therefore, the design and synthesis of p-type polymer cathodes offer opportunities for high reaction potential and long cycle life organic non-aqueous RMBs and RABs.

The correlation between electrochemical behaviors of the OEMs in aqueous RZBs containing carbonyl, imine, secondary/ tertiary amine groups, and their molecular structure is summarized in Fig. 20c. Analogous to non-aqueous RMBs and RABs, the high-molecular-weight organic compounds and polymers display better cycle life in aqueous RZBs as well. Two polymers (PexTTF and P(DA70-stat-SSA30) in Table 8), which are not included in Fig. 20c, even show stable cycle life of 10 000 and 50 000 cycles, confirming the exceptional cyclic stability of polymers. Due to the high redox potential of Zn anode (2.28 V versus Li/Li⁺), most carbonyl group-based OEMs show low reaction potential (≤ 1 V). To overcome this challenge, introducing electron-withdrawing functional groups into the OEMs could enhance the reaction potentials, and employing p-type OEMs as cathodes can also increase the reaction potentials due to the anion insertion mechanism. Therefore, the design and synthesis of anion insertion-based

p-type polymer cathodes are also promising for high-reactionpotential and long-cycle-life aqueous RZBs.

Another challenge of OEMs in MRBs is the low specific capacity, which limits the energy density of organic MRBs. Increasing the molecular weight of organic compounds and polymers decreases the solubility and enhances the cyclic stability of organic MRBs, but it also leads to a low specific capacity. The ratio of the number of active redox centers to the molecular weight of an organic compound or repeating unit in the polymer determines the theoretical specific capacity of OEMs. To enhance the specific capacity, an effective method is to incorporate multi-electroactive centers in one organic framework, which increases the active redox centers per organic compound or repeating unit in the polymer. However, the specific capacity of OEMs in MRBs is lower than the theoretical capacity due to the low electronic conductivity and moderate reaction kinetics. To improve the conductivity, there are three strategies: (1) enlarging long-term π conjugated structure in OEMs, which facilitates the electron transfer in the organic framework; (2) employing π - π stacking interaction between OEMs and carbon materials such as graphene and carbon nanotubes. The high conductivity and insolubility of carbon materials not only promote the electron transfer but also alleviates the dissolution of OEMs; (3) synthesizing large surface area porous OEMs, which provide more active sites for the electrochemical reaction and shorten the ion diffusion pathways. With the increased conductivity, specific capacity, and rate capability, OEMs will be remarkably improved for developing high-energy and high-power MRBs. However, the energy density of state-of-the-art OEMs is still lower than the inorganic counterparts, organic MRBs are promising alternatives to LIBs and LABs for grid-scale stationary energy storage, where cost, cycle life, and environmental impact are more critical than energy density. Developing lithium-free and cobalt-free battery technology based on low-cost and abundant organic/polymer materials and multivalent metals (Mg/Al/Zn) could enhance the sustainability, affordability, and environmental benignity of energy storage devices. Therefore, searching for high potential, high capacity, and high stability polymeric cathode materials is essential for the development and applications of MRBs.

Though the development of organic MRBs is slower than LIBs and other inorganic battery systems, the demand for affordable, sustainable, and environmentally benign energy storage devices attracts enormous research interests toward this field. There are still several challenges that need to be solved before we can obtain exceptional OEMs. Promising approaches to overcome these challenges could draw inspirations from recent investigations on the design and synthesis of advanced OEMs in alkali-ion batteries due to the universal nature of organic electrodes in various rechargeable batteries. For example, a further increase of reaction potential and specific capacity of organic MRBs can be achieved by tuning the molecular structure and electron-withdrawing functional groups or cation (Mg²⁺) substitution.

In addition to develop advanced OEMs, the electrolyte also plays a critical role in optimizing the electrochemical performance of organic MRBs. Here, we have summarized the promising electrolytes for non-aqueous and aqueous MRBs to guide the other researchers in this field. The electrolytes in aqueous MRBs are more cost-effective than those in non-aqueous MRBs. In aqueous RMBs, MgSO₄ and Mg(NO₃)₂ are suitable salts to achieve long cycle life aqueous RMBs, while AlCl₃ and Ca(NO₃)₂ are the promising electrolyte salts for aqueous RABs and RCBs, respectively. The lowcost and abundant ZnSO₄ salt is promising for high-performance aqueous RZBs, and Zn(CF₃SO₃)₂ also demonstrates potential as an electrolyte salt for high capacity and stable aqueous RZBs. To date, OEMs in non-aqueous RZBs using 0.5 M Zn(CF₃SO₃)₂/DMF electrolyte deliver the best cycle life of 20000 cycles, while Mg(TFSI)2 in an ether-based electrolyte is promising for nonaqueous RMBs, because it enables reversible Mg2+ storage and enhances the energy density. In non-aqueous RABs, the electrolyte composed of AlCl3 and ionic liquid (EMIC) is widely used and enables reversible electrodeposition of metallic Al on the anode. However, the high cost of EMIC restricts its practical application. Deep eutectic solvents, as ionic liquid analogs formed by mixing a strong Lewis acidic metal halide with a Lewis basic ligand, have gained significant attention due to their low cost and comparable physical and electrochemical properties. 158-161 Due to the strong intermolecular interaction between different components, deep eutectic solvents provide various advantages, such as high safety, high structural flexibility, and excellent thermal and chemical stability, becoming a new class of cost-effective ionic liquids for electrochemical energy storage. 162-164 After Abood et al. 165 first synthesized deep eutectic solvents by mixing AlCl₃ and an oxygen donor amide ligand such as urea or acetamide, AlCl₃-based deep eutectic solvents have been successfully applied in RABs. 166-171 In the deep eutectic solvent-based electrolyte, the [AlCl₂·nAmide]⁺ cations enable the reversible Al plating/stripping. 172,173 While most RABs based on deep eutectic solvent use graphite as the cathode, they also have great potential for applications in non-aqueous organic RABs.

Although great progress has been achieved, there are still some challenges with the current scientific research and practical applications of organic MRBs: (1) large amounts of conductive carbons (usually 30 wt% or more) are added in the organic electrode due to the low electronic conductivity of OEMs, decreasing the capacity and energy density of organic MRBs. In addition, some expensive carbon materials, such as CNTs and graphene, are used to enhance the conductivity of the organic electrode, increasing the cost of MRBs; (2) the relatively low reaction potential of OEMs, especially n-type OEMs, decreases the energy density of MRBs; (3) the low tapped densities of OEMs caused by the presence of light elements (C, H, O, N, and S) result in the low volumetric energy density of MRBs; (4) the synthetic procedure of some high-performance OEMs such as carbonyl and imine polymers is very time- and energy-consuming, enhancing their production cost.

To promote the development of OEMs for practical applications, we outline several possible directions for advanced OEMs in MRBs. (1) Employing molecular engineering for the combination of OEMs and conductive substrates, which can dramatically improve the electronic conductivity and rate capability to achieve fast charge batteries; (2) the complex cation, $AlCl^{2^+}$ or $AlCl_2^+$ rather than Al^{3^+} , involves in the electrochemical redox reaction of RABs, lowering the battery energy density. Novel organic electrolytes and further structural optimization of OEMs are required to achieve Al^{3^+} redox reaction and improve the energy density of organic RABs; (3) despite the various characterization techniques that have been applied to research the charge storage mechanisms of OEMs in MRBs, additional methods including *in situ* TEM and CryoEM, are still needed to provide a clearer understanding of the structural changes of OEMs during the charge/discharge process; (4) in MRBs, the transport of multivalent ions between the electrolyte and OEMs occurs during the charge/discharge processes, more research efforts are demanded to understand the interfacial properties and achieve stable and ionic conductive SEI layer for high-performance organic MRBs.

Advancing technologies greatly promote the development of scientific research. The traditional process of developing new materials uses the trial-and-error method and involves cumbersome experimental steps, a long development cycle, and a vast amount of resources. To date, by relying on artificial intelligence (AI), computational chemistry has become increasingly predictive in a variety of applications, such as energy harvesting and storage, catalyst, and drug design. 174 A subfield of AI that has attracted considerable research interest in recent years is machine learning, which relies upon statistical algorithms and builds a model to make predictions without human intervention. The basic steps involved in the construction of a model are data collection, data representation, choice a learner, and model optimization. 175 Organics are among the first subjects which have the potential of computational methods in laboratory practice. 176 Machine learning can automate discovery, synthesis, and characterization of new compounds, including OEMs. The use of machine learning in molecular chemistry is quite advanced because molecules can be easily described in a manner amenable to algorithmic interpretation. 177,178 Hence, the search for improved OEMs can be accelerated by machine learning through the following routes: (1) standardized databases. The basis of machine learning is in the vast amount of knowledge in databases that already exist. Although there has been a wealth of scientific literature on OEMs, it is difficult to automatically extract due to the proliferation and heterogeneous nature of different journals and databases. Publicly accessible structure and property databases can be established to improve the interoperability between data and metadata.¹⁷⁹ (2) Text mining. Compared to a similar area, image recognition, which has millions of input datasets, high-quality data points in chemistry or materials are often limited to thousands. Text mining, especially high precision text mining from smaller datasets, needs to be developed to increase the model accuracy of machine learning. 180 (3) Quantum learning. Compared with classical computing which processes bits that are either 1 or 0, quantum learning can process qubits that are both 1 and 0 at the same time using the quantum superposition states, which can further accelerate the extraction of information from databases. 181,182 This new generation of machine learning has an enormous potential to promote OEMs development.

There are plenty of approaches to further improve the battery performance of OEMs. With the rapid growth of smart technology and grid-scale energy storage, the opportunities and applications of advanced MRBs will promote the development of cost-effective and environmentally benign OEMs.

Conflicts of interest

The authors declare no competing interests.

Acknowledgements

This research was supported by the US National Science Foundation Award No. 2000102 and the George Mason University, College of Science Postdoctoral Fellowship. The authors also acknowledge the support from the George Mason University Quantum Science & Engineering Center.

References

- 1 Y. Lu and J. Chen, Nat. Rev. Chem., 2020, 4, 127-142.
- 2 Y. Lu, Q. Zhang, L. Li, Z. Niu and J. Chen, Chem, 2018, 4, 2786–2813.
- 3 T. B. Schon, B. T. McAllister, P. F. Li and D. S. Seferos, *Chem. Soc. Rev.*, 2016, 45, 6345–6404.
- 4 S. Muench, A. Wild, C. Friebe, B. Häupler, T. Janoschka and U. S. Schubert, *Chem. Rev.*, 2016, **116**, 9438–9484.
- 5 C. P. Grey and J. M. Tarascon, Nat. Mater., 2016, 16, 45-56.
- 6 D. Larcher and J. M. Tarascon, Nat. Chem., 2015, 7, 19–29.
- 7 S. Tan, D. J. Payne, J. P. Hallett and G. H. Kelsall, *Curr. Opin. Electrochem.*, 2019, 16, 83–89.
- 8 C. Cui, X. Ji, P. F. Wang, G. L. Xu, L. Chen, J. Chen, H. Kim, Y. Ren, F. Chen, C. Yang, X. Fan, C. Luo, K. Amine and C. Wang, ACS Energy Lett., 2020, 5, 224–231.
- 9 A. Choudhary and E. Prasad, Global Lithium-Ion Battery Market to \$100.43 Billion by 2025 at 17.1% CAGR;
 K. Yeware and E. Prasad, Lead-Acid Battery Market Outlook 2026, reports by Allied Market Research, 2020.
- 10 J. Muldoon, C. B. Bucur and T. Gregory, Chem. Rev., 2014, 114, 11683-11720.
- 11 S. Lee, G. Kwon, K. Ku, K. Yoon, S. K. Jung, H. D. Lim and K. Kang, Adv. Mater., 2018, 1704682.
- 12 X. B. Cheng, R. Zhang, C. Z. Zhao and Q. Zhang, *Chem. Rev.*, 2017, **117**, 10403–10473.
- 13 Q. Liu, H. Wang, C. Jiang and Y. Tang, Energy Storage Mater., 2019, 23, 566–586.
- 14 Y. Xu, M. Zhou and Y. Lei, Mater. Today, 2018, 21, 60-78.
- 15 K. Qin, J. Baucom, D. Liu, W. Shi, N. Zhao and Y. Lu, Small, 2020, 16, 2000794.
- 16 R. Zhang, S. Wen, N. Wang, K. Qin, E. Liu, C. Shi and N. Zhao, Adv. Energy Mater., 2018, 8, 1800914.
- 17 D. Lin, Y. Liu, Z. Liang, H. W. Lee, J. Sun, H. Wang, K. Yan, J. Xie and Y. Cui, *Nat. Nanotechnol.*, 2016, **11**, 626–632.
- 18 M. Mao, T. Gao, S. Hou and C. Wang, Chem. Soc. Rev., 2018, 47, 8804–8841.

- 19 J. Xie and Q. Zhang, Small, 2019, 15, 1805061.
- 20 C. Luo, O. Borodin, X. Ji, S. Hou, K. J. Gaskell, X. Fan, J. Chen, T. Deng, R. Wang, J. Jiang and C. Wang, PANS, 2018, 115, 2004-2009.
- 21 Y. Park, D. S. Shin, S. H. Woo, N. S. Choi, K. H. Shin, S. M. Oh, K. T. Lee and S. Y. Hong, Adv. Mater., 2012, 24, 3562-3567.
- 22 N. Patil, A. Aqil, F. Ouhib, S. Admassie, O. Inganäs, C. Jérôme and C. Detrembleur, Adv. Mater., 2017, 29, 1703373.
- 23 Y. Liang, C. Luo, F. Wang, S. Hou, S. C. Liou, T. Qing, Q. Li, J. Zheng, C. Cui and C. Wang, Adv. Energy Mater., 2018, 1802986.
- 24 C. Luo, G. L. Xu, X. Ji, S. Hou, L. Chen, F. Wang, J. Jiang, Z. Chen, Y. Ren, K. Amine and C. Wang, Angew. Chem., Int. Ed., 2018, 57, 2879-2883.
- 25 M. Lee, J. Hong, J. Lopez, Y. Sun, D. Feng, K. Lim, W. C. Chueh, M. F. Toney, Y. Cui and Z. Bao, Nat. Energy, 2017, 2, 861-868.
- 26 D. L. Williams, J. J. Byrne and J. S. Driscoll, J. Electrochem. Soc., 1969, 116, 2-5.
- 27 P. G. Pickup and R. A. Osteryoung, J. Am. Chem. Soc., 1984, 106, 2294-2299.
- 28 A. G. Macdiarmid, J.-C. Chiang, M. Halpern, W.-S. Huang, S.-L. Mu, L. D. Nanaxakkara, S. W. Wu and S. I. Yaniger, Mol. Cryst. Liq. Cryst., 1985, 121, 173-180.
- 29 G. Kumar, A. Sivashanmugam, N. Muniyandi, S. K. Dhawan and D. C. Trivedi, Synth. Met., 1996, 80, 279-282.
- 30 I. A. Rodríguez-Pérez, Y. Yuan, C. Bommier, X. Wang, L. Ma, D. P. Leonard, M. M. Lerner, R. G. Carter, T. Wu, P. A. Greaney, J. Lu and X. Ji, J. Am. Chem. Soc., 2017, 139, 13031-13037.
- 31 Y. Liang, Z. Tao and J. Chen, Adv. Energy Mater., 2012, 2, 742-769.
- 32 B. Häupler, A. Wild and U. S. Schubert, Adv. Energy Mater., 2015, 5, 1402034.
- 33 J. J. Shea and C. Luo, ACS Appl. Mater. Interfaces, 2020, 12, 5361-5380.
- 34 C. Luo, J. J. Shea and J. Huang, J. Power Sources, 2020, 453, 227904.
- 35 J. Hong, M. Lee, B. Lee, D. H. Seo, C. B. Park and K. Kang, Nat. Commun., 2014, 5, 5335.
- 36 B. Pan, J. Huang, Z. Feng, L. Zeng, M. He, L. Zhang, J. T. Vaughey, M. J. Bedzyk, P. Fenter, Z. Zhang, A. K. Burrell and C. Liao, Adv. Energy Mater., 2016, 6, 1600140.
- 37 H. Glatz, E. Lizundia, F. Pacifico and D. Kundu, ACS Appl. Energy Mater., 2019, 2, 1288-1294.
- 38 C. Luo, X. Ji, S. Hou, N. Eidson, X. Fan, Y. Liang, T. Deng, J. Jiang and C. Wang, Adv. Mater., 2018, 30, 1706498.
- 39 M. Armand, S. Grugeon, H. Vezin, S. Laruelle, P. Ribière, P. Poizot and J. M. Tarascon, Nat. Mater., 2009, 8, 120-125.
- 40 P. Poizot, J. Gaubicher, S. Renault, L. Dubois, Y. Liang and Y. Yao, Chem. Rev., 2020, 120, 6490-6557.
- 41 G. Dai, Y. He, Z. Niu, P. He, C. Zhang, Y. Zhao, X. Zhang and H. Zhou, Angew. Chem., Int. Ed., 2019, 58, 9902-9906.
- 42 F. Liu, T. Wang, X. Liu and L. Z. Fan, Adv. Energy Mater., 2020, 2000787.

- 43 A. Jouhara, N. Dupré, A. C. Gaillot, D. Guyomard, F. Dolhem and P. Poizot, Nat. Commun., 2018, 9, 4401.
- 44 H. Sano, H. Senoh, M. Yao, H. Sakaebe and T. Kiyobayashi, Chem. Lett., 2012, 41, 1594-1596.
- 45 H. Senoh, H. Sakaebe, H. Sano, M. Yao, K. Kuratani, N. Takeichi and T. Kivobayashi, J. Electrochem. Soc., 2014, 161, A1315-A1320.
- 46 B. Pan, D. Zhou, J. Huang, L. Zhang, A. K. Burrell, J. T. Vaughey, Z. Zhang and C. Liao, J. Electrochem. Soc., 2016, 163, A580-A583.
- 47 J. Bitenc, T. Pavčnik, U. Košir and K. Pirnat, Materials, 2020, 13, 506.
- 48 T. Debashis, H. M. Viswanatha, M. N. K. Harish and S. Sampath, J. Electrochem. Soc., 2020, 167, 070561.
- 49 L. Cui, L. Zhou, K. Zhang, F. Xiong, S. Tan, M. Li, Q. An, Y. M. Kang and L. Mai, Nano Energy, 2019, 65, 103902.
- 50 J. Tian, D. Cao, X. Zhou, J. Hu, M. Huang and C. Li, ACS Nano, 2018, 12, 3424-3435.
- 51 Q. Ju, Y. Shi and J. Kan, Synth. Met., 2013, 178, 27-33.
- 52 Y. NuLi, Z. Guo, H. Liu and J. Yang, Electrochem. Commun., 2007, 9, 1913-1917.
- 53 N. Oyama, T. Tatsuma, T. Sato and T. Sotomura, Nature, 1995, 373, 598-600.
- 54 J. Li, H. Zhan, L. Zhou, S. Deng, Z. Li and Y. Zhou, Electrochem. Commun., 2004, 6, 515-519.
- 55 H. K. Henry and S. B. Lee, ChemRxiv, 2018, DOI: 10.26434/ chemrxiv.6716012.v1.
- 56 J. Bitenc, K. Pirnat, T. Bančič, M. Gaberšček, B. Genorio, A. Randon-Vitanova and R. Dominko, ChemSusChem, 2015, 8, 4128-4132.
- 57 Y. Liang, R. Feng, S. Yang, H. Ma, J. Liang and J. Chen, Adv. Mater., 2011, 23, 640-643.
- 58 Z. Song, Y. Qian, X. Liu, T. Zhang, Y. Zhu, H. Yu, M. Otani and H. Zhou, Energy Environ. Sci., 2014, 7, 4077-4086.
- 59 J. Bitenc, K. Pirnat, E. Žagar, A. Randon-Vitanova and R. Dominko, J. Power Sources, 2019, 430, 90-94.
- 60 J. Bitenc, K. Pirnat, G. Mali, B. Novosel, A. Randon Vitanova and R. Dominko, Electrochem. Commun., 2016, 69, 1-5.
- 61 A. Vizintin, J. Bitenc, A. Kopač Lautar, J. Grdadolnik, A. Randon Vitanova and K. Pirnat, ChemSusChem, 2020, 13, 2328-2336.
- 62 H. Dong, Y. Liang, O. Tutusaus, R. Mohtadi, Y. Zhang, F. Hao and Y. Yao, Joule, 2019, 3, 782-793.
- 63 S. H. Strauss, Chem. Rev., 1993, 93, 927-942.
- 64 T. Bančič, J. Bitenc, K. Pirnat, A. Kopač Lautar, J. Grdadolnik, A. Randon Vitanova and R. Dominko, J. Power Sources, 2018, **395**, 25-30.
- 65 Z. Song, H. Zhan and Y. Zhou, Angew. Chem., Int. Ed., 2010, 49, 8444-8448.
- 66 C. R. Deblase, K. Hernández-Burgos, J. M. Rotter, D. J. Fortman, D. Dos, S. Abreu, R. A. Timm, I. C. N. Diógenes, L. T. Kubota, H. D. Abruña and W. R. Dichtel, Angew. Chem., Int. Ed., 2015, 54, 13225-13229.
- 67 J. Benson, S. Boukhalfa, A. Magasinski, A. Kvit and G. Yushin, ACS Nano, 2012, 6, 118-125.

- 68 J. Biemolt, P. Jungbacker, T. Van Teijlingen, N. Yan and G. Rothenberg, *Materials*, 2020, **13**, 425.
- 69 X. Fan, F. Wang, X. Ji, R. Wang, T. Gao, S. Hou, J. Chen, T. Deng, X. Li, L. Chen, C. Luo, L. Wang and C. Wang, *Angew. Chem., Int. Ed.*, 2018, 57, 7146–7150.
- 70 H. Wu, K. Wang, Y. Meng, K. Lu and Z. Wei, *J. Mater. Chem.* A, 2013, 1, 6366–6372.
- 71 Y. Wang, Z. Liu, C. Wang, Y. Hu, H. Lin, W. Kong, J. Ma and Z. Jin, *Energy Storage Mater.*, 2020, **26**, 494–502.
- 72 D. Lu, H. Liu, T. Huang, Z. Xu, L. Ma, P. Yang, P. Qiang, F. Zhang and D. Wu, J. Mater. Chem. A, 2018, 6, 17297–17302.
- 73 Q. Chen, Y. N. Nuli, W. Guo, J. Yang, J. L. Wang and Y. G. Guo, *Acta Phys.-Chim. Sin.*, 2013, **29**, 2295–2299.
- 74 S. Y. Ha, Y. W. Lee, S. W. Woo, B. Koo, J. S. Kim, J. Cho, K. T. Lee and N. S. Choi, *ACS Appl. Mater. Interfaces*, 2014, 6, 4063–4073.
- 75 M. Miroshnikov, K. Mahankali, N. K. Thangavel, S. Satapathy, L. M. R. Arava, P. M. Ajayan and G. John, *ChemSusChem*, 2020, 13, 2186–2204.
- 76 M. Li, J. Lu, X. Ji, Y. Li, Y. Shao, Z. Chen, C. Zhong and K. Amine, *Nat. Rev. Mater.*, 2020, 5, 276–294.
- 77 M. Mao, C. Luo, T. P. Pollard, S. Hou, T. Gao, X. Fan, C. Cui, J. Yue, Y. Tong, G. Yang, T. Deng, M. Zhang, J. Ma, L. Suo, O. Borodin and C. Wang, *Angew. Chem., Int. Ed.*, 2019, 58, 17820–17826.
- 78 L. Kong, M. Zhong, W. Shuang, Y. Xu and X. H. Bu, *Chem. Soc. Rev.*, 2020, **49**, 2378–2407.
- 79 R. Sun, S. Hou, C. Luo, X. Ji, L. Wang, L. Mai and C. Wang, Nano Lett., 2020, 20, 3880–3888.
- 80 A. B. Ikhe, N. Naveen, K. S. Sohn and M. Pyo, *Electrochim. Acta*, 2018, **283**, 393–400.
- 81 G. A. Elia, K. Marquardt, K. Hoeppner, S. Fantini, R. Lin, E. Knipping, W. Peters, J. F. Drillet, S. Passerini and R. Hahn, *Adv. Mater.*, 2016, **28**, 7564–7579.
- 82 Y. Ru, S. Zheng, H. Xue and H. Pang, J. Mater. Chem. A, 2019, 7, 14391–14418.
- 83 Y. Zhang, S. Liu, Y. Ji, J. Ma and H. Yu, *Adv. Mater.*, 2018, **30**, 1706310.
- 84 H. Yang, H. Li, J. Li, Z. Sun, K. He, H. M. Cheng and F. Li, *Angew. Chem., Int. Ed.*, 2019, **58**, 11978–11996.
- 85 P. G. Pickup and R. A. Osteryoung, *J. Electroanal. Chem.*, 1985, **195**, 271–288.
- 86 L. Janiszewska and R. Osteryoung, *J. Electrochem. Soc.*, 1987, **134**, 2787–2794.
- 87 J. Tang and R. A. Osteryoung, Synth. Met., 1991, 45, 1-13.
- 88 L. M. Goldenberg and R. A. Osteryoung, *Synth. Met.*, 1994, **64**, 63–68.
- 89 N. Koura, H. Ejiri and K. Takeishi, *J. Electrochem. Soc.*, 1993, **140**, 602–605.
- 90 K. Ui, Y. Kuma and N. Koura, *Electrochemistry*, 2006, 7, 536–538.
- 91 N. S. Hudak, J. Phys. Chem. C, 2014, 118, 5203-5215.
- 92 M. Walter, K. V. Kravchyk, C. Böfer, R. Widmer and M. V. Kovalenko, *Adv. Mater.*, 2018, 30, 1705644.
- 93 J. Bitenc, N. Lindahl, A. Vizintin, M. Abdelhamid, R. Dominko and P. Kohansson, *Energy Storage Mater.*, 2020, 24, 379–383.

- 94 D. J. Kim, D. J. Yoo, M. T. Otley, A. Prokofjevs, C. Pezzato, M. Owczarek, S. J. Lee, J. W. Choi and J. F. Stoddart, *Nat. Energy*, 2019, 4, 51–59.
- 95 Y. Liang and Y. Yao, Nat. Energy, 2019, 4, 10-11.
- 96 J. Zhou, X. Yu, J. Zhou and B. Lu, *Energy Storage Mater.*, 2020, **31**, 58-63.
- 97 D. Selvakumaran, A. Pan, S. Liang and G. Cao, J. Mater. Chem. A, 2019, 7, 18209–18236.
- 98 A. Guerfi, J. Trottier, I. Boyano, I. De Meatza, J. A. Blazquez, S. Brewer, K. S. Ryder, A. Vijh and K. Zaghib, *J. Power Sources*, 2014, 248, 1099–1104.
- 99 T. J. Simons, M. Salsamendi, P. C. Howlett, M. Forsyth, D. R. Macfarlane and C. Pozo-Gonzalo, *ChemElectroChem*, 2015, 2, 2071–2078.
- 100 N. Wang, X. Dong, B. Wang, Z. Guo, Z. Wang, R. Wang, X. Qiu and Y. Wang, *Angew. Chem., Int. Ed.*, 2020, 59, 14577–14583.
- 101 Z. Zhao-Karger and M. Fichtner, *Front. Chem.*, 2019, 7, 1–12.
- 102 R. C. Massé, E. Uchaker and G. Cao, Sci. China Mater., 2015, 58, 715–766.
- 103 Z. Ma, D. R. MacFarlane and M. Kar, *Batteries Supercaps*, 2019, 2, 115–127.
- 104 B. T. McAllister, L. T. Kyne, T. B. Schon and D. S. Seferos, Joule, 2019, 3, 620–624.
- 105 R. Y. Wang, C. D. Wessells, R. A. Huggins and Y. Cui, *Nano Lett.*, 2013, 13, 5748–5752.
- 106 M. Krogsgaard, M. A. Behrens, J. S. Pedersen and H. Birkedal, *Biomacromolecules*, 2013, **14**, 297–301.
- 107 N. Patil, A. Mavrandonakis, C. Jérôme, C. Detrembleur, J. Palma and R. Marcilla, ACS Appl. Energy Mater., 2019, 2, 3035–3041.
- 108 Y. J. Kim, W. Wu, S. E. Chun, J. F. Whitacre and C. J. Bettinger, *Adv. Mater.*, 2014, **26**, 6572–6579.
- 109 H. Lee, N. F. Scherer and P. B. Messersmith, *Proc. Natl. Acad. Sci. U. S. A.*, 2006, **103**, 12999–13003.
- 110 Y. Liang, Y. Jing, S. Gheytani, K. Y. Lee, P. Liu, A. Facchetti and Y. Yao, *Nat. Mater.*, 2017, 16, 841–848.
- 111 L. Chen, J. L. Bao, X. Dong, D. G. Truhlar, Y. Wang, C. Wang and Y. Xia, ACS Energy Lett., 2017, 2, 1115–1121.
- 112 L. Chen, W. Li, Y. Wang, C. Wang and Y. Xia, *RSC Adv.*, 2014, **4**, 25369–25373.
- 113 F. Wang, X. Fan, T. Gao, W. Sun, Z. Ma, C. Yang, F. Han, K. Xu and C. Wang, ACS Cent. Sci., 2017, 3, 1121–1128.
- 114 V. Verma, S. Kumar, W. Manalastas, R. Satish and M. Srinivasan, *Adv. Sustainable Syst.*, 2019, 3, 1800111.
- 115 R. Cang, Y. Song, K. Ye, K. Zhu, J. Yan, J. Yin, G. Wang and D. Cao, *J. Electroanal. Chem.*, 2020, **861**, 113967.
- 116 F. Wu, H. Yang, Y. Bai and C. Wu, Adv. Mater., 2019, 31, 1806510.
- 117 R. J. Gummow, G. Vamvounis, M. B. Kannan and Y. He, Adv. Mater., 2018, 30, 1801702.
- 118 Z. Li, O. Fuhr, M. Fichtner and Z. Zhao-Karger, *Energy Environ. Sci.*, 2019, **12**, 3496–3501.
- 119 S. Gheytani, Y. Liang, F. Wu, Y. Jing, H. Dong, K. K. Rao, X. Chi, F. Fang and Y. Yao, *Adv. Sci.*, 2017, **4**, 1700465.

- 120 R. Cang, C. Zhao, K. Ye, J. Yin, K. Zhu, J. Yan, Y. Gao, G. Wang and D. Cao, ChemSusChem, 2020, 13, 3911-3918.
- 121 H. Li, L. Ma, C. Han, Z. Wang, Z. Liu, Z. Tang and C. Zhi, Nano Energy, 2019, 62, 550-587.
- 122 P. He, Q. Chen, M. Yan, X. Xu, L. Zhou, L. Mai and C.-W. Nan, EnergyChem, 2019, 1, 100022.
- 123 B. Tang, L. Shan, S. Liang and J. Zhou, Energy Environ. Sci., 2019, 12, 3288-3304.
- 124 A. Kitani, M. Kaya and K. Sasaki, J. Electrochem. Soc., 1986, 133, 1069-1073.
- 125 G. Mengoli and M. Musiani, J. Appl. Electrochem., 1987, 17, 515-524.
- 126 M. S. Rahmanifar, M. F. Mousavi and M. Shamsipur, J. Power Sources, 2002, 110, 229-232.
- 127 J. Zhang, D. Shan and S. Mu, J. Power Sources, 2006, 161, 685-691.
- 128 C. Chen, X. Hong, A. Chen, T. Xu, L. Lu, S. Lin and Y. Gao, Electrochim. Acta, 2016, 190, 240-247.
- 129 H.-Y. Shi, Y.-J. Ye, K. Liu, Y. Song and X. Sun, Angew. Chem., 2018, 130, 16597-16601.
- 130 X. Li, R. Lv, S. Zou, B. Na, P. Liu, Y. Ma and H. Liu, Compos. Sci. Technol., 2019, 180, 71-77.
- 131 Y. Liu, L. Xie, W. Zhang, Z. Dai, W. Wei, S. Luo, X. Chen, W. Chen, F. Rao, L. Wang and Y. Huang, ACS Appl. Mater. Interfaces, 2019, 11, 30943-30952.
- 132 F. Wan, L. Zhang, X. Wang, S. Bi, Z. Niu and J. Chen, Adv. Funct. Mater., 2018, 28, 1804975.
- 133 C. Kim, B. Y. Ahn, T. S. Wei, Y. Jo, S. Jeong, Y. Choi, I. D. Kim and J. A. Lewis, ACS Nano, 2018, 12, 11838-11846.
- 134 Y. Zhao, Y. Wang, Z. Zhao, J. Zhao, T. Xin, N. Wang and J. Liu, Energy Storage Mater., 2020, 28, 64-72.
- 135 J. Wang, J. Liu, M. Hu, J. Zeng, Y. Mu, Y. Guo, J. Yu, X. Ma, Y. Qiu and Y. Huang, J. Mater. Chem. A, 2018, 6, 11113-11118.
- 136 Z. Cai and C. Hou, J. Power Sources, 2011, 196, 10731-10736.
- 137 Z. Cai, J. Guo, H. Yang and Y. Xu, J. Power Sources, 2015, 279, 114-122.
- 138 H. Karami, M. F. Mousavi and M. Shamsipur, J. Power Sources, 2003, 117, 255-259.
- 139 J. Huang, Z. Wang, M. Hou, X. Dong, Y. Liu, Y. Wang and Y. Xia, Nat. Commun., 2018, 9, 2906.
- 140 D. Bin, W. Huo, Y. Yuan, J. Huang, Y. Liu, Y. Zhang, F. Dong, Y. Wang and Y. Xia, Chem, 2020, 6, 968-984.
- 141 A. Lahiri, L. Yang, G. Li and F. Endres, ACS Appl. Mater. Interfaces, 2019, 11, 45098-45107.
- 142 X. Li, X. Xie, R. Lv, B. Na, B. Wang and Y. He, Energy Technol., 2019, 7, 1801092.
- 143 S. Liu, H. Zhu, B. Zhang, G. Li, H. Zhu, Y. Ren, H. Geng, Y. Yang, Q. Liu and C. C. Li, Adv. Mater., 2020, 2001113.
- 144 Y. Zhao, L. Ma, Y. Zhu, P. Qin, H. Li, F. Mo, D. Wang, G. Liang, Q. Yang, W. Liu and C. Zhi, ACS Nano, 2019, 13, 7270-7280.
- 145 D. Kundu, P. Oberholzer, C. Glaros, A. Bouzid, E. Tervoort, A. Pasquarello and M. Niederberger, Chem. Mater., 2018, 30, 3874-3881.
- 146 Q. Zhao, W. Huang, Z. Luo, L. Liu, Y. Lu, Y. Li, L. Li, J. Hu, H. Ma and J. Chen, Sci. Adv., 2018, 4, eaao1761.

- 147 Z. Guo, Y. Ma, X. Dong, J. Huang, Y. Wang and Y. Xia, Angew. Chem., 2018, 130, 11911-11915.
- 148 G. Dawut, Y. Lu, L. Miao and J. Chen, Inorg. Chem. Front., 2018, 5, 1391-1396.
- 149 Y. Zhang, Y. Liang, H. Dong, X. Wang and Y. Yao, J. Electrochem. Soc., 2020, 167, 070558.
- 150 S. Zhang, W. Zhao, H. Li and Q. Xu, ChemSusChem, 2020,
- 151 X. Yue, H. Liu and P. Liu, Chem. Commun., 2019, 55, 1647-1650.
- 152 X. Wang, L. Chen, F. Lu, J. Liu, X. Chen and G. Shao, ChemElectroChem, 2019, 6, 3644-3647.
- 153 R. Cang, K. Ye, K. Zhu, J. Yan, J. Yin, K. Cheng, G. Wang and D. Cao, J. Energy Chem., 2020, 45, 52-58.
- 154 A. M. Khayum, M. Ghosh, V. Vijayakumar, A. Halder, M. Nurhuda, S. Kumar, M. Addicoat, S. Kurungot and R. Banerjee, Chem. Sci., 2019, 10, 8889-8894.
- 155 K. Koshika, N. Sano, K. Oyaizu and H. Nishide, Macromol. Chem. Phys., 2009, 210, 1989-1995.
- 156 K. Koshika, N. Chikushi, N. Sano, K. Oyaizu and H. Nishide, Green Chem., 2010, 12, 1573-1575.
- 157 B. Haüpler, C. Rössel, A. M. Schwenke, J. Winsberg, D. Schmidt, A. Wild and U. S. Schubert, NPG Asia Mater., 2016, 8, e283.
- 158 C. Florindo, F. Lima, B. D. Ribeiro and I. M. Marrucho, Curr. Opin. Green Sustainable Chem., 2019, 18, 31-36.
- 159 C. Zhang, L. Zhang and G. Yu, Acc. Chem. Res., 2020, 53, 1648-1659.
- 160 E. L. Smith, A. P. Abbott and K. S. Ryder, Chem. Rev., 2014, 114, 11060-11082.
- 161 M. Forsyth, P. C. Howlett, A. E. Somers, D. R. MacFarlane and A. Basile, npj Mater. Degrad., 2017, 1, 18.
- 162 L. Zhang, C. Zhang, Y. Ding, K. Ramirez-Meyers and G. Yu, Joule, 2017, 1, 623-633.
- 163 C. Zhang, Y. Ding, L. Zhang, X. Wang, Y. Zhao, X. Zhang and G. Yu, Angew. Chem., Int. Ed., 2017, 56, 7454-7459.
- 164 Y. Wang and H. Zhou, Energy Environ. Sci., 2016, 9, 2267–2272.
- 165 H. M. A. Abood, A. P. Abbott, A. D. Ballantyne and K. S. Ryder, Chem. Commun., 2011, 47, 3523-3525.
- 166 M. Li, B. Gao, C. Liu, W. Chen, Z. Shi, X. Hu and Z. Wang, Electrochim. Acta, 2015, 180, 811-814.
- 167 M. Li, B. Gao, W. Chen, C. Liu, Z. Wang, Z. Shi and X. Hu, Electrochim. Acta, 2015, 185, 148-155.
- 168 W. Chu, X. Zhang, J. Wang, S. Zhao, S. Liu and H. Yu, Energy Storage Mater., 2019, 22, 418-423.
- 169 N. Bogolowski and J. F. Drillet, *Electrochim. Acta*, 2018, 274, 353-358.
- 170 S. C. Wu, Y. Ai, Y. Z. Chen, K. Wang, T. Y. Yang, H. J. Liao, T. Y. Su, S. Y. Tang, C. W. Chen, D. C. Wu, Y. C. Wang, A. Manikandan, Y. C. Shih, L. Lee, Y. L. Chueh, Y. L. Chueh and Y. L. Chueh, ACS Appl. Mater. Interfaces, 2020, 12, 27064-27073.
- 171 N. Canever, N. Bertrand and T. Nann, Chem. Commun., 2018, 54, 11725-11728.
- 172 M. Angell, C. J. Pan, Y. Rong, C. Yuan, M. C. Lin, B. J. Hwang and H. Dai, PANS, 2017, 114, 834-839.

- 173 H. Jiao, C. Wang, J. Tu, D. Tian and S. Jiao, *Chem. Commun.*, 2017, 53, 2331–2334.
- 174 M. Arita, D. R. Bowler and T. Miyazaki, *J. Chem. Theory Comput.*, 2014, **10**, 5419–5425.
- 175 K. T. Butler, D. W. Davies, H. Cartwright, O. Isayev and A. Walsh, *Nature*, 2018, **559**, 547–555.
- 176 E. J. Corey and W. T. Wipke, Science, 1969, 166, 178-192.
- 177 T. I. Oprea and A. Tropsha, *Drug Discovery Today: Technol.*, 2006, 3, 357–365.
- 178 T. Sterling and J. J. Irwin, *J. Chem. Inf. Model.*, 2015, 55, 2324–2337.
- 179 W. W. M. Fleuren and W. Alkema, *Methods*, 2015, 74, 97–106.
- 180 E. Kim, K. Huang, A. Saunders, A. McCallum, G. Ceder and E. Olivetti, *Chem. Mater.*, 2017, **29**, 9436–9444.
- 181 A. Steane, Rep. Prog. Phys., 1963, 59, 1665-1735.
- 182 A. Aspuru-Guzik, A. D. Dutoi, P. J. Love and M. Head-Gordon, *Science*, 2005, **309**, 1704–1707.